AFRL-VA-WP-TR-2001-3005

MULTIPLE SITE DAMAGE IN FLAT PANEL TESTING

CAPT. DANIEL B. SHRAGE

AIR VEHICLES DIRECTORATE
AIR FORCE RESEARCH LABORATORY
2790 D STREET, STE 306W
WRIGHT-PATTERSON AIR FORCE BASE, OH 45433-7542

OCTOBER 2000

**FINAL REPORT FOR PERIOD OF 13 MAY 1999 – 08 DECEMBER 1999**

AIR VEHICLES DIRECTORATE
AIR FORCE RESEARCH LABORATORY
AIR FORCE MATERIEL COMMAND
WRIGHT-PATTERSON AIR FORCE BASE, OH 45433-7542

NOTICE

USING GOVERNMENT DRAWINGS, SPECIFICATIONS, OR OTHER DATA INCLUDED IN THIS DOCUMENT FOR ANY PURPOSE OTHER THAN GOVERNMENT PROCUREMENT DOES NOT IN ANY WAY OBLIGATE THE U.S. GOVERNMENT. THE FACT THAT THE GOVERNMENT FORMULATED OR SUPPLIED THE DRAWINGS, SPECIFICATIONS, OR OTHER DATA DOES NOT LICENSE THE HOLDER OR ANY OTHER PERSON OR CORPORATION; OR CONVEY ANY RIGHTS OR PERMISSION TO MANUFACTURE, USE, OR SELL ANY PATENTED INVENTION THAT MAY RELATE TO THEM.

THIS REPORT IS RELEASABLE TO THE NATIONAL TECHNICAL INFORMATION SERVICE (NTIS). AT NTIS, IT WILL BE AVAILABLE TO THE GENERAL PUBLIC, INCLUDING FOREIGN NATIONS.

THIS TECHNICAL REPORT HAS BEEN REVIEWED AND IS APPROVED FOR PUBLICATION.

DANIEL B. SHRAGE, Capt, USAF
Lead Engineer
Aircraft Structural Integrity
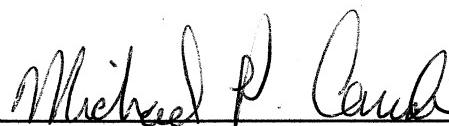
MICHAEL P. CAMDEN
Acting Chief
Analytical Structural Mechanics Branch

DAVID M. PRATT, PhD
Technical Advisor
Structures Division

Do not return copies of this report unless contractual obligations or notice on a specific document require its return.

REPORT DOCUMENTATION PAGE

Form Approved
OMB No. 074-0188

1. AGENCY USE ONLY (Leave blank)	2. REPORT DATE OCTOBER 2000	3. REPORT TYPE AND DATES COVERED Final, 05/13/1999 – 12/08/1999	
4. TITLE AND SUBTITLE MULTIPLE SITE DAMAGE IN FLAT PANEL TESTING		**5. FUNDING NUMBERS** N/A	
6. AUTHOR(S) Capt. Daniel B. Shrage			
7. PERFORMING ORGANIZATION NAME(S) AND ADDRESS(ES) AIR VEHICLES DIRECTORATE AIR FORCE RESEARCH LABORATORY 2790 D STREET, STE 306W WRIGHT-PATTERSON AIR FORCE BASE, OH 45433-7542		**8. PERFORMING ORGANIZATION REPORT NUMBER**	
9. SPONSORING / MONITORING AGENCY NAME(S) AND ADDRESS(ES) AIR VEHICLES DIRECTORATE AIR FORCE RESEARCH LABORATORY AIR FORCE MATERIEL COMMAND WRIGHT-PATTERSON AIR FORCE BASE, OH 45433-7542 POC: Capt. Daniel B. Shrage, AFRL/VASM, (937) 255-6104 x242		**10. SPONSORING / MONITORING AGENCY REPORT NUMBER** AFRL-VA-WP-TR-2001-3005	

11. SUPPLEMENTARY NOTES:

12a. DISTRIBUTION / AVAILABILITY STATEMENT Approved for public release; distribution unlimited.	12b. DISTRIBUTION CODE

13. ABSTRACT *(Maximum 200 Words)*

The report aimed to experimentally verify analytic models that predict the residual strength of representative aircraft structures, such as wide panels, that are subjected to multiple site damage (MSD). As today's transport aircraft become older, the possibility exists for predetermined analysis to be invalidated by the onset of MSD. The MSD can be caused by cyclic loading on the fuselage structure over its life, and the resulting weakening in the structure must be considered as a potential safety risk during repairs and inspections.

Four types of flat joints that represented production joints in narrow and wide body transport aircraft were damaged and then tested for residual strength. Testing included recording crack extension. Equipment used to examine damage included a traveling optical microscope, strain gages (for examining axial and rosette segments of joints), and a crack opening displacement gage to measure local and global deformations. The tests were displacement controlled using a linear voltage displacement transducer allowing the measurement of crack progression after the peak strength of the panel had been reached. The average reduction in residual strength for 0.050-inch damage site was 21.45 percent, while the average for 0.100-inch damage was 27.88 percent.

14. SUBJECT TERMS			15. NUMBER OF PAGES 108
			16. PRICE CODE
17. SECURITY CLASSIFICATION OF REPORT Unclassified	18. SECURITY CLASSIFICATION OF THIS PAGE Unclassified	19. SECURITY CLASSIFICATION OF ABSTRACT Unclassified	20. LIMITATION OF ABSTRACT SAR

| NSN 7540-01-280-5500 | | | Standard Form 298 (Rev. 2-89)
Prescribed by ANSI Std. Z39-18
298-102 |

TABLE OF CONTENTS

LIST OF FIGURES

LIST OF TABLES

1. Introduction

The Multiple Site Damage (MSD) Testing and Analysis program is one of six technology thrusts in the Federal Aviation Administration's (FAA) Widespread Fatigue Damage (WFD) Evaluation program. The prime contractor to the FAA is The Boeing-Long Beach Company. The Air Force Research Laboratory, Air Vehicles Directorate, Structures Division, Analytical Structural Mechanics Branch (AFRL/VASM) is participating in five of the six technology areas; WFD Initiation, Small Crack Study, Equivalent Initial Flaw Size (EIFS), MSD in Flat Panels, and MSD in an Aft Pressure Bulkhead. The MSD in Curved Panels program is an effort solely executed by Boeing and the FAA. Costs in the MSD in Flat Panels testing are shared between the FAA and AFRL/VASM. The panels were tested at AFRL/VASM using the Wide Panel Test Facility (Figure 1). Via the FAA, Boeing fabricated 16 production-like joints to be tested at AFRL/VASM, Wright-Patterson AFB, OH. For the core program, three of each joint type were tested, for a total of 12 test panels (Figures 2-5). Additionally, there is a supplemental test program planned, with the remaining four panels. Boeing also provided materials for four lab-quality specimens to be manufactured and tested at AFRL/VASM. These lab-quality specimens will also be included in the supplemental test program. This program will test the panels without buckling guides and the strain data will be recorded using a three-dimensional visual image correlation system (VIC 3-D). This system captures the full field displacements at each load step, and those displacement fields can be converted to strains. The results of the supplemental tests will be presented as an addendum to this report.

With the existence of large lead cracks in built-up structure, the ability to accurately predict the residual strength and damage tolerance is critical in ensuring flight safety and in determining inspection criteria. The flat panel testing is designed to simulate aircraft structure and improve the field level techniques for evaluating existing damage, by providing verified models for life prediction at given damage states. To that end, each of the flat panel specimens has a long lead crack (12.82 – 14.8 inches) in the critical row applicable to each panel. A critical row in a joint is the row of rivets known as the initial failure point. The critical row in these joints is dependent on the individual joint configuration, but several similarities occur. In joint types I (Figure 2) and II (Figure 3), the joint is asymmetric and the critical row is the outside row in the sheet with the largest countersunk holes. Joint types III (Figure 4) and IV (Figure 5) are both symmetric, but the critical row is the outermost row of rivets, determined from prior testing. Which of the outermost rows will be critical was also determined prior to panel manufacture, through both panel testing and on-aircraft experience.

The residual strength and damage tolerance characteristics of splice joints with MSD vary significantly depending upon the initial size and distribution of the MSD flaws. The data gathered in this test program are used to validate current residual strength prediction models, as well as Finite Element Analysis (FEA) models that simulate the underlying behavior of the joints. Each of the flat panels was manufactured with a configuration of MSD in a number of rivets adjacent to the lead crack. Joint types I, III, and IV contain six rivet holes on each side of the lead crack, with joint type II having seven holes receiving MSD. The MSD is placed in the holes adjacent to the lead crack along the critical row, on both sides of each hole, parallel to the lead crack. The MSD is manufactured as a through crack, with the length of the MSD measured from the straight shank of the hole.

The objective of the MSD study is to generate data, crack opening displacement, crack length, and strain fields in the critical areas of typical fuselage longitudinal and circumferential splice joints subject to static loading.

2. Background

In the WFD Evaluation program both testing and analysis of fuselage skin splice joints is addressed; however, since this report covers only the experimental portion, only references to experimental residual strength tests are discussed. The purpose of this background information is to show only what experimental work has been accomplished. Results of residual strength testing of fuselage skin-like components have been widely reported in open literature since the Aloha accident in 1988.[1] Much of the earlier work, 1989 – 1994, focused on predicting the first and subsequent linkup of adjacent cracks; however, in hindsight, these results are not meaningful in an engineering sense as it is now widely recognized that the important parameter from a fail safety point of view is the load (or stress) at final structural failure. Most, if not all, test programs have been designed to validate linkup or residual strength prediction methods. The most widely cited test program was accomplished by Foster-Miller, Inc. and comprised 12 unstiffened, flat; 3 unstiffened, curved; and 6 stiffened, curved panels.[2] The flat panel tests consisted of a single, centrally located lead crack with three different MSD cracking scenarios ahead of the lead crack. The curved panel test series used three different cracking scenarios as well as two different stiffener selections, one light and one heavy.

Dawicke, Newman, Sutton, and Amstutz conducted residual strength tests of 25 flat, unstiffened sheets to study the effect of the crack history on residual strength.[3] The crack history in their investigation was defined as how the crack was initiated in the specimen - whether by using a jeweler's saw, fatigue precracking at a low stress range, or fatigue precracking at a high stress range. To measure the fracture parameter of interest, the critical crack tip opening displacement (CTOD), the highly accurate digital imaging system developed by Sutton of the University of South Carolina was used.[4]

To study the effect of dynamic fracture and its effects on crack arrest, Kosai, Shimamoto, Yu, Walker, Kobayashi, and Tan conducted 21 axial rupture tests of small-scale models of an idealized fuselage.[5] A thin-sheet axial cylinder was used for 10 specimens without axial stiffeners and 11 specimens with axial stiffeners. For the stiffened case, nine different scenarios were considered.

Full-scale residual strength tests of both narrow and wide body fuselage structure were conducted by the Boeing Commercial Airplane Group as reported by Miller, Gruber, Wilkins, and Worden.[6] The narrow and wide body fuselage cylinders contained a large test section where a test panel with the crack configuration of interest was installed. Four narrow- and two wide-body tests were completed to study the effect of crack extension and arrest as a function of fuselage diameter. Additional insight was obtained on the phenomenon of controlled decompression via fuselage skin flapping.

De Wit, Fields, Mordfin, Low, and Harne tested large-scale thin-sheet aluminum specimens to study the fracture behavior of panels nearly two times as large as any previously tested.[7,8] Their focus was to determine if there is a specimen dimension parameter affecting residual strength test results and thus residual strength prediction methodologies. The test specimens were flat, unstiffened panels with various lead and MSD crack scenarios. In addition, several test specimens were added to study the boundary of plastic collapse and fracture.

To study the effects of stiffener size (stiffness) and MSD crack size in front of the lead crack, Heinimann conducted 12 tests on flat, stiffened panels.[9] The test portion of this work was similar to the flat panel portion of that reported in reference [2].

To investigate the effect of the mode-mixity on residual strength, Helm, Sutton, and Boone, tested seven specimens subjected to tension and in-plane shear and five specimens subjected to tension and torsion.[10] In addition to studying the mode-mixity effect, they also determined the effect of grain orientation on the CTOD fracture parameter.

Residual strength pressure tests of stringer- and frame-stiffened aluminum fuselage (wide-body) panels were tested by Young, Rouse, Ambur, and Starnes to study the effect of internal pressure and axial tension on two cracking scenarios.[11] The two specimens were quite large, resembling those tested by Boeing.[6] The extent of stable tearing before panel failure was also studied in detail, as this is of prime interest in validating the crack tip opening angle (CTOA) failure criterion. As is always the case with tests of this configuration, the crack arrest capability of the frame (circumferential) stiffeners under the given cracking scenario can also be assessed. Jeong, Bakuckas, and Samavedam completed similar test work using the FAA Aging Aircraft Test Fixture designed and operated by Foster-Miller, Inc.[12][13]

As part of a material performance comparison, Bray, Bucci, Kulak, Warren, Grandt, Golden, and Sexton performed three series of residual strength tests using 2524-T3 aluminum sheet material.[14] One test series focused on residual strength and the other two test series addressed specific crack growth propagation phenomena. The residual strength test series was designed to assess the effect of MSD on residual strength of unstiffened and stiffened flat panels.

Smith, Mouak, Saville, Myose, and Horn tested 22 unstiffened and 12 stiffened flat panels subject to axial tension to validate their modification to the Swift linkup criterion.[15] The Swift linkup criterion was shown to be inaccurate for certain cracking scenarios; thus, the test matrix of Smith et al. was designed to investigate a variety of panel width and thickness, lead and MSD crack lengths (and thus ligament lengths) for both stiffened and unstiffened flat panels.[16]

The effect of crack buckling on residual strength predictions was investigated by Dawicke, Gullerud, Dodds, and Hampton using three compact tension (CT) and nine middle cracked tension (MT) specimens of varying widths while maintaining a constant crack length to specimen width ratio (a/W).[17] Crack face buckling is known to be a function of a/W. The amount of crack face buckling was controlled by the use of guide plates along the full length and width of the specimens.

Testing of riveted lap joint specimens was accomplished by Silva, Concalves, Oliviera, and de Castro. The tests employed a total of 10 unconstrained specimens in a matrix of WFD initiation and residual strength testing configurations. The stress measurement system, SPATE, and strain gages were used to characterize the three-dimensional stress state that the panels were experiencing under tensile loading and to draw conclusions from the panel response in fatigue and final failure.[18]

3. Experimental Investigation

For this study, the panels are representative of actual aircraft joints and are subjected to remote tensile loads. These loads are distributed over the entire width of the panel. The tensile load simulates the hoop stress caused by internal cabin pressurization, as well as longitudinal fuselage bending loads.

The AFRL's Wide Panel Test Facility was designed and constructed specifically for the EIFS and MSD test programs. A digital computer was used to control the closed loop, servo hydraulic load frames. The maximum specimen dimensions are 48 by 86 inches at loads up to 100 kips with a factor of safety of 2. Each frame is equipped with a 20 power traveling optical microscope (TOM) mounted to a stage that can translate along the length or across the width of the specimen. The translation stage is attached to a digital readout accurate to 0.5 milliinch. The purpose of the TOM is to measure crack lengths during the test. Two linear voltage displacement transducers (LVDT) are attached to the panel so quantities in the specimen length direction, i.e. overall panel elongation, can be measured. The two LVDTs are necessary as the test is displacement controlled. The first LVDT connects to the displacement control system and provides the input for the load cell. As the LVDT controller is manipulated, the load cell responds until the programmed displacement is met. The load is then the resultant of the desired displacement necessary to avoid failing the panel due to load shedding under constant load. However, the data recording system is separate from the load control system, so the second LVDT connects to the data acquisition system and records the overall panel displacement during the testing.

A crack opening displacement gage (COD) was also utilized during the testing, attached with two knife edges glued to the panel directly above and below the lead crack on the centerline of the panel. The COD has a gage length of 0.5 inch, with a 0.25 inch maximum displacement measurement. The COD gage is used to measure the opening of the crack at the centerline. The resolution of the LVDT/COD system is ±0.01 milliinch. The data recording system can sample at 10 data points per second with all data being stored electronically. In the current configuration, all strain gage data was recorded, as well as load, LVDT, and COD data.

Additionally, the tests were recorded with two high-speed cameras, at a rate of 500 frames a second. This video provides a split picture of both ends of the lead crack to show the stable growth and linkup during testing. The video has an overlay of the load and LVDT readings to give a reference point for the image.

Crack measurement was accomplished using the TOM at each end of the lead crack, as well as the MSD sites, where applicable. An initial measurement was taken before each load was applied, referencing a marked zero point on the panel. At each load interval, both ends of the lead crack, as well as the MSD sites, where applicable, were visually inspected for crack extension.

3.1 Test Articles

The MSD specimen panels are based on fuselage splice joint designs that have been used in commercial aircraft for many years. Four types were chosen: two longitudinal lap-splice joints, one longitudinal butt-splice joint, and one circumferential butt-splice joint. Aluminum doublers were bonded with FM73® to the specimen ends to prevent failure in or near the grip area. This was accomplished in accordance with the MSD Study Test Plan.[19] The adhesive cures at 250 °F. The specimen is heated from room temperature to 250 °F in 1 hour, held for 1 hour at a pressure of 40±5 psi, and then cooled to room temperature. The overall specimen dimensions are 48 by 72 inches with 48 by 60 inches outside the grip area.

The type I longitudinal lap-splice joint skin is made of 0.063-inch-thick 2024-T3 aluminum clad sheet with a 7075-T6 aluminum doubler and longeron. Similarly, the type II longitudinal lap-splice joint skin is made of 0.063-inch-thick 2024-T3 aluminum clad sheet with a 7075-T6 longeron and no doubler. The type III longitudinal butt-splice joint skin, doubler, and splice plate is made of 0.09" thick 2024-T3 aluminum clad sheet with a 7150-T61511 longeron. The type IV circumferential butt-splice joint skin is made of 0.063-

4

inch-thick 2024-T3 aluminum clad sheet with 7075-T6 doubler and splice plate. For the longitudinal joints, the material orientation of the skin in relation to the applied load is the transverse-long (TL) direction, whereas for the circumferential joint, the material orientation is in the long-transverse (LT) direction. These four joint types are shown in Figures 2-5, depicting the layups of the joint structures, including skin and stiffeners, generated by a study of initial quality in lap-splice joints.[20] The figures also contain terminology used for the different parts of each panel that are explained here. The skin side of the panel is the side of the panel that would be the aircraft skin, given an actual aircraft structure. This side of the panel is also termed the near side, as all videotaping and crack length measurements were taken from this side, to best see the cracks. The opposite side of the panel contains the internal structure found in the splices typical of transport aircraft. This is termed the longeron side of the panel or the far side of the panel, in this test setup.

Each of the joint types has three different configurations, differentiated by the existence and size of MSD in the critical row, as seen in Table 1.

Table 1. Lead and MSD Crack Configurations

Joint Type	Panel ID	Splice Type	Lead Crack Length (in)	MSD Size (in)
Type I	-1-1	Longitudinal Lap	13.9	NONE
	-1-2	Longitudinal Lap	13.9	0.050"
	-1-3	Longitudinal Lap	13.9	0.100"
Type II	-501-1	Longitudinal Lap	12.82	NONE
	-501-2	Longitudinal Lap	12.82	0.050"
	-501-3	Longitudinal Lap	12.82	0.100"
Type III	-503-1	Longitudinal Butt	14.8	NONE
	-503-2	Longitudinal Butt	14.8	0.050"
	-503-3	Longitudinal Butt	14.8	0.100"
Type IV	-505-1	Circumferential Butt	13.9	NONE
	-505-2	Circumferential Butt	13.9	0.050"
	-505-3	Circumferential Butt	13.9	0.100"

Each of the four joint types was instrumented with strain gages (see Table 2) having a multi-axial grid with the loading axis parallel to the longitudinal axis of the strain gage grid.

Table 2. MicroMeasurements® Strain Gage Type

Type	Option	Lot Number	Resistance in Ohms at 24 °C	Gage Factor (24 °C)	Transverse Sensitivity (24 °C)	Code
EA-13-062AQ-350	W	R-A55BF00	350.0±0.3%	2.145±0.5%	0.7±0.2%	062116-956
EA-13-250BF-350	W	R-A59AF06	350.0±0.3%	2.105±0.5%	0.2±0.2%	082414-2463
WA-13-060WR-120	W	A55AF00	120.0±0.5%	2.16 Nom.	1.2±0.2%	072812-809
WK-13-060WR-350	N/A	D-K14FF25	350.0±0.4%	2.25 Nom.	-1.1 Nom.	911820

The smaller gages, EA-13-062AQ-350, were used at the anticipated location of maximum stress in the critical outer rivet row. The larger gages, EA-13-250AQ-350, were used to determine the global response of the panel. Finally, the rosettes, WA-13-060WR120 were used in locations to capture the out-of-plane deformation resulting from transverse displacements and the transverse, shear, and axial strains at those points. These strains are captured from the tensile and bending strains generated by the pairs of rosettes. The rosettes will also capture the strain from crack face buckling. The diagram of the strain gage placement for each joint type can be found in Figures 6 through 9. In all panels, strain gages 21 through 24 are rosettes and are not shown on the figures, to avoid muddling the figures. At all locations on the panels, the strain gages are mounted back-to-back, one gage on each side of the sheet, the mean strain between the

two gages is the tensile component and half the strain difference between front and back gages is the bending component, calculated using the following equations:

$$\varepsilon_{mean} = \varepsilon_t = \frac{\varepsilon_{front} + \varepsilon_{back}}{2} \qquad\qquad \varepsilon_b = \frac{\varepsilon_{front} - \varepsilon_{back}}{2} \tag{1}$$

where

    ε_t = normal strain due to tension

    ε_b = normal strain due to bending

    ε_{front}, ε_{back} = normal strain from gages that are back-to-back.

For each of the panels, the front side is considered the skin side, while the backside is considered the longeron side. Additionally, the rosettes record ε_{xx} and ε_{yy}, which can then be converted into the principal strains ε_1 and ε_2, useful in model validation.

3.2 Antibuckling Guides

The antibuckling guides were designed to prevent crack face buckling during the test, as well as provide resistance to secondary bending, ideally confining the crack extension to Mode I. Mode I failure is an in-plane tearing due only to remote tensile loading. Since the panels are of finite width and are not connected to frames, the Poisson contraction of the panel induces an out-of-plane displacement. As the current prediction models use a purely Mode I failure criterion, the tests use antibuckling guides to prevent the secondary bending and crack face buckling. The guides are comprised of half-inch-thick A36 steel plates, with horizontal I-beam stiffeners at the top and bottom of each plate. However, since the crack must be observed during the testing, there is by necessity a gap in the antibuckling guides. To provide the separation needed, the guides were divided into two separate halves. The top pair of guide plates was suspended from the top grip by steel links and the bottom pair was supported by steel links attached to the bottom grip. This was done to provide support for the antibuckling guides that would be separate from the panel itself. On the skin side of the panel, there was a 1-inch separation between the guides, with the separation on the longeron side dependent on the joint type. Figure 10 shows the antibuckling guides for all joint types. The five rectangles across the antibuckling guide are a visual depiction of the longeron side supports included in the assembly; the stiffeners on the longeron side of the panel were placed at two 10-inch intervals from either side of the centerline. The supports consist of ¾-inch bolts with plastic caps resting on 2- by 2-inch steel squares placed on the longeron for the lap-splices. For the butt-splice, the plastic caps were placed directly against the panel, in areas between rivets. To prevent pre-straining the panel, the bolts were tightened only enough to ensure that they remained in place. Figures 11 and 12 depict the supports used in each of the joint types.

Phenolic sheets were also part of the antibuckling guide assembly, attached to the guide plates with industrial adhesive. The phenolic sheets consist of laminated sheet; fine weave fiberglass, in accordance with material specification MIL-P-15035. The adhesive used was 3M Super77 Spray Adhesive. Before the installation of the guide plates onto each panel, the sheets were cleaned using acetone and a film of lubricant was applied to prevent friction from the guides affecting the loading of the panel. The lubricant used was LPS® Magnum Teflon® Lubrication. Reduction of friction is critical to the test accuracy, as friction between the antibuckling guides and the panel will result in a load transfer from the specimen to its support. This load transfer creates a situation in which results obtained are inaccurate, as the specimen will be experiencing less than the recorded load, leading to an overestimation of the panel's residual strength. Additionally, as shown in Figures 6 through 9, far-field strain gages are situated underneath the antibuckling guides to capture the secondary bending and global tensile response of the panel. To prevent the gages from being crushed under the phenolic plates, separate configurations for the phenolic blocks on the antibuckling guides and spaces between the phenolic plates to rout the strain gage wires were included in the antibuckling guide design.

3.3 Test Procedure

The test procedure is similar to ASTM E561: R-Curve Testing. In this reference, no specific design is put forth for the antibuckling guides. The only requirement is that "the plates shall be so designed to prevent sheet kinking about the crack plane and sheet wrinkling along the specimen width".[21] The antibuckling guide plates are assembled onto the test panel. The entire assembly is then placed in the load frame and the strain gages are connected to the data collection system. The LVDT and COD gages are both set up on the panel and connected to the data collection system. The video recording setup is then placed in front of the panel.

The initial loading is a strain survey. The max load for the survey is 15 kips, and is performed three times. During the survey, all of the data channels are printed and reviewed at load levels of 5, 10, and 15 kips. This strain survey verifies that the load is being applied symmetrically, as well as ensures that all strain gage data is linear and repeatable. While the strain data is initially highly nonlinear, this region is confined to less than 10 kips. This was the primary reason for the 15-kip load; it places the strain outside of the initial nonlinear deformation, but the stress induced would be low enough to make it extremely unlikely that crack extension or permanent crack opening would be created in the specimens.

A reference zero is set near the limit of travel of the TOM. This zero is then marked on the panel for future reference and from that zero point, an initial measurement is taken of the cracks. Once extension occurs, the lead crack lengths are measured at each subsequent load level and the adjacent rivet holes are visually inspected. Additionally, as each linkup occurs, the loading is stopped and the crack extension measured.

One concern during all of the residual strength testing was ensuring that the load was applied symmetrically. Even though the test frame was designed as a two-force member and should straighten itself out with the application of load, it has been determined that the friction in each clevis combined with the weight of the loading strut can actually skew the load to one side or another, unless the setup is manually aligned with each test. This was accomplished by leveling the top of the loading strut and ensuring that equal spacing is present on each side of the bottom grip.

This procedure is continued until final failure of the panel. After failure, the panel is removed from the frame and the antibuckling guides are removed from the assembly. The overall panel components and the fracture surfaces are photographed. These photos are included as Appendix B.

4. Results and Discussion

Twelve specimens were tested in our investigation of MSD effects on a residual strength; three of each joint type. The testing was successful in recording the required data described in the Introduction section of the report. The crack length, COD, and strain fields were acquired in the ways discussed above. By using the three configurations, the effect of MSD size on residual strength can be determined. The residual strength of the panel decreased with the presence of MSD in the rivets adjacent to the lead crack. A description of each specimen is recorded in Table 3. Also included in this table are the linkup loads and stresses that each of the panels experienced, as well as the peak loads and stresses. A linkup is defined as the instantaneous propagation of the crack into the next rivet hole. A summary of the events during each test is included as Appendix A. These residual strength reductions are also shown graphically in Figure 13.

Table 3. Table of Linkup and Peak Loads

Panel ID	First Linkup Load (kips)	First Linkup Stress (ksi)	Percent Reduction Due to MSD	Peak Load (kips)	Peak Stress (ksi)	Percent Reduction Due to MSD
-1-1	46.57	15.40	-	69.51	22.99	-
-1-2	45.05	14.90	3.2	52	17.20	25.2
-1-3	37.87	12.52	18.7	52.69	17.42	24.2
-501-1	46	15.21	-	62	20.50	-
-501-2	40	13.23	13.0	54.35	17.97	12.3
-501-3	34	11.24	26.1	45.07	14.90	27.3
-503-1	69.47	16.08	-	108.77	25.18	-
-503-2	61.74	14.29	11.1	79.11	18.31	27.3
-503-3	52.88	12.24	23.9	71.78	16.62	34.0
-505-1	58.04	19.19	-	75.32	24.91	-
-505-2	46.66	15.43	19.6	59.53	19.69	21.0
-505-3	41.42	13.70	28.6	55.77	18.44	26.0

For Table 3, the stress data was calculated using the following equation:

$$\sigma = \frac{P_{REMOTE}}{A_{REMOTE}},$$ (2)

where
   P_{REMOTE} = Remote tensile load (lb)
   A_{REMOTE} = Far-field cross-sectional area (sq. in.).

The primary purpose of the data in Table 3 is to verify the residual strength predictions that Boeing has generated. To that end, the peak load and stress are given and not the final failure load.

The strain data was used to examine the severity of secondary bending and crack face buckling in the joint during static loading. This data is used to ascertain the fidelity of the testing in trying to simulate a Mode I failure and show to what degree out-of-plane deformation affected the test data. This is discussed in subsequent sections.

4.1 Crack Extension

The existence and size of MSD in a built-up structure will affect the overall stiffness and residual strength of the joint. However, the damage tolerance characteristics of the wide panel specimens remain difficult to quantify. The ability to predict the residual strength of the remaining structure and determine the level of repair is critical to ensure safety. As shown in Figures 14 through 17, the total lead crack length is plotted against the load, for each of the joint types, as well as the comparison of the three configurations of MSD size. In each case, the introduction of MSD decreased the residual strength of the panel. The results are presented here according to joint type.

4.1.1 Joint Type I

This is a production representative version of a longitudinal lap-splice on a narrow body transport aircraft. Figure 14 shows the recorded crack extension for each of the MSD configurations tested. The initial concern is that the crack has progressed symmetrically. As shown in Figure 18, this shows the half crack extension for each of the panels in the series.

The first panel in the series is MSD 1-1 and displays symmetric crack growth through the first linkup. At the second linkup, it appeared that either side could progress, but only the right side did and the load was then shed, preventing the left side from progressing. The loading was restarted after measurement and the left side linked-up at a slightly lower load than previously caused the right side linkup. The most reasonable explanation is that manufacturing and material variability will cause each panel to favor one side or the other at peak load. While the difference between the linkup loads for each side of the panel might be very similar, as the load increases, it will hit the stress necessary to linkup one side first and then will shed before the other side can compensate.

Panel 1-2 saw similar phenomena; the first linkup was simultaneous, but the remaining linkups all occurred between loads of 51 and 52 kips. There was a slightly higher force necessary to cause linkups on the right side of the panel and that load was not attained until the left side had linked up several times. However, the panel could have completely failed, but for the hole without MSD on the left side of the panel, which stopped the crack. There was a near simultaneous linkup of three rivets on the left side of the panel, together with a corresponding shedding of load. At this point, the crack had progressed beyond the rivets with MSD and the crack stopped at a hole without MSD. The panel also experienced one linkup on the right side of the panel, but the crack progression stopped there. The most probable explanation for this phenomenon is related to testing displacement control. As the lead crack progresses through the panel, the LVDT reads the overall deformation of the panel and adjusts the load to achieve the desired length. When the panel fails, it is due to the fast fracture in which the panel is yielding much faster than the system can shed the load. Once the crack entered that hole, the crack tip was now the blunt notch of the rivet hole, which slowed the crack down and enabled the system to shed enough load such that the overall length of the panel had stabilized. Loading then resumed and final failure occurred without further linkups.

Panel 1-3 also displays symmetric crack growth and experienced simultaneous initial linkup. The linkups after that were also at very close loads, with a tendency more to the left side of the panel. In this panel, both sides extended through several holes with MSD to the first hole without MSD and then stopped, with a large shedding of load, seemingly for the same reason as panel 1-2.

4.1.2 Joint Type II

This is a production representative version of a longitudinal lap-splice on a narrow body transport aircraft. Figure 15 shows the recorded crack extension for each of the MSD configurations tested. The first phenomenon noted is that the residual strength of the panels in this series seemed to be affected much less by the introduction of MSD into the panel than the other joint types. In the other joint types, doublers are present in the design and the critical row is a row connecting a doubler to one of the skins in the joint

9

(Figures 2, 4 and 5). However, for joint type II, there is no doubler, and the critical row is a direct connection between both of the skins and a lower cross-sectional area through the joint.

Again, the half-crack extension versus load information was used to determine if the crack maintained symmetry (Figure 19). For panel 501-1, the panel maintained symmetric extension throughout most of the testing. While the cracks favored one side or another during the stable growth between the holes, the linkups all occurred simultaneously. The sole exception to this was the third linkup, which occurred only on the left side.

Panel 501-2 was very similar to panel 501-1 except for the fact the first linkup was experienced only by the left side of the lead crack, and after bringing the load back to slightly above the peak, the right side linked. The panel maintained that process until final failure was reached, where the final linkup before failure occurred only on the left side.

Finally, panel 501-3 displayed the behavior typically associated with the extensive MSD introduced into the fastener holes in the row of the lead crack. There was significant crack extension, but at a much lower load; also, the crack showed some signs of asymmetric behavior, but the cracks had extended to nearly identical lengths at the time of final fracture. After every linkup, there was a slight amount of load shedding, depending on how many linkups occurred. If only one hole linked, as in the first two events, the load shed on the order of 4 to 5 kips. However, when the crack linked near the end of the panel's life, there was an approximately 10-kip loss of load. It was at this time the that cracks extended to the same hole: the last hole with MSD. The loading continued at that point until fast fracture occurred.

4.1.3 Joint Type III

This is a production representative version of a longitudinal butt-splice on a wide-body transport aircraft. Figure 16 shows the recorded crack extension for each of the MSD configurations tested. The half-crack extension for all of the specimens is graphically shown in Figure 20.

For panels 503-1 and 503-3, the crack extension was limited and symmetric. The linkups occurred simultaneously, in terms of load applied, and there was no final extension before failure. In other words, after the load shed with the second linkup, there was no more extension of the MSD cracks or the lead crack from the MSD notch before final fracture occurred.

In panel 503-2, there was a slight difference. The panel experienced a linkup in which the left side linked initially and the load was not noticeably shed. The initial linkup load was only very slightly exceeded when the right side linked. This is assumed to be almost a simultaneous link. However, once loading was resumed, the left side crack progressed slightly ahead of the right side crack and finally linked with the adjacent hole. The right side, however, did not linkup, but as loading resumed, panel failure occurred before the right side could link past the first adjacent rivet.

4.1.4 Joint Type IV

This is a production representative version of a circumferential butt-splice on a wide-body transport aircraft. Figure 17 shows the recorded crack extension for each of the MSD configurations tested. The half-crack extension is shown in Figure 21. All panels tested showed large out-of-plane deformation (approximately 0.5 inch).

The first panel (505-1) testing progressed unexceptionally through the first linkup, but as shown in Figure 17, the knife edge holding the COD gage disbonded from the panel. This occurred at approximately 75 kips. The panel was brought down to 1 kip and the knife edge was reattached. The clip gage was then reinstalled and the loading resumed. The loading progressed to 70 kips when crack extension was seen.

This was recorded and the test continued. At a slightly higher load than the panel experienced when the knife edge disbonded, the left side of the lead crack linked to the adjacent rivet. The load shed approximately 5 kips, and then testing resumed. The right side then linked before the peak load could be reached again, and load was shed again. Final fracture occurred before the peak load could be reachieved.

Panel 505-2 progressed more in accordance with the established testing. The linkups were simultaneous and the load dropped to approximately 6 kips, then as the loading resumed, failure occurred before the peak was reached. However, the clip gage disbonded again, this time at approximately 55 kips. The gage was reattached and the testing continued without incidence until the final fracture. The second and last linkup occurred simultaneously and the load was shed approximately 6 kips. The final fracture occurred before further events took place. After conferring with the technicians, it was determined that the adhesive in use was beyond its recommended shelf life and replacement adhesive was acquired. This was assumed to be the cause of the disbond.

That was not the case, however, as the clip gage disbonded a final time during the testing of 505-3. During this test, the right side linked first, with an approximately 2 kip load shed. The initial linkup load was surpassed when the left side linked up. At that point the disbond occurred. The remainder of the test was similar to the testing of panel 503-2, in which one side linked and before the other side could link and equal out the net section of the panel, final fracture occurred. Additionally, as the disbonds were repeatable, it is assumed that the high deformation of the panel at the crack, a result of crack face buckling, was the cause. As the bottom of the panel deformed, the clip gage would rotate; this caused the adhesive to experience a pullup load instead of a shear load.

4.2 Secondary Bending

All splice types are symmetrical joints and, as such, generate secondary bending due to the eccentricity of the load path through the joint. One consideration for this testing is that the antibuckling guides were designed to prevent both crack face buckling and secondary bending by constraining all types of out-of-plane deformation. However, out-of-plane deformations do occur, given the large area that cannot be adequately constrained when dealing with built-up structure (i.e., longerons or large numbers of blind fasteners on the longeron side of the panels). This bending generates higher than normal stresses at the outer rows of the joint, making the outer row critical. The outer row is considered to be the farthest row of rivets from the center of the joint. In a joint where one of the sheets is countersunk, the area transferring the load will be less; therefore, that point will usually become the critical area.

Examining the strain gages parallel to the loading axis can capture this secondary bending. For the joint types I, III, and IV, the gages are numbered 1 through 4 for the top half of the joint and 13/14 through 19/20 for the bottom half. For joint type II, the gages are numbered 1/2, 7/8 and 17 through 20. Utilizing this data, the secondary bending is examined with respect to MSD in each of the different joint types, as well as both far-field strain and strain along the critical crack row. These results can then be compared to the tensile strain in those areas to determine the ratio of load that is directed into the secondary bending. The degree of secondary bending is typically given by the bending factor, k.

$$k = \frac{\sigma_{bending}}{\sigma_{tension}} ,$$

(3)

4.2.1 Joint Type I

The first set of data is the secondary bending in each of the three MSD configurations from the joint type I series, comparing strain both above and below the crack (Figure 22). The bending strains at peak load can be compared with the tensile strains and the results are shown in Table 4. The results show that the bending strain seems to increase with the introduction of MSD, especially the 0.100-inch size MSD. However, this effect seemed to be seen only on the lower or bottom half of the panel. Since the strain

11

recording is accurate to only +/-50 με, it is difficult to give significance to the bending factor in the upper half or top of the joint.

Table 4. Comparison of Bending and Tensile Strains Above and Below Joint Type I

Panel ID	Top Tension Strain	Top Bending Strain	Bending Factor, k	Bottom Tension Strain	Bottom Bending Strain	Bending Factor, k
MSD 1-1	3139.48	165.6	0.05	3003.77	19.44	0.006
MSD 1-2	2283.99	68.23	0.03	2235.06	223.29	0.10
MSD 1-3	2114.00	185.16	0.09	1880.67	677.18	0.36

The only area that exhibits a significant bending factor is the panel with the largest MSD, but it does appear that the effect increases with the increased size of MSD.

4.2.2 Joint Type II

Using the bending factor (k), the ratio of bending tensile strain can be determined for the 501 series of panels. This is shown in Table 5. However, the top far-field tension strain cannot be determined for panel 501-2. During either the assembly of the antibuckling guides or the installation of the panel into the frame, strain gages 2 and 8 were damaged. These were the far-field strain gages above the joint line of the panel (see Figure 9). From the data that is presented, however, the bending factor significance is extremely low, essentially zero, and shows the effectiveness of the antibuckling guides in preventing secondary bending in the panels of this series. The strains are shown graphically in Figure 23.

Table 5. Comparison of Bending and Tensile Strains Above and Below Joint Type II

Panel ID	Top Tension Strain	Top Bending Strain	Bending Factor, k	Bottom Tension Strain	Bottom Bending Strain	Bending Factor, k
MSD 501-1	2861.47	7.37	0.003	2859.99	-127.94	-0.04
MSD 501-2	N/A	N/A	N/A	2102.545	-58.805	-0.03
MSD 501-3	1970.96	131.59	0.07	2032.48	71.38	0.04

4.2.3 Joint Type III

Using the bending factor (k), the ratio of bending tensile strain can be determined for the 503 series of panels. This is shown in Table 6. The strains are shown graphically in Figure 24. The bending factor of the panels in this series has a maximum of 10 percent of the tensile strain and shows the effectiveness of the antibuckling guides during the testing. Additionally, the bending factor does not clearly relate to the size of the MSD, but does appear to be greater for the bottom half of the panel than for the top half of the panel.

Table 6. Comparison of Bending and Tensile Strains Above and Below Joint Type III

Panel ID	Top Tension Strain	Top Bending Strain	Bending Factor, k	Bottom Tension Strain	Bottom Bending Strain	Bending Factor, k
MSD 503-1	3662.29	87.75	0.02	3325.32	280.95	0.08
MSD 503-2	2560.92	28.71	0.01	2343.48	238.97	0.10
MSD 503-3	2202.36	43.79	0.02	2051.20	26.94	0.01

4.2.4 Joint Type IV

For the last series, the bending factor is determined from the strain recorded at the peak load during the testing, as was done for the other joint types. The data is shown in Table 7, and the entire load versus strain curves are shown in Figure 25. Again, the designs of the antibuckling guides are apparently effective in the prevention of secondary bending.

Table 7. Comparison of Bending and Tensile Strains Above and Below Joint Type IV

Panel ID	Top Tension Strain	Top Bending Strain	Bending Factor, k	Bottom Tension Strain	Bottom Bending Strain	Bending Factor, k
MSD 505-1	3427.47	2.89	0.00	3108.91	214.62	0.07
MSD 505-2	2642.32	255.59	0.10	2256.51	192.42	0.09
MSD 505-3	2373.83	168.58	0.07	2289.49	253.47	0.11

There were also strain gages placed along the critical crack row in the panels without the presence of MSD. Figure 26 shows the critical row secondary bending for each of the joint types on the left side of the crack. This figure shows only the strain up to the first linkup, to isolate the global response of the panel during the initial loading. This shows the effectiveness of the antibuckling guides. The strain gage data exhibited in this figure include the gages on the left side of the crack, both the outer and inner. The bending strain to tensile strain ratio at the peak load from the figure is denoted in Table 8.

Table 8 – Comparison of Bending and Tensile Strains Along Critical Crack Row

Panel ID	Strain Gages	Peak Tensile Strain	Peak Bending Strain	Bending Factor – k
MSD 1-1	5/6	1553.92	759.59	0.489
	7/8	1581.24	640.84	0.405
MSD 501-1	13/14	2788.065	1166.445	0.418
	15/16	2979.735	852.405	0.286
MSD 503-1	5/6	2009.045	117.115	0.058
	7/8	1819.325	601.135	0.330
MSD 505-1	5/6	1766.740	743.030	0.421
	7/8	2141.270	726.220	0.339

4.3 Crack Face Buckling

Crack face buckling is caused by the Poisson contraction of the panel during tensile loading. The contraction of the thin sheet laterally will tend to bow the sheet out-of-plane. The critical aspect of crack face buckling is its affect on crack extension. The out-of-plane deformation adds to both the complexity of the analysis and prediction of residual strength. This added complexity comes from the incorporation of a failure criterion verified in predicting crack resistance with several modes of crack extension. In the past, the modeling of crack progression and crack opening has been restricted to Mode I problems. However, the out-of-plane displacement above and below the crack on all panels and all configurations shows how the other tearing modes also affect the crack progression. To quantify the state of strain in the center of the panel, the panels were each fitted with rosettes along the centerline of the panel, where possible, directly above and below the center of the lead crack. In one instance, the gages were slightly off center to accommodate a rivet head on the centerline of the crack. The strains generated from these gages show that as the crack progresses, the primary strain seen by the panel in this area is a transverse compression, as well

as a transverse bending. Both of these strains are generated by the same phenomenon. As the panel is loaded, the Poisson contraction will create compression loading perpendicular to the loading direction. To alleviate this strain, there is an out-of-plane deformation, and a bending about the centerline of the panel occurs. This bending is termed crack face buckling and has a significant impact on the progression of the lead crack and the residual strength of the panel. This effect is somewhat dampened by the addition of the antibuckling guides, but was not relieved completely.

Also resisting the out-of-plane deformation is the longeron installed in the splice structure. This resistance is demonstrated by comparing the crack face buckling present in joint type IV with other joints containing a longeron (Figure 27). Figure 27 shows the strain data from the transverse leg of the rosette on the side of the crack with a longeron and in the case of joint type IV, the side of the crack with the doublers. Additionally, to isolate the effect of the longeron on the crack face buckling, all of the joint types for Figure 27 are without MSD. Figure 27 shows that while the bending of the panels is similar initially, the panel without a longeron changes drastically as the crack progresses. This could be seen during the test, as all of the panels with a longeron were deforming outward or away from the joint, while the joint type IV panels were deforming inward. If the panel was on an aircraft, this would be analogous to either a bulging in the skin for the lap-splices and a dimpling of the skin at the circumferential splice. Furthermore, the constraints placed against the longeron side of all of the joints served only to limit the deformation in a small area, while the rest of the lead crack deformed in between the supports (shown in Figures 11 and 12) to approximately 0.75 inch. This is an approximate measurement taken from the difference above and below the crack face.

Another way to capture the effect of the longeron is to compare the transverse bending strain on either side of the lead crack (Figure 28). In the first figure, the transverse bending strain is compared between the different joint types using the strain gage on the half of the panel with the longeron. In Figure 28, joint types I, II, and III are compared using the strain gages on the top and bottom of the crack to show the difference in crack face buckling depending on the side with the longeron. Again, the data was used from the panels without MSD. The data show how joint types III and I separate during the testing, with the top skin bending inward as the bottom skin bends outward. This was apparent during the testing, in which deformations out-of-plane were easily visible, upward of approximately 0.5 inch.

To measure the crack face buckling outside of the influence of the crack and the joint, rosettes were used to capture the far-field strain gages on the right side of the panel and determine if the presence of MSD would have some effect. This is shown in Figures 29 and 30, containing the transverse bending and tensile strain data for each of the configurations of the joint type I series. The trends are similar between the tensile and bending gages, an area in which the amount of strain increases with the presence of MSD at a given load. The transverse tensile strain shows that the panel is indeed under transverse compression, as would be assumed to be the case due to Poisson contraction. Again, the antibuckling guides were used to prevent the out-of-plane displacement, and the guides for this configuration actually extended over the gages, with channels cut out of the phenolic blocks to leave space for the gages and wires. However, the critical aspect of Figure 30 is that the presence of the MSD appears to have a much greater affect on the load versus strain curve than that of the size of the MSD, similar to the effect of MSD on crack extension.

5. Conclusions

From this testing, several conclusions can be drawn. These relate to both the effects of MSD size in comparison between panels of a particular joint type, as well as comparisons between the joint types.

1. Damage tolerance of the joints. The ability of the joints in the wide-body aircraft to withstand damage is severely affected by the presence of MSD in the joint (joint types III and IV). Joint types I and II showed the ability to withstand much longer lead cracks and could hold a reduced load at those points.
2. Except for the 501 series, the existence of MSD has a larger effect on the reduction in residual strength than the length of MSD. For the 501 series, while the reduction in residual strength appears to correspond in a linear fashion with the MSD size, it is dangerous to interpolate between the points and assume a linear relationship without further testing.
3. Load required for initial extension is affected similarly by the introduction of MSD as that of the residual strength. There were exceptions to this, but by and large, the percentage reduction of the residual strength with MSD was similar to the reduction in load necessary to facilitate detectable cracking.
4. For all specimens some crack face buckling was present in the form of visible out-of-plane deformation. Also, the calculated bending factors for the transverse strain gages directly above and below the crack demonstrate bending of up to 45 percent of the tensile strain. Therefore, while the antibuckling guides are effective at preventing the secondary bending about the splice line, they do not appear to be effective at containing the crack face buckling.

6. Recommendations

     While this testing is useful for the prediction of residual strength with lap-splice joints with known MSD states, more tests are required to adequately capture the MSD phenomenon. Additional testing of panels with lap-splice joints should include an improved design of antibuckling guides to prevent the crack face buckling and provide more support to the joint from the longeron side of the panel. This is difficult to design, given that the longeron side of a riveted lap joint will have an uneven surface. Unfortunately, this is critical to the data accuracy if the analysis is to be constrained to two dimensions.

     Another option is to prepare riveted lap joint specimens representative of aircraft structure and perform residual strength tests without the antibuckling guides. The strains measured on the panels could be correlated to FEA, as well as compared to previous testing, to determine the effect of the out-of-plane deformation on the residual strength. This is currently planned as a supplemental test program. This program will test the panels without buckling guides and the strain data will be recorded using VIC 3-D. This system captures the full field displacements at each load step and those displacement fields can be converted to strains. The results of the supplemental tests will be presented as an addendum to this report.

7. References

[1] Aircraft Accident Report: Aloha Airlines, Flight 243, Boeing 737-200, N73711, near Maui, Hawaii, April 28, 1988, NTSB/AAR-89/03. Washington DC: U.S. National Transportation Safety Board, 1989.

[2] D. Broek, David Y. Jeong, and David Thomson. "Testing of Flat and Curved Panels with Multiple Cracks." Proceedings of the 17th Symposium of the International Committee on Aeronautical Fatigue, 9-11 June 1993, Stockholm, Sweden.

[3] D. S. Dawicke, J. C. Newman, Jr., M. A. Sutton, and B. E. Amstutz. "Stable Tearing Behavior of a Thin-Sheet Material with Multiple Cracks." NASA Technical Memorandum 109131, July 1994.

[4] B.E. Amstutz, M. A. Sutton, D.S. Dawicke, and J. C. Newman. "An Experimental Study of CTOD for Mode I/Mode II Stable Crack Growth in Thin 2024-T3 Aluminum Specimens." Fracture Mechanics: Volume 26, ASTM STP1256, Walter G. Reuter, John H. Underwood and James C. Newman, Jr., Eds. American Society for Testing and Materials, Philadelphia, 1995.

[5] M. Kosai, A. Shimamoto, C. -T. Yu, S. I. Walker, A. S. Kobayashi, and P. Tan. "Axial Crack Propagation and Arrest in Pressurized Fuselage." Presented at the FAA/NASA International Symposium, Advanced Structural Integrity Methods for Airframe Durability and Damage Tolerance, May 4-6, 1994, Hampton, Virginia.

[6] M. Miller, M. L. Gruber, K. E. Wilkins, and R. E. Worden. "Full Scale testing and Analysis of Fuselage Structure." Proceedings of FAA/NASA International Symposium on Advanced Structural Integrity Methods for Airframe Durability and Damage Tolerance, 4-6 May 1994, Hampton, VA, NASA-CP-3274.

[7] Roland De Wit, R. J. Fields, L. Mordfin, S. R. Low III, and D. Harne. "Fracture Behavior or Large-Scale Thin-Sheet Aluminum Alloy." Proceedings of FAA/NASA International Symposium on Advanced Structural Integrity Methods for Airframe Durability and Damage Tolerance, 4-6 May 1994, Hampton, VA, NASA-CP-3274.

[8] Roland De Wit, R. J. Fields, S. R. Low III, D. E. Harne, and T. Foeke. "Fracture Testing of Large-Scale Thin-Sheet Aluminum Alloy." DOT/FAA/AR-95/11, 1996.

[9] M. Heinimann and A. Grandt Jr. "Analysis of Stiffened Panels with Multiple Site Damage." Proceedings of the 1996 USAF Aircraft Structural Integrity Program Conference, 3-5 Dec 1996, San Antonio, TX, WL-TR-97-4055.

[10] Jeffrey D. Helm, M. A. Sutton, and M. L. Boone. "CTOD Measurements in 2024-T3 for Residual Strength Modeling." Proceedings of the First Joint DoD/FAA/NASA Conference on Aging Aircraft, 8-10 July 1997, Ogden, UT.

[11] Richard D. Young, M. Rouse, D. R. Ambur, and J. H. Starnes, Jr. "Residual Strength Pressure Tests and Nonlinear Analysis of Stringer- and Frame-Stiffened Aluminum Fuselage Panels with Longitudinal Cracks." Proceedings of the Second Joint NASA/FAA/DoD Conference on Aging Aircraft, 31 Aug – 3 Sep 1998, Williamsburg, VA. NASA-CP-1999-208982.

[12] David Y. Jeong, J. G. Bakuckas, and G. Samavedam. "Analytical and Test Evaluations on the Linkup of Multiple Cracking in Stiffened Fuselage Panels." Proceedings of the Second Joint NASA/FAA/DoD Conference on Aging Aircraft, 31 Aug – 3 Sep 1998, Williamsburg, VA. NASA-CP-1999-208982.

[13] David Y. Jeong, S. J. Kokkins, S. B. MacPherson, T. H. Flournoy, J .V. Canha, G. W. Neat, and D. E. Nieser. "Full-Scale Testing of Fuselage Panels Obtained from Retired Aircraft. " Proceedings of USAF Aircraft Structural Integrity Program Conference, 01 Dec – 03 1998, San Antonio, TX.

[14] Gary H. Bray, R. J. Bucci, C. J. Warren, A. F. Grandt, Jr., P. J. Golden, and D. G. Sexton. "Benefits of Improved Fuselage Skin Sheet Alloy 2524-T3 in Multi-Site Damage Scenarios." Proceedings of the Second Joint NASA/FAA/DoD Conference on Aging Aircraft, 31 Aug – 3 Sep 1998, Williamsburg, VA. NASA-CP-1999-208982.

[15] Bert Smith, A. Mouak, P. Saville, R. Myose, and W. Horn. "Improved Engineering Methods for Determining the Critical Strengths of Aluminum Panels with Multiple Site Damage in Aging Aircraft." Proceedings of the Second Joint NASA/FAA/DoD Conference on Aging Aircraft, 31 Aug – 3 Sep 1998, Williamsburg, VA. NASA-CP-1999-208982.

[16] Bert Smith, A. L. Hijazi, A. K. M. Haque, and R. Y. Myose. "Modified Linkup Models for Determining the Strength of Stiffened Panels with Multiple Site Damage." Proceedings of the Third Joint DoD/NASA/FAA Conference on Aging Aircraft, 20-23 September, 1999, Albuquerque, NM.

[17] David S. Dawicke, A. S. Gullerud, R. H. Dodds, and R. W. Hampton. "Residual Strength Predictions with Crack Buckling." Proceedings of the Second Joint NASA/FAA/DoD Conference on Aging Aircraft, 31 Aug – 3 Sep 1998, Williamsburg, VA. NASA-CP-1999-208982.

[18] Lucas M Silva, J. P. Concalves, F. M. F. Oliviera, and P. M. S. T. de Castro. "Multiple Site Damage in Riveted Lap Joint Specimens." Proceedings of the Third Joint DoD/NASA/FAA Conference on Aging Aircraft, 20-23 September, 1999, Albuquerque, NM.

[19] James Lo. Multiple Site Damage (MSD) Study Test Procedure, The Boeing Company, 1998.

[20] J. Hsu and J. Yu. "Initial Quality of Typical Aircraft Fuselage Splice Joints Investigated in WFD Program." Proceedings of ICES, Atlanta, GA, 1998.

[21] Standard Practice for R-Curve Determination. ASTM Standards. Vol. 03.01, Metals Test Methods and Analytical Procedures, E561, pp. 509-521, 1999

LIST OF ACRONYMS

ACRONYM	DESCRIPTION
AFRL/VASM	Air Force Research Laboratory/Analytical Structural Mechanics Branch
ASTM	American Society for Testing and Materials
COD	Crack Opening Displacement
CT	Compact Tension
CTOA	Crack Tip Opening Angle
CTOD	Crack Tip Opening Displacement
DOT	Department of Transportation
EIFS	Equivalent Initial Flaw Size
FEA	Finite Element Analysis
LT	Longitudinal Transverse
LVDT	Linear Voltage Displacement Transducer
MSD	Multiple Site Damage
MT	Middle Tension
TL	Transverse Long
TOM	Traveling Optical Microscope
VIC 3-D	Three Dimensional Visual Image Correlation
WFD	Widespread Fatigue Damage

Figures
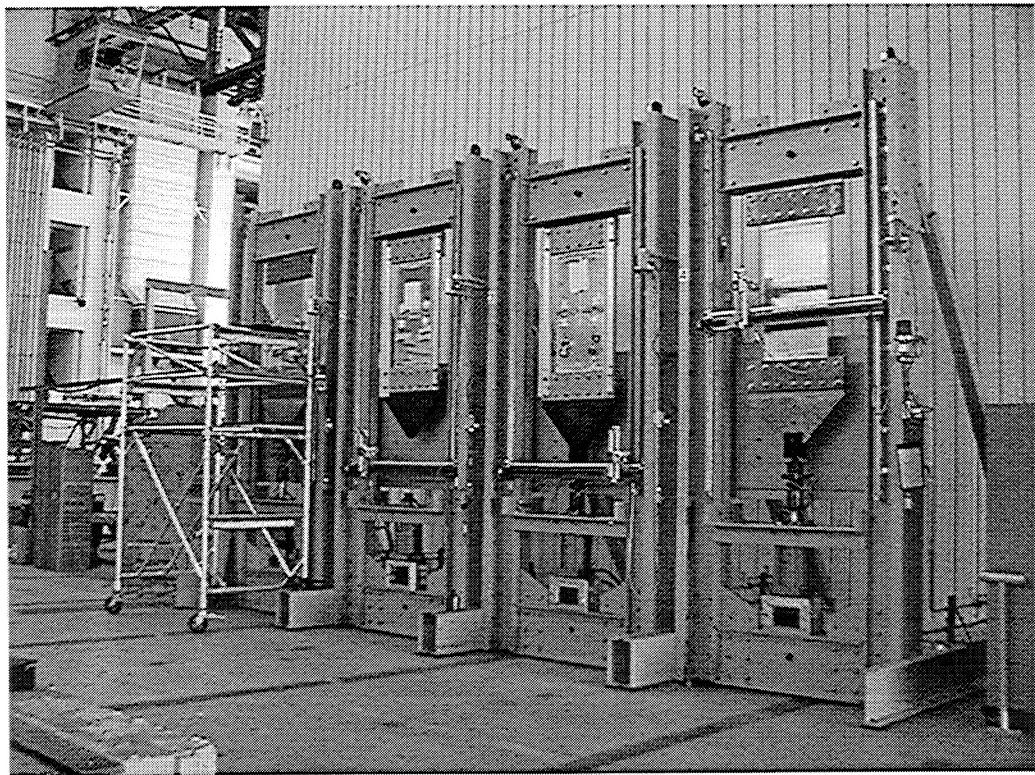
Figure 1. Wide Panel Test Facility
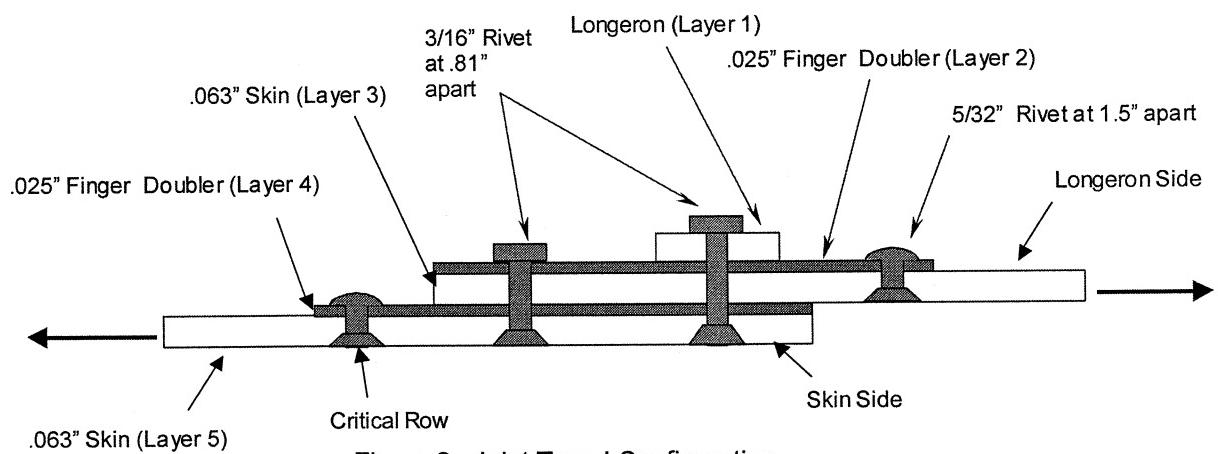
Figure 2. Joint Type I Configuration
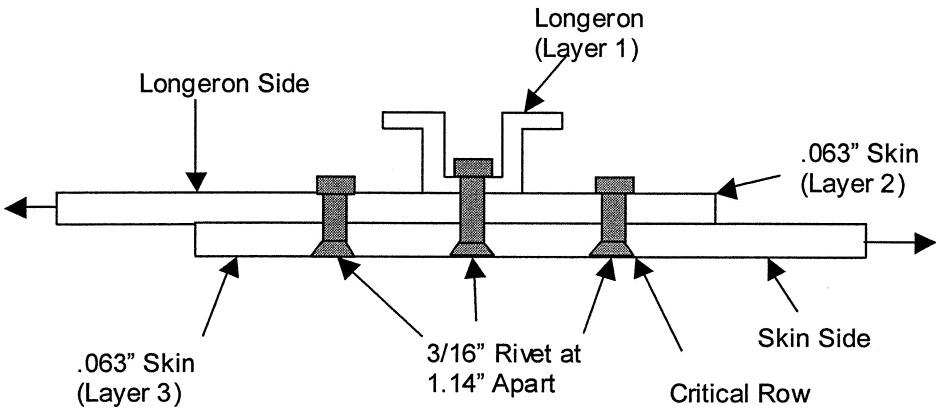
Figure 3. Joint Type II Configuration
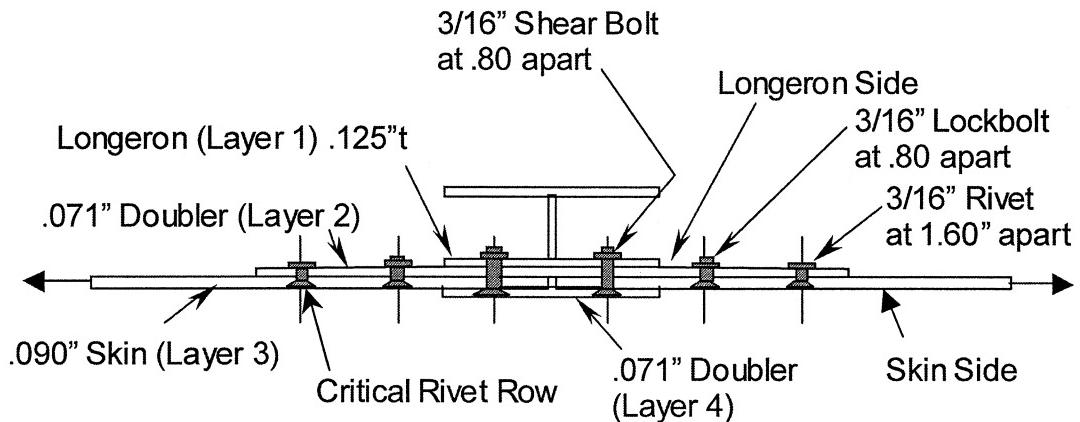
Figure 4. Joint Type III Configuration
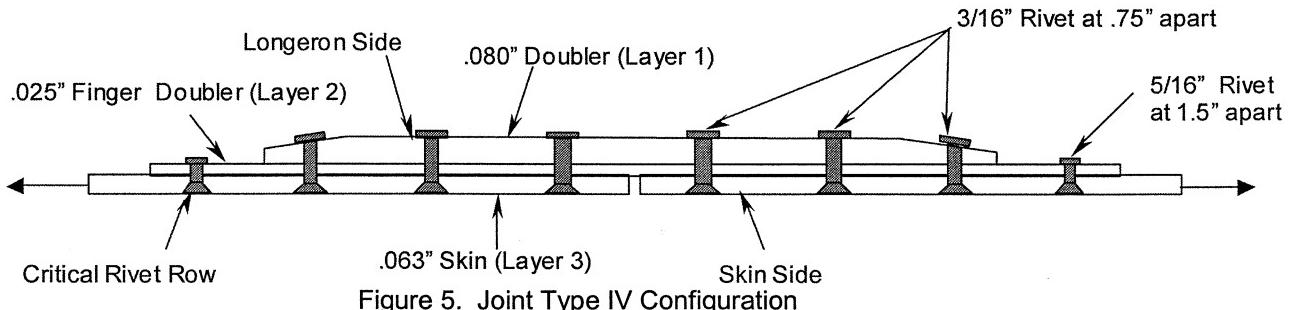
Figure 5. Joint Type IV Configuration

21

SKIN SIDE

48.00 (REF.)

EA-13-120WR-350 ROSETTE
STRAIN GAGE (BACK-TO-BACK
ON PANEL NO. -1-1 ONLY)

Strain Gages 1, 2
Strain Gages 21, 22
Strain Gages 9, 10
Strain Gages 3, 4
Strain Gages 11, 12
Strain Gages 7, 8
17.25

Strain Gages 5, 6
Strain Gages 13, 14
Strain Gages 15, 16
Strain Gages 23, 24
11.25
Strain Gages 17, 18
Strain Gages 19, 20

T
N

CRITICAL FASTENER ROW

℄ SYM.
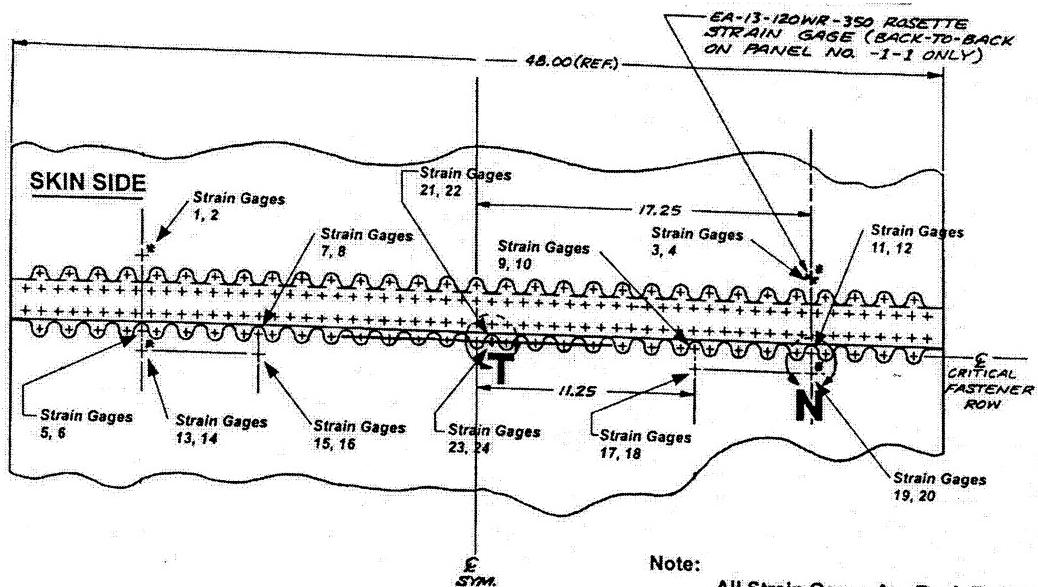
Note:
All Strain Gages Are Back-To-Back
* Indicates Install on -1-2 and -1-3
Odd No's on Near Side
Even No's on Far Side

SPLICE TYPE 1

-1-1, -1-2, -1-3

Figure 6. Gage Placement of Joint Type 1

SKIN SIDE

48.00 (REF.)

Strain Gages 21, 22
Strain Gages 5, 6
Strain Gages 1, 2
Strain Gages 3, 4
11.97 (REF.)
Strain Gages 7, 8

U
S

Strain Gages 9, 10
Strain Gages 11, 12
Strain Gages 13, 14
Strain Gages 15, 16
Strain Gages 17, 18
Strain Gages 23, 24
16.53 (REF.)
Strain Gages 19, 20

CRITICAL FASTENER ROW

℄ SYM

EA-13-120WR-350 ROSETTE
STRAIN GAGE (BACK-TO-BACK
ON PANEL NO -501-1 ONLY)
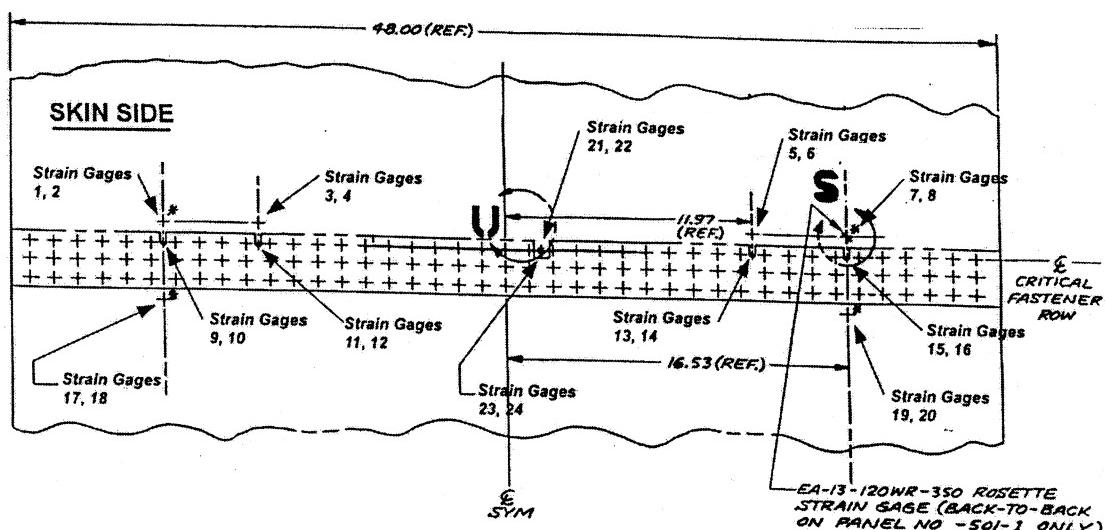
SPLICE TYPE 2

-501-1, -501-2, -501-3

Notes:
All Strain Gages Are Back-To-Back
* Indicates Install on -501-2 and -501-3
Odd No's on Near Side
Even No's on Far Side

Figure 7. Gage Placement of Joint Type II

22
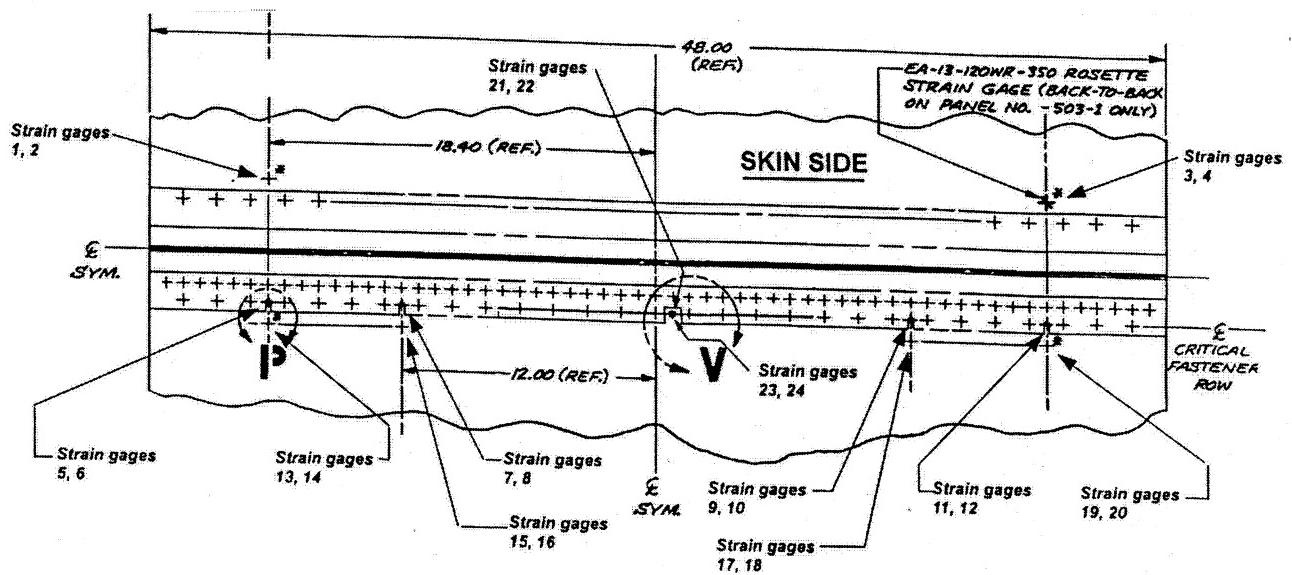
SPLICE TYPE 3

-503-1, -503-2, -503-3

Notes:

All Strain Gages Are Back-To-Back
* Indicates Install on -503-2 and -503-3
Odd No's on Near Side
Even No's on Far Side

Figure 8. Gage Placement of Joint Type III
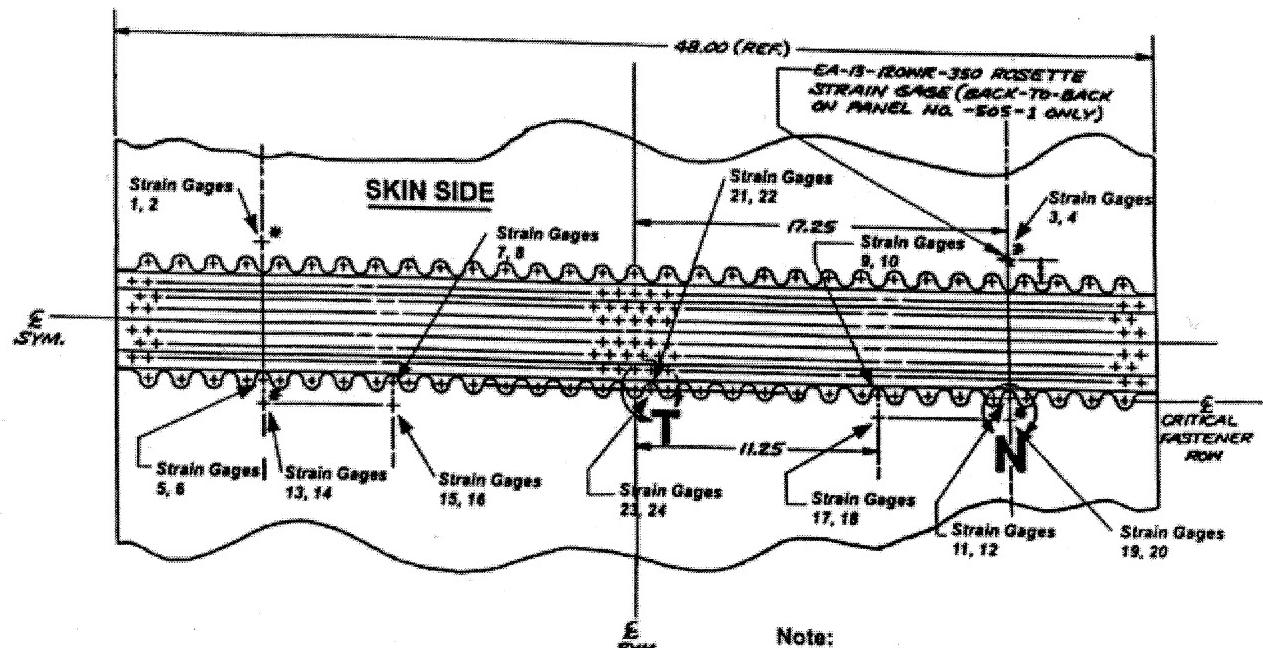
SPLICE TYPE 4

-505-1, -505-2, -505-3

Note:

All Strain Gages Are Back-To-Back
* Indicates Install on -505-2 and -505-3
Odd No's on Near Side
Even No's on Far Side

Figure 9.   Gage placement of Joint Type IV

23
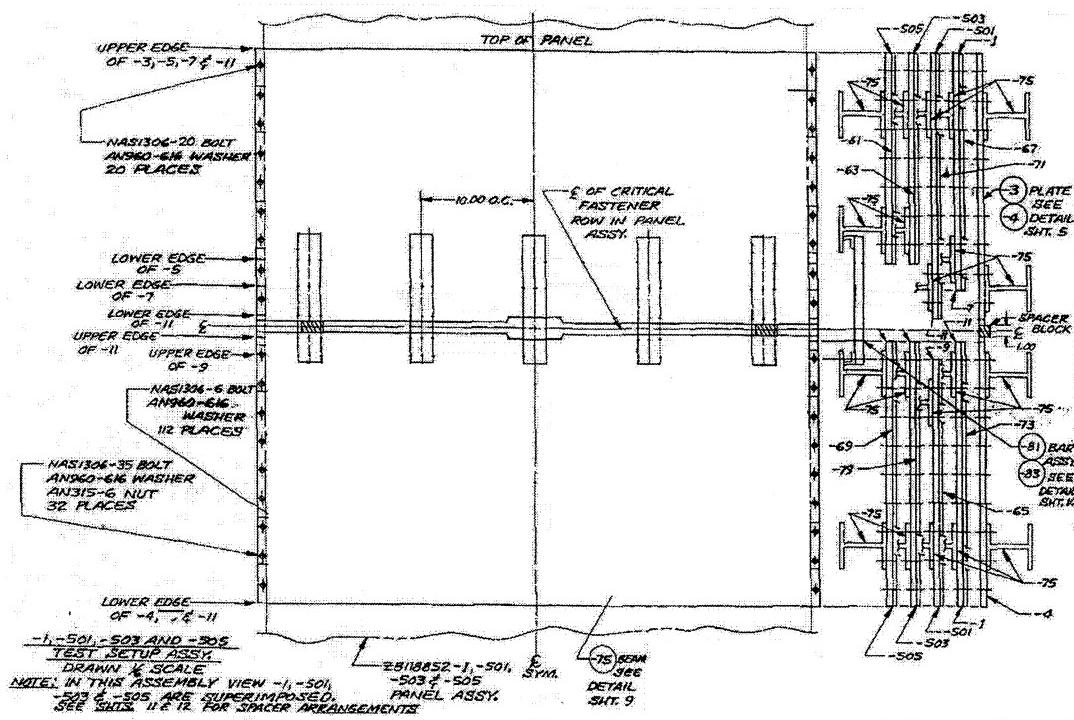
Figure 10.   Anti-bucking Guide Diagram for All Joint Types
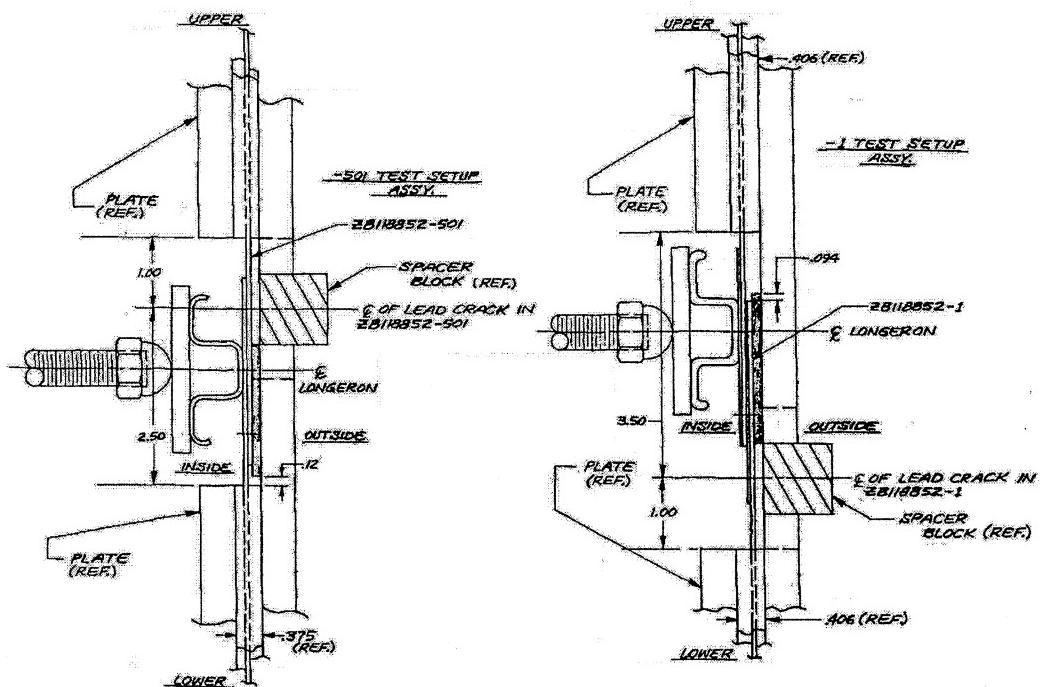
Figure 11. Anti-buckling supports for Joint Types I and II

24
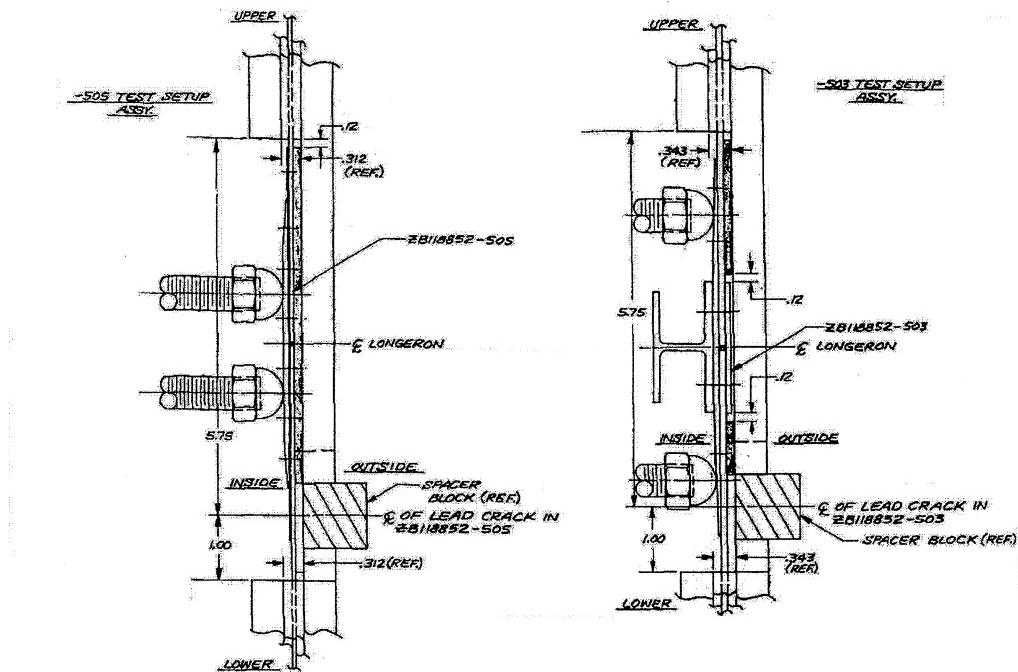
Figure 12.   Anti-buckling supports for Joint Types III and IV
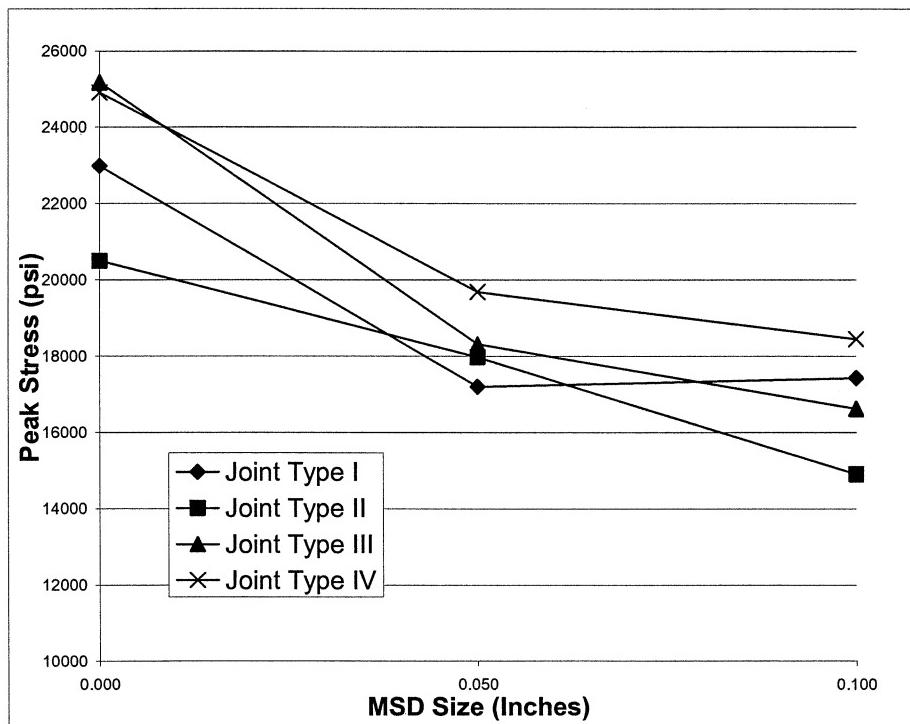
Figure 13. Effect of MSD Size on Peak Stress

25
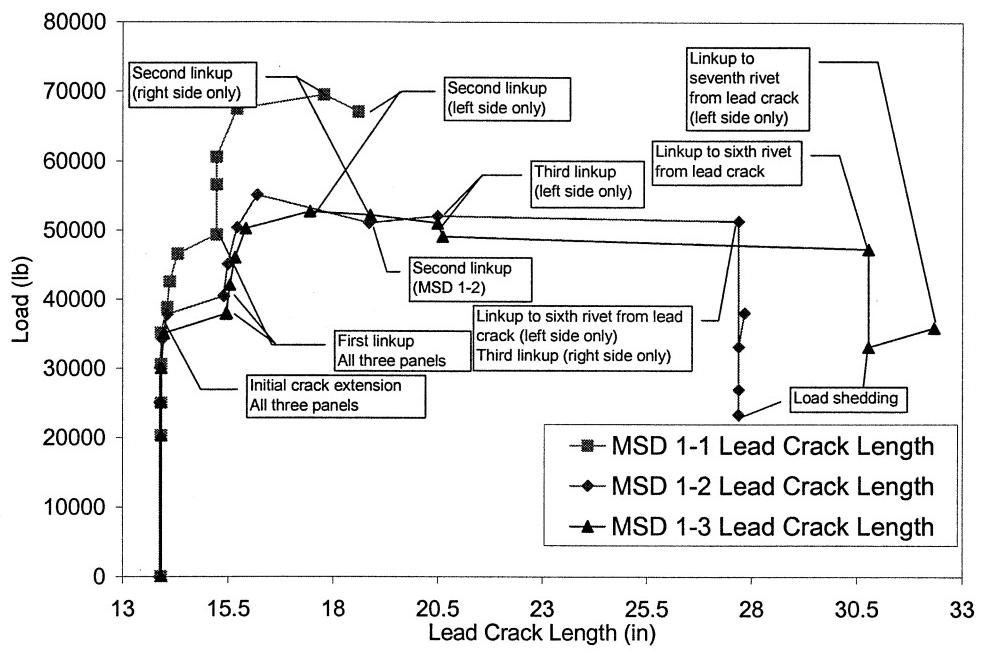
Figure 14. Joint Type I Lead Crack Lengths
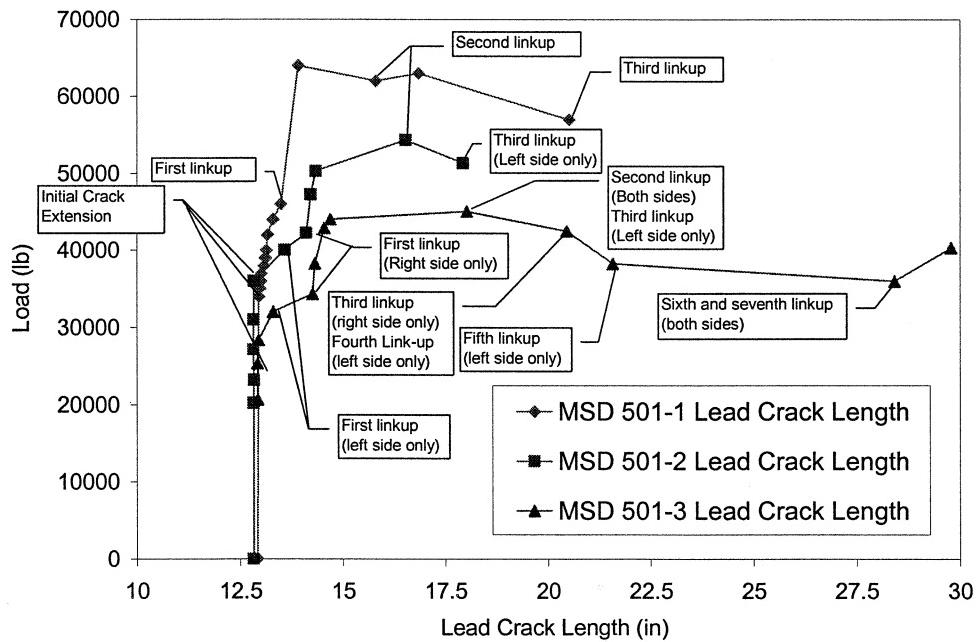
Figure 15. Joint Type II Lead Crack Lengths
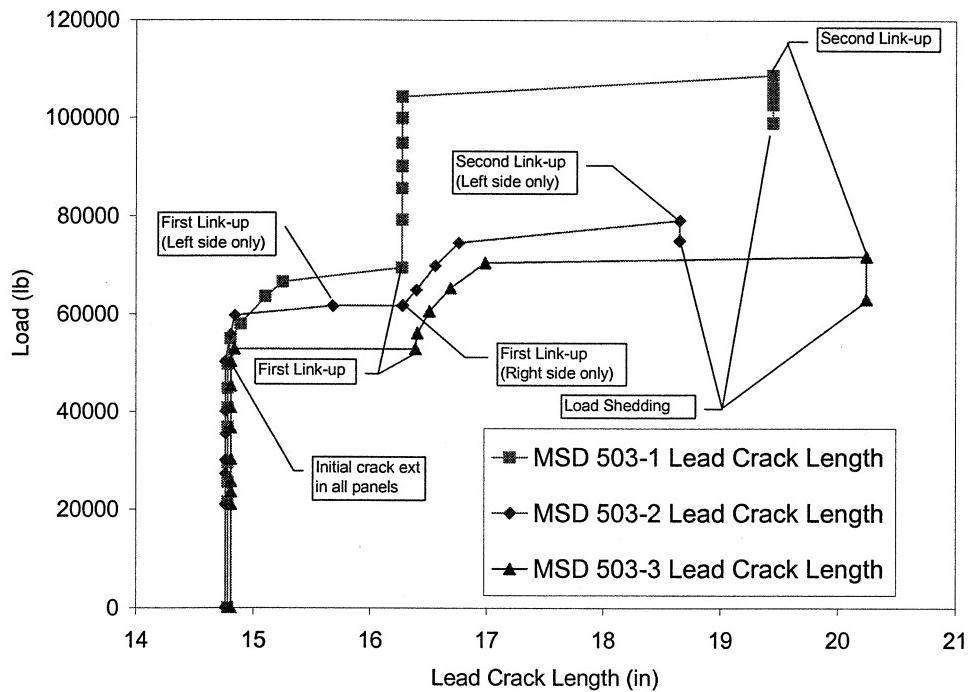
Figure 16. Joint Type III Lead Crack Lengths
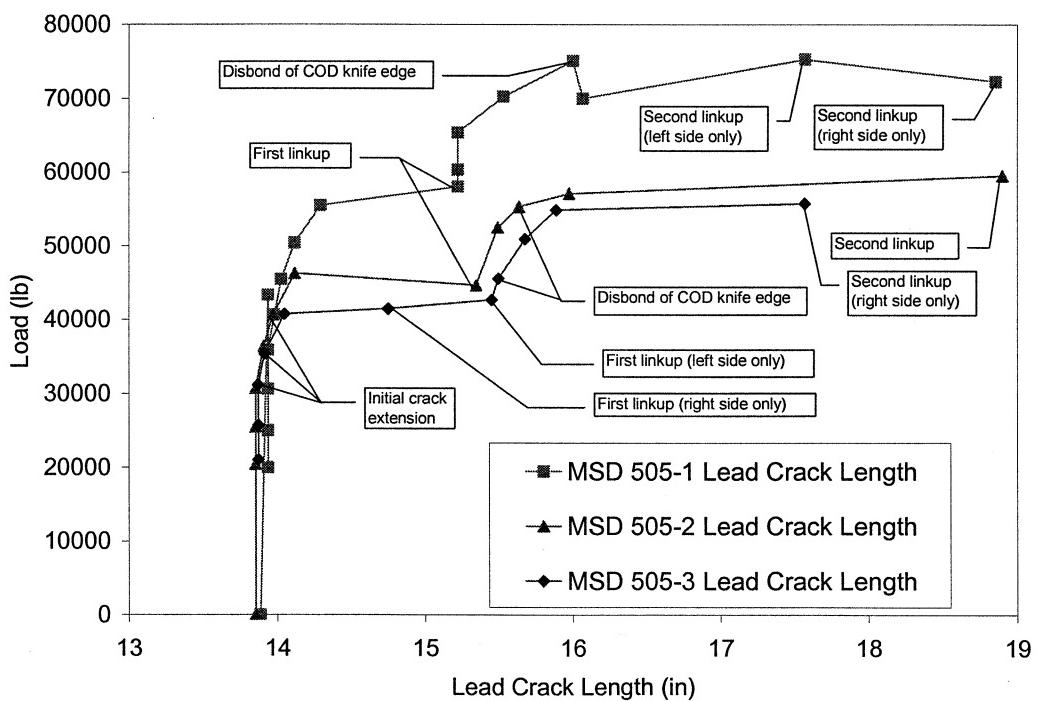
Figure 17. Joint Type IV Lead Crack Lengths
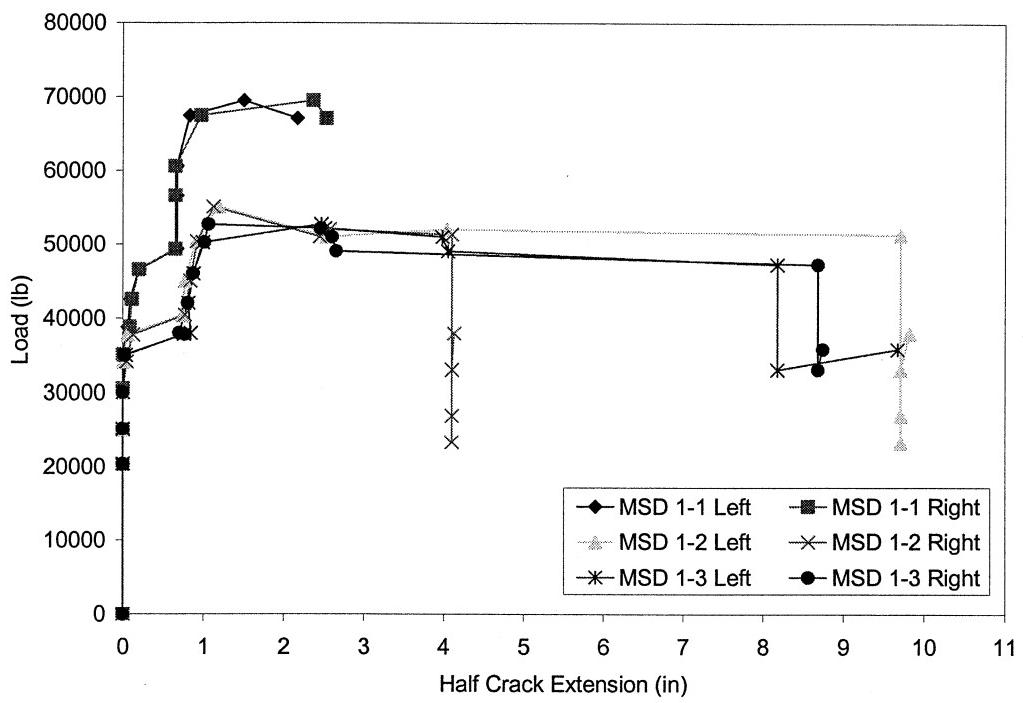
Figure 18. Joint Type I Half Crack Extension
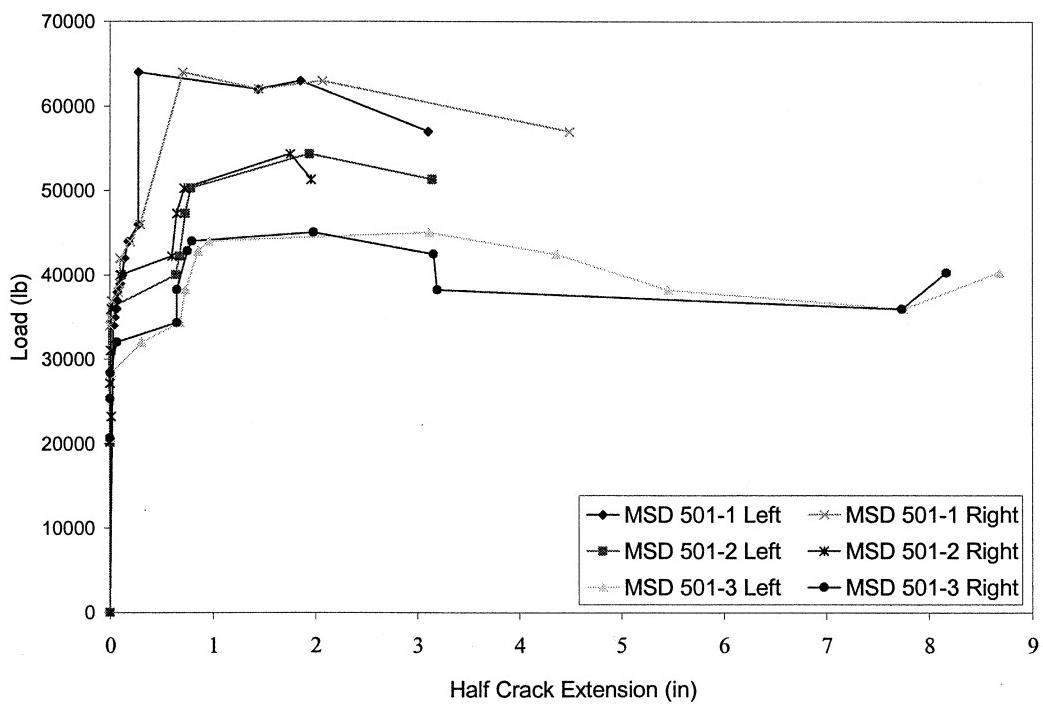
Figure 19. Joint Type II Half Crack Extension

28
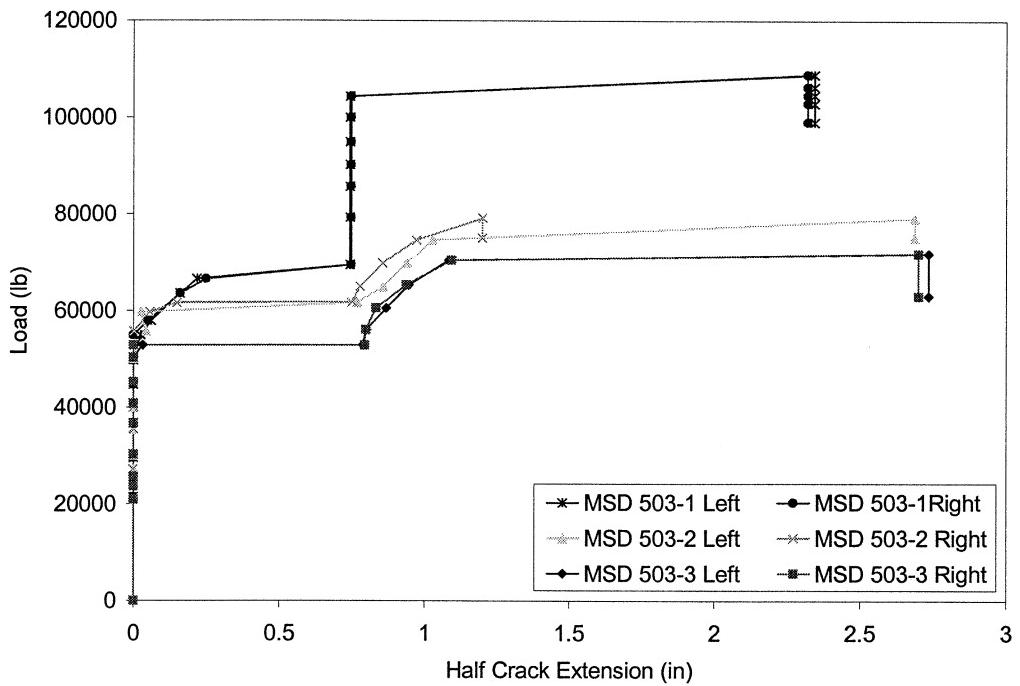
Figure 20. Joint Type III Half Crack Extension
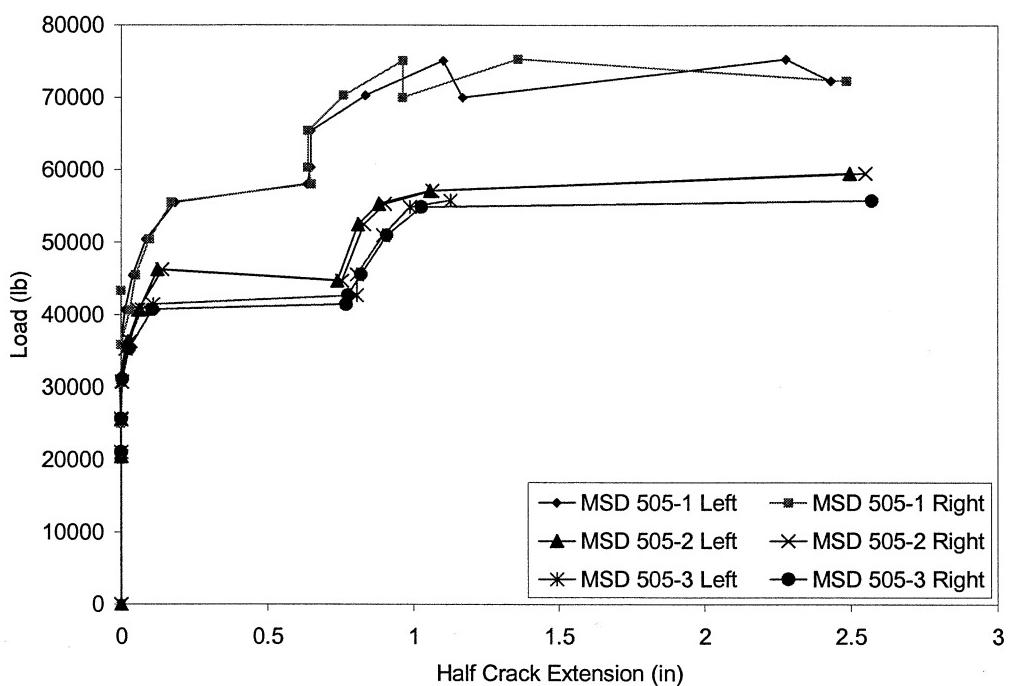
Figure 21. Joint Type IV Half Crack Extension
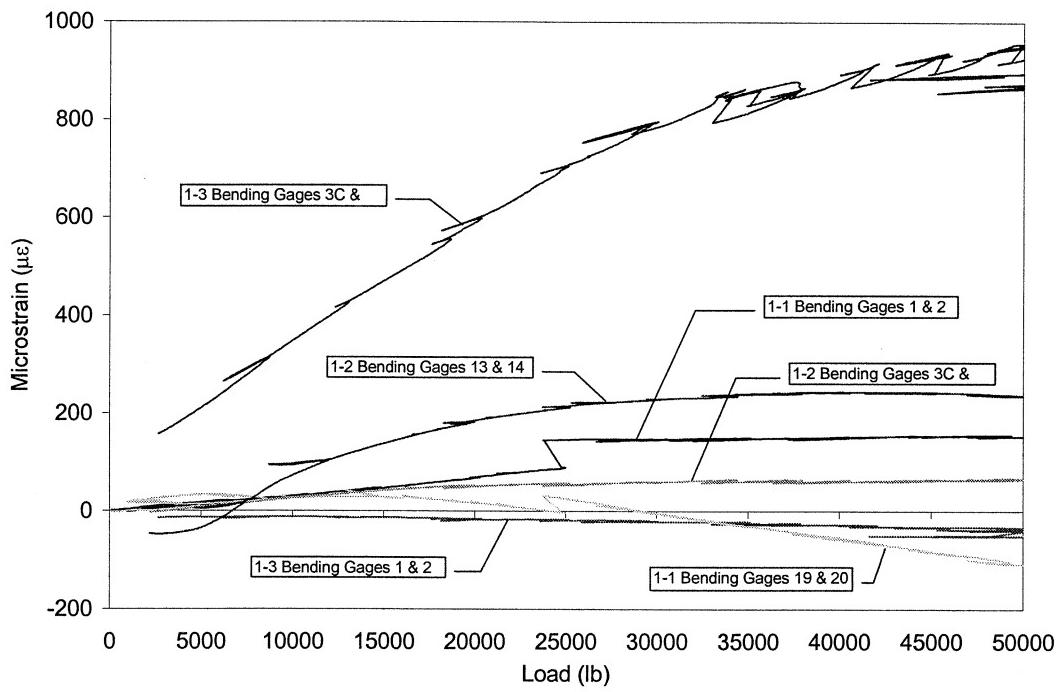
Figure 22. Secondary Bending Comparison in Joint Type I Panels
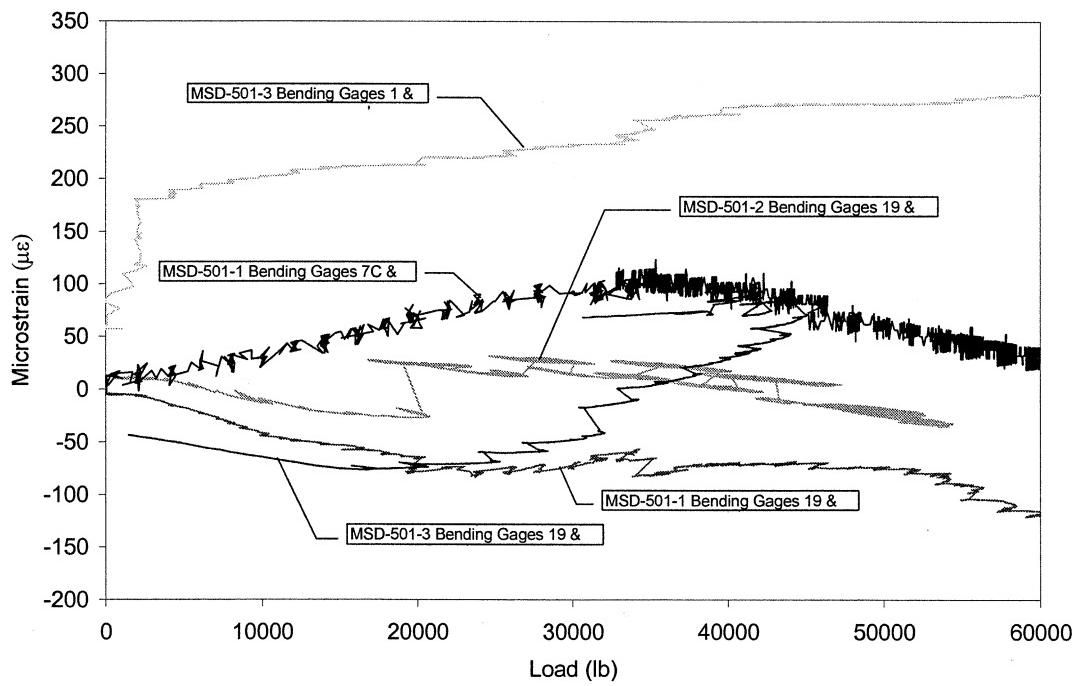
Figure 23. Secondary Bending Comparison in Joint Type II Panels

30
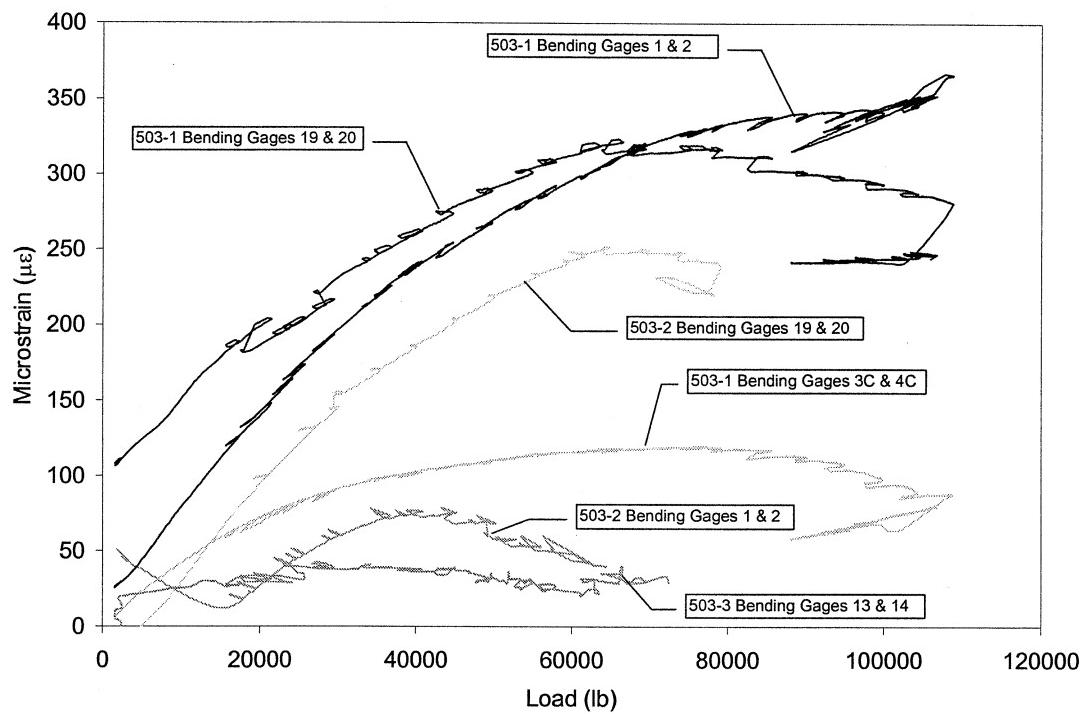
Figure 24. Secondary Bending Comparison in Joint Type III Panels
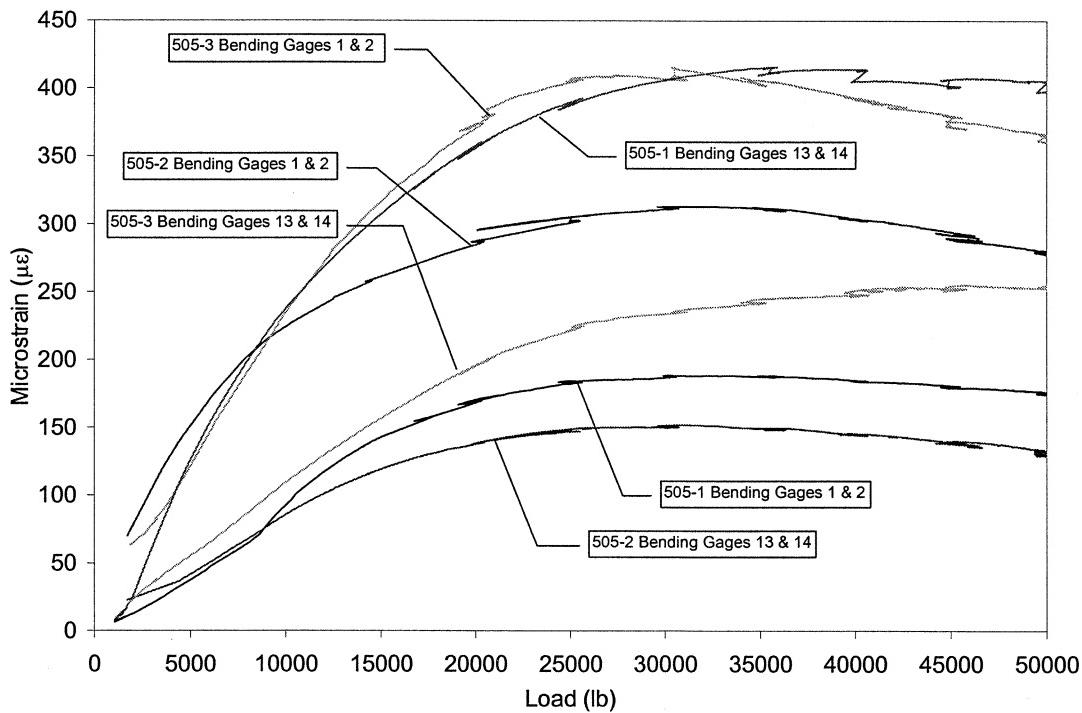
Figure 25. Secondary Bending Comparison in Joint Type IV Panels
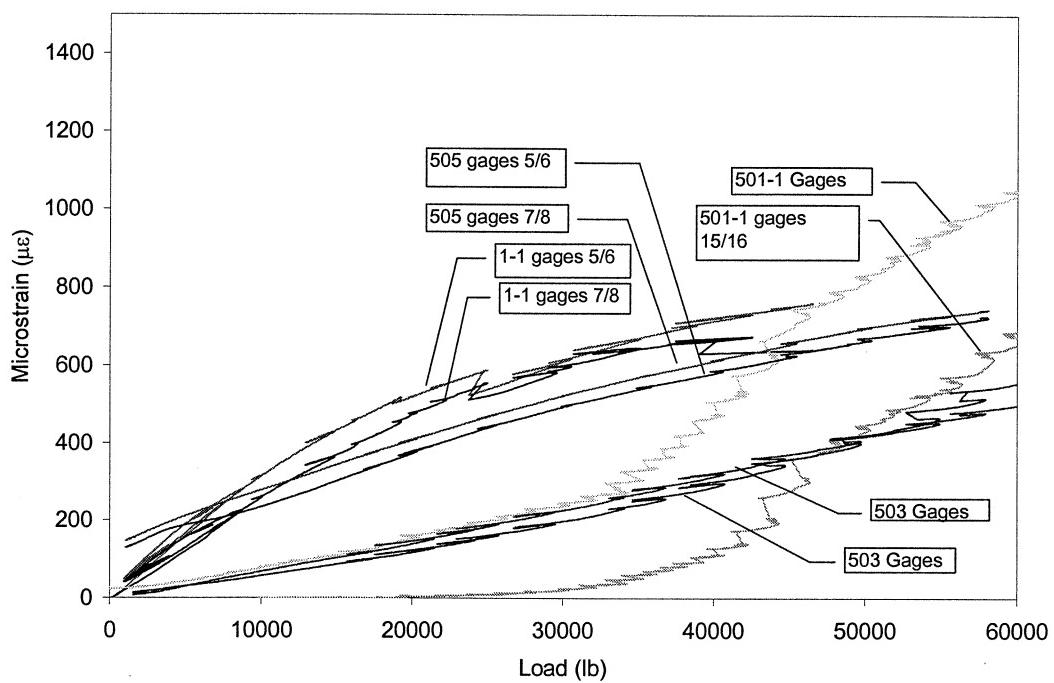
Figure 26. Secondary Bending Comparison Along Critical Row in Panels without MSD
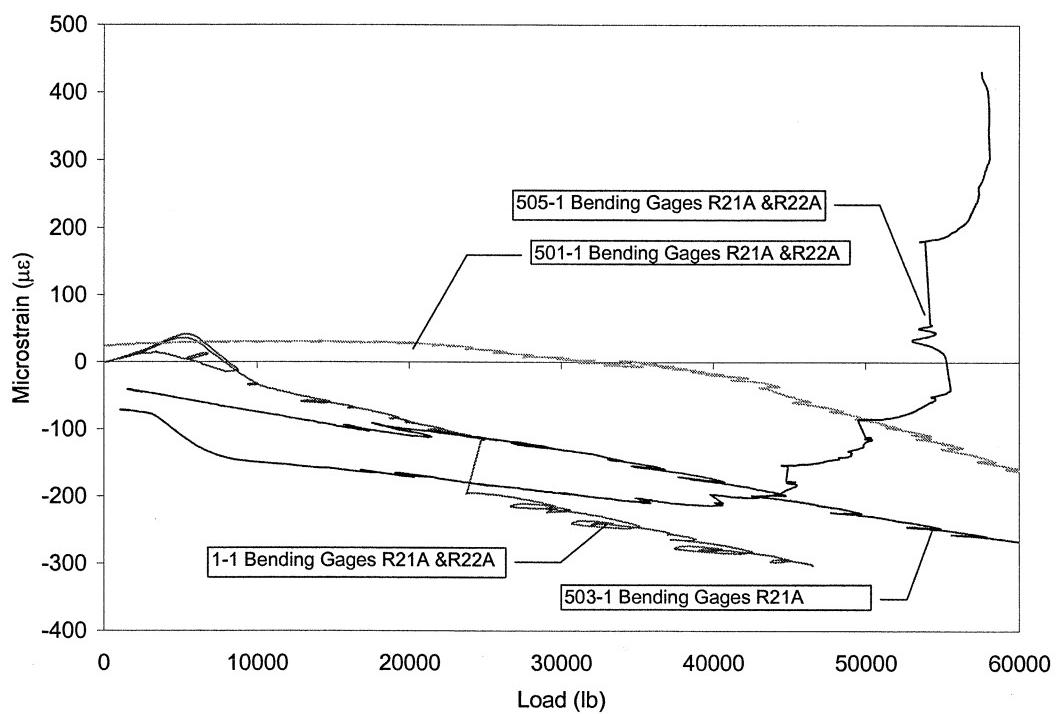
Figure 27. Crack Face Buckling Strain Comparison in Panels without MSD

32
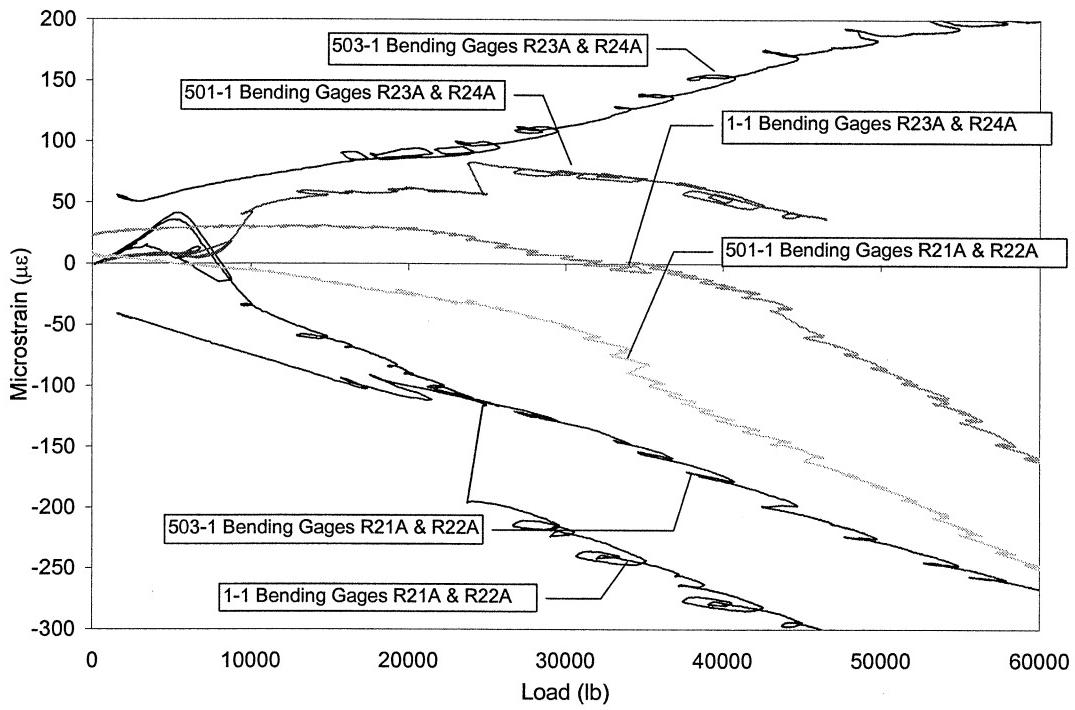
Figure 28. Crack Face Buckling Strain Comparison in Panels without MSD
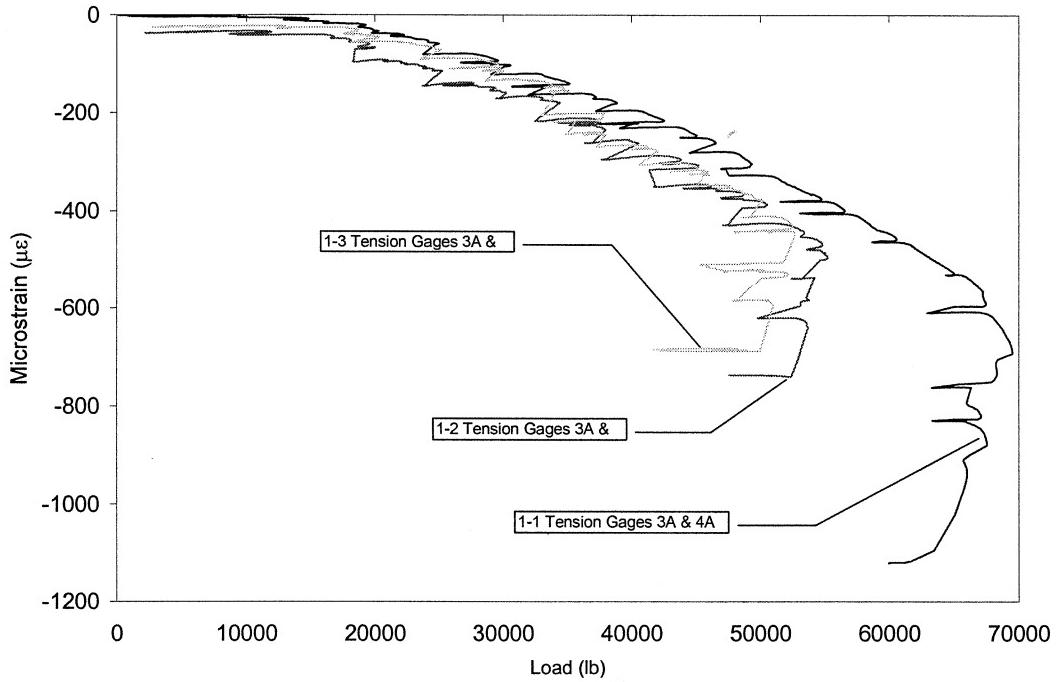
Figure 29. Transverse Tensile Strain in Joint Type I Panels

33
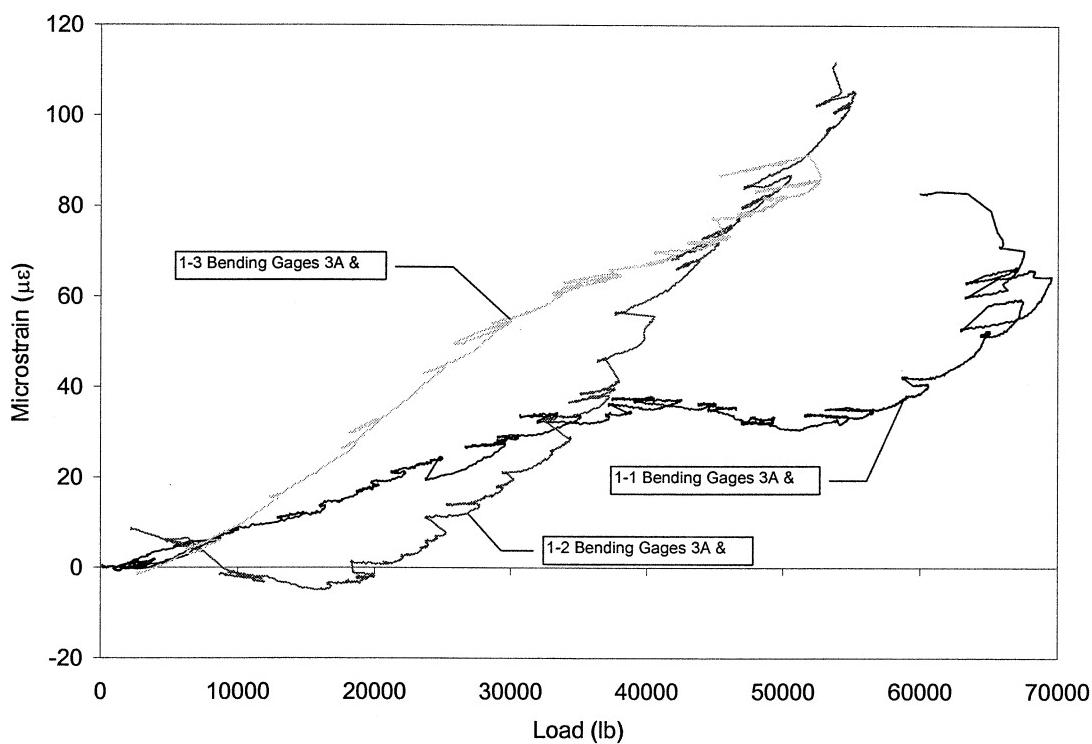
Figure 30. Transverse Bending Strain in Joint Type I Panels
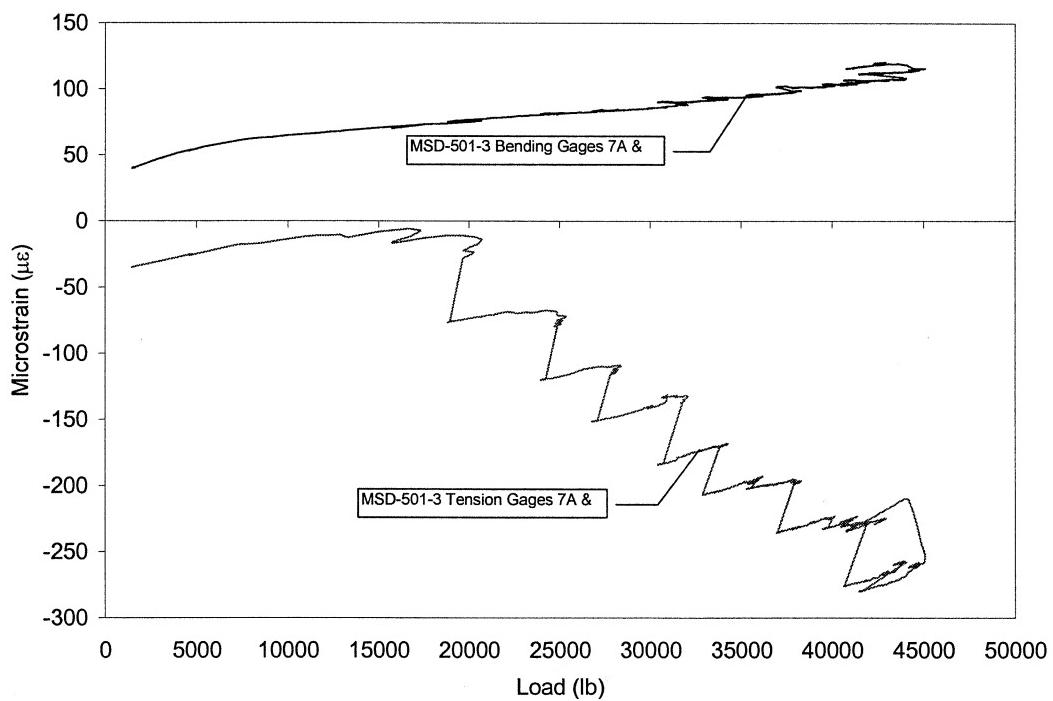
Figure 31. Transverse Strain in Joint Type II Panel 503-3

34
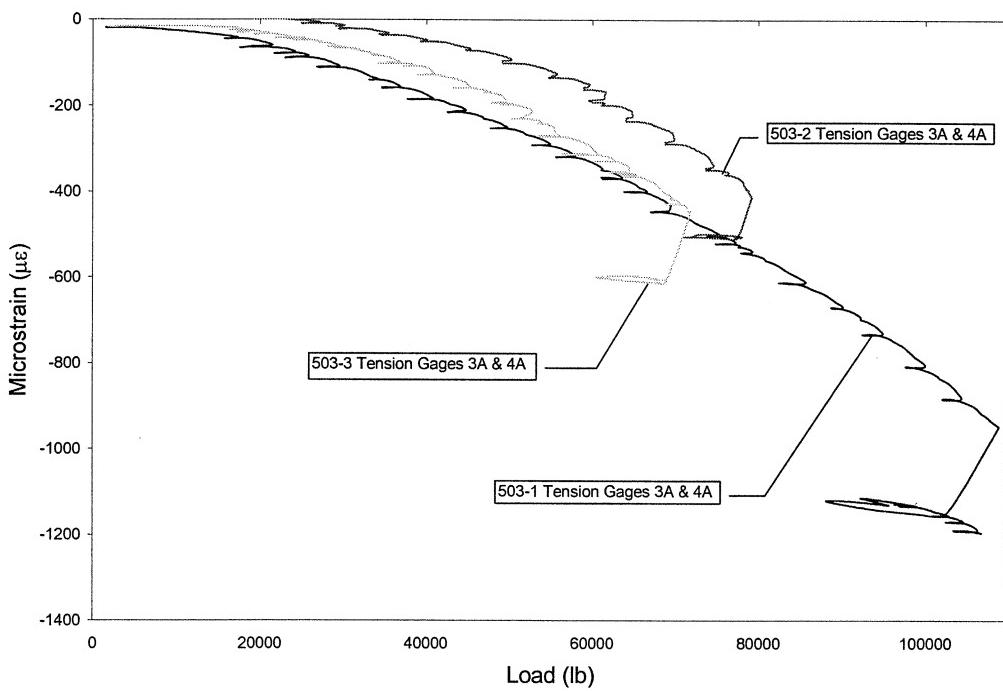
Figure 32. Transverse Tensile Strain in Joint Type III Panels
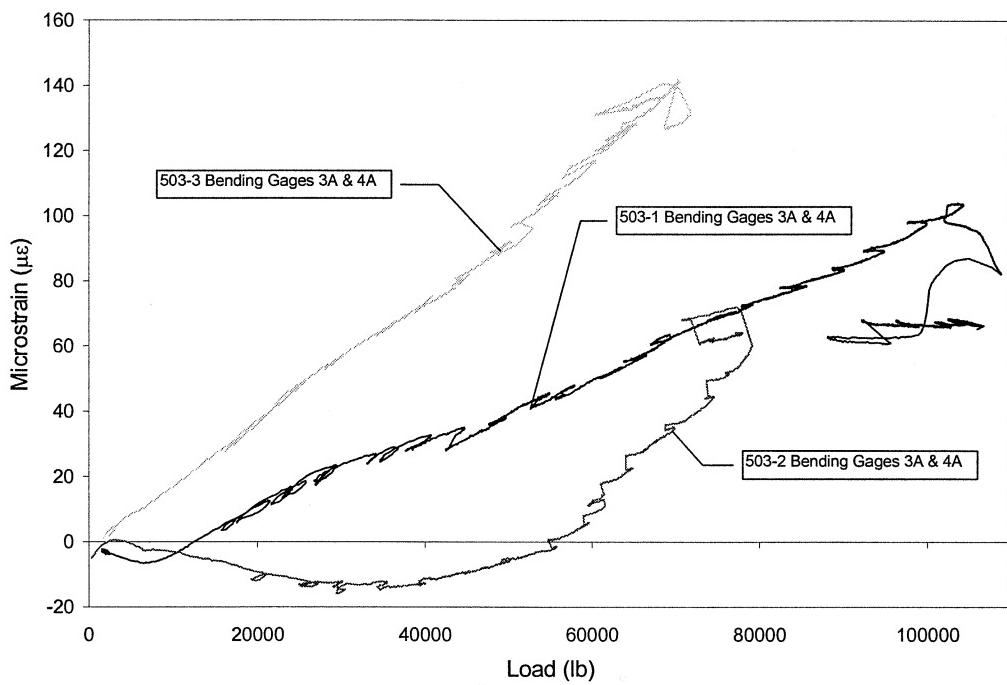
Figure 33. Transverse Bending Strain in Joint Type III Panels

35
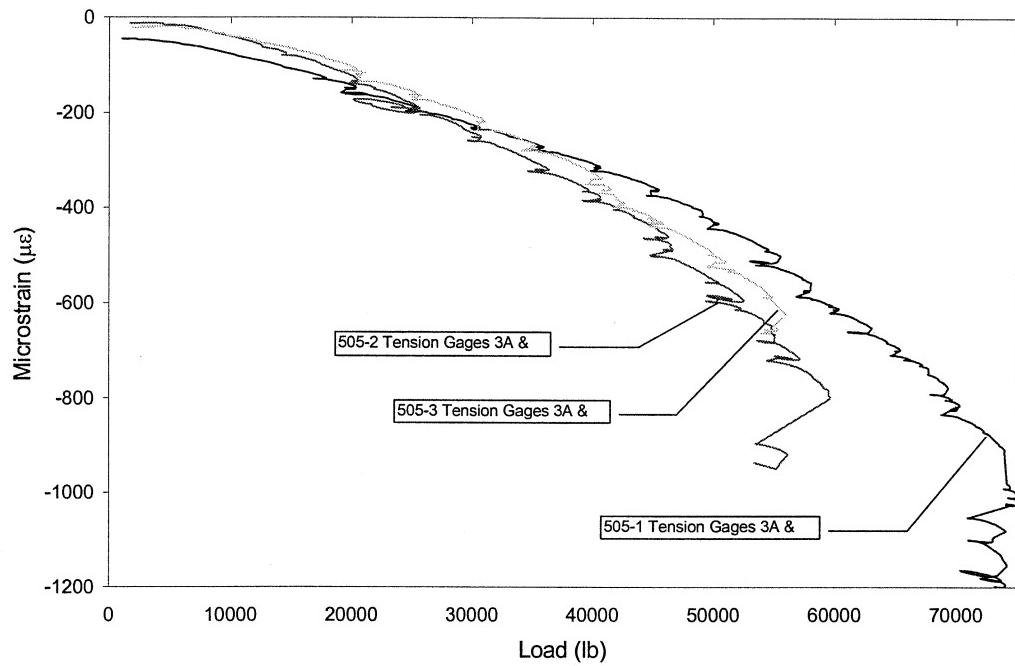
Figure 34. Transverse Tension Strain in Joint Type IV Panels
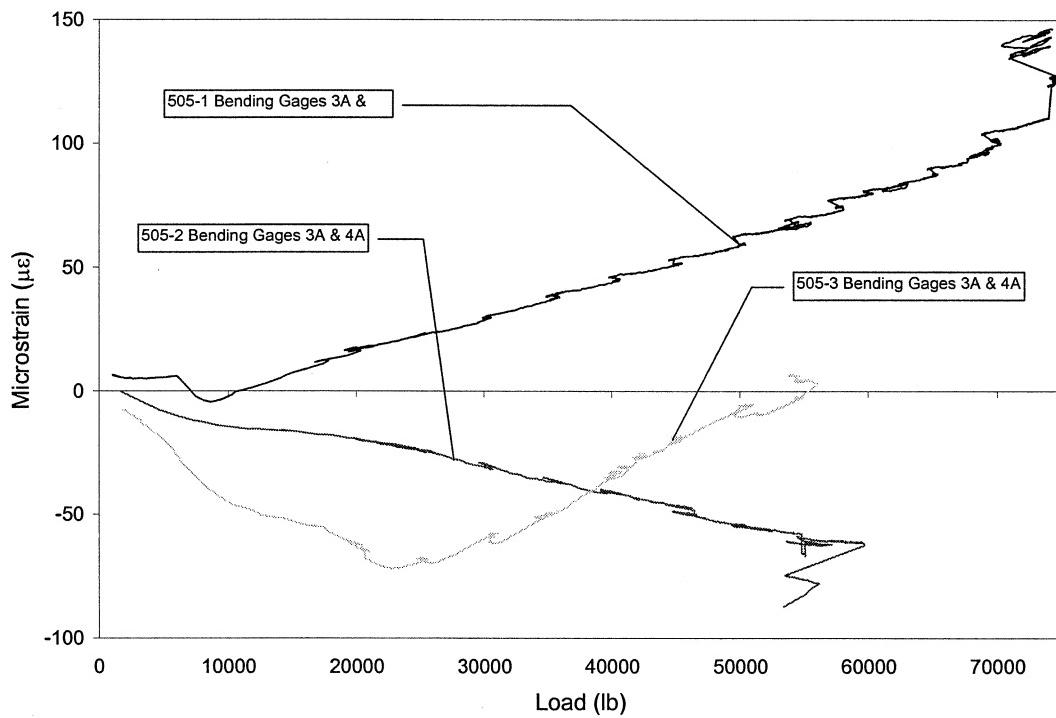
Figure 35. Transverse Bending Strain in Joint Type IV Panels

36

Appendix A

Test History

MSD-1-1 (TYPE I)

Load (lb)   Event

35161	Initial crack extension
49351	First linkup
69513	Second linkup (right side only)
67082	Second linkup (left side)
67491	Final failure

MSD-1-2 (TYPE I)

Load (lb)   Event

34223	Initial crack extension
40431	First linkup
51000	Second linkup (left side only)
52000	Third linkup (left side only)
51300	Left side only. Linkup through four fasteners Third linkup (right side only)
38727	Final failure

MSD-1-3 (TYPE I)

Load (lb)   Event

35081	Initial crack extension
37869	First linkup
52687	Second linkup (left side only)
52135	Second linkup (right side only)
50979	Third linkup (left side only)
47268	Linkup to sixth rivet (both sides)
35884	Final failure

MSD-501-1 (TYPE II)

Load (lb)   Event

34000	Initial crack extension (left side only)
35000	Initial crack extension (right side only)
46000	First linkup
62000	Second linkup
57000	Third linkup (left side only)
57035	Final failure

MSD-501-2 (TYPE II)

Load (lb)   Event

31000	Initial crack extension
40000	First linkup (left side only)
42000	First linkup (right side only)
54349	Second linkup (both sides)
51350	Third linkup (left side only)
46551	Final failure

MSD-501-3 (TYPE II)

Load (lb)   Event

25334	Initial crack extension
32028	First linkup (left side only)

34352	First linkup (right side only)
45065	Second linkup (both sides) Third linkup (left side only)
42500	Third linkup (right side only) Fourth linkup (left side only)
38277	Fifth linkup (left side only)
36000	Sixth and Seventh linkup (both sides)
40323	Final failure

MSD-503-1 (TYPE III)

Load (lb)	Event
54903	Initial crack extension (left side only)
57905	Initial crack extension (right side only)
69465	First linkup (both sides)
108767	Second linkup (both sides)
106587	Final failure

MSD-503-2 (TYPE III)

Load (lb)	Event
55746	Initial crack extension (right side only)
59660	Initial crack extension (left side only)
61596	First linkup (left side only)
61739	First linkup (right side only)
79114	Second linkup (left side only)
78191	Final failure

MSD-503-3 (TYPE III)

Load (lb)	Event
52875	First linkup (both sides)
71777	Second linkup (both sides)
68651	Final failure

MSD-505-1 (TYPE IV)

Load (lb)	Event
40637	Initial crack extension (both sides)
58037	First linkup (both sides)
75125	Disbond of COD knife edge
75321	Second linkup (left side only)
72300	Second linkup (right side only)
74269	Final failure

MSD-505-2 (TYPE IV)

Load (lb)	Event
36316	Initial crack extension (both sides)
46662	First linkup (both sides)
55312	Disbond of COD knife edges
59529	Second linkup (both sides)
55901	Final failure

MSD-505-3 (TYPE IV)

Load (lb)	Event
31139	Initial crack extension (both sides)
41422	First linkup (right side only)
42679	First linkup (left side only)
45558	Disbond of COD knife edges
55770	Second linkup (right side only)
54666	Final failure

MSD 1-1
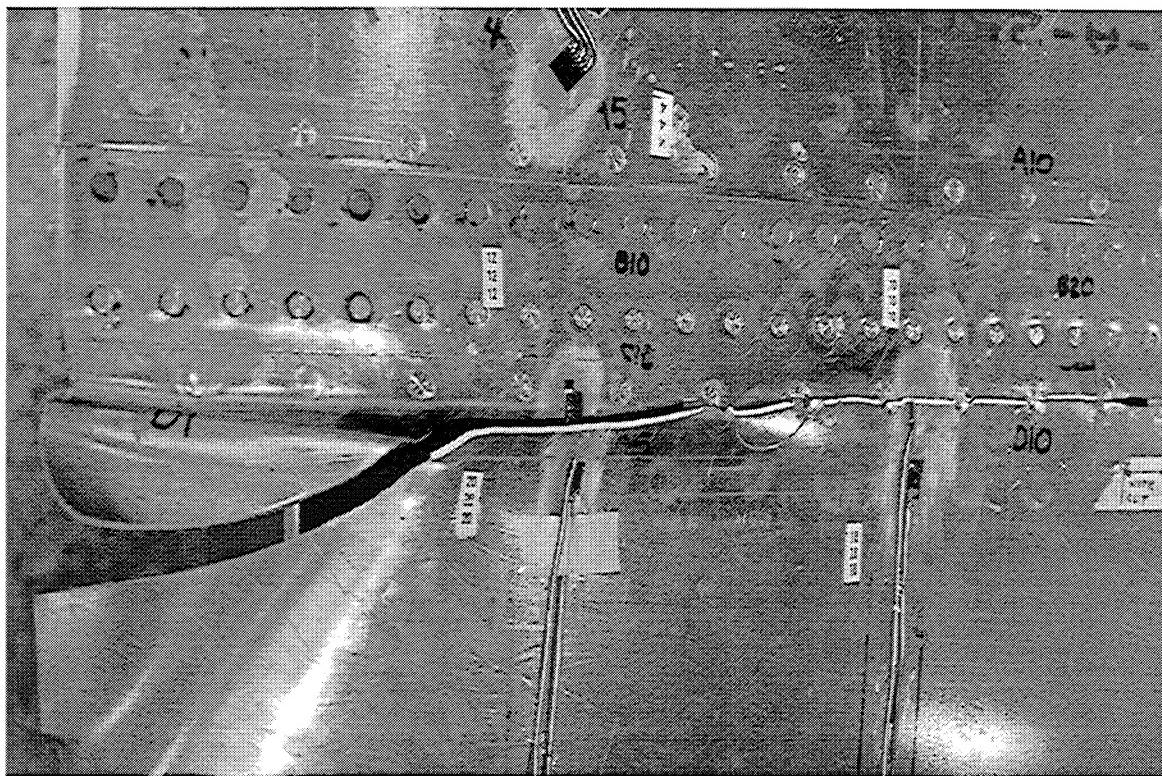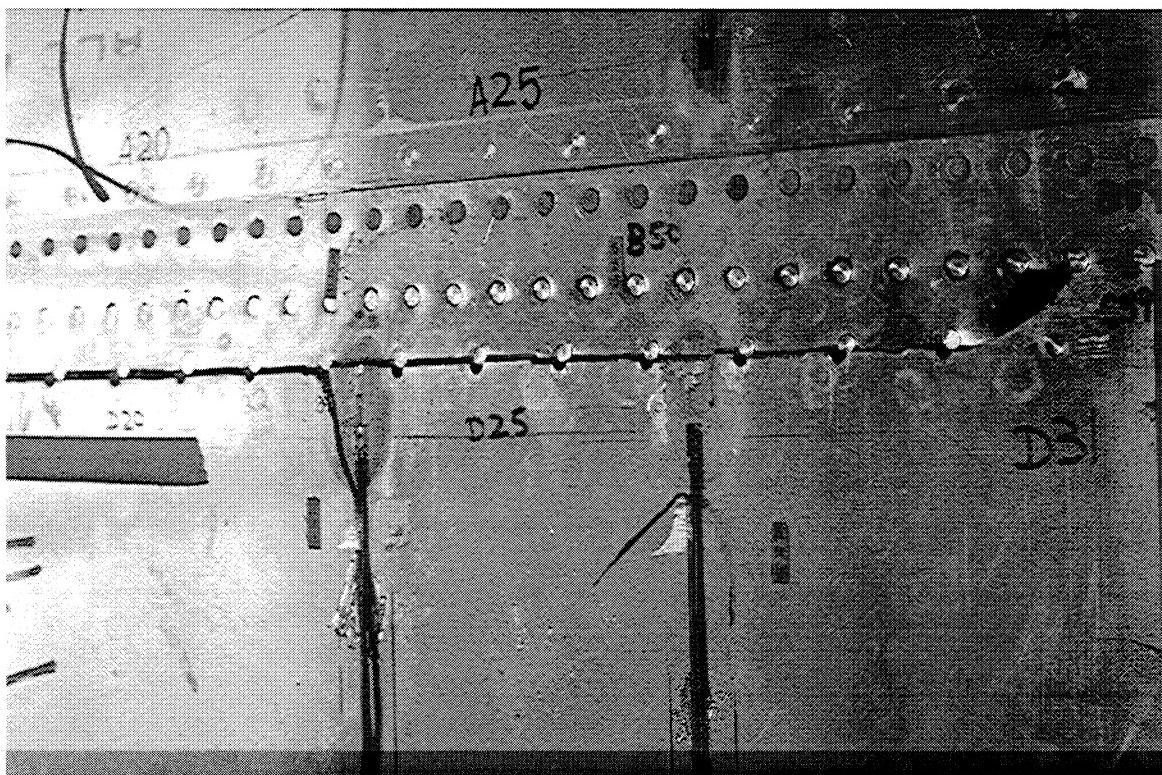
Figure 37

Figure 38
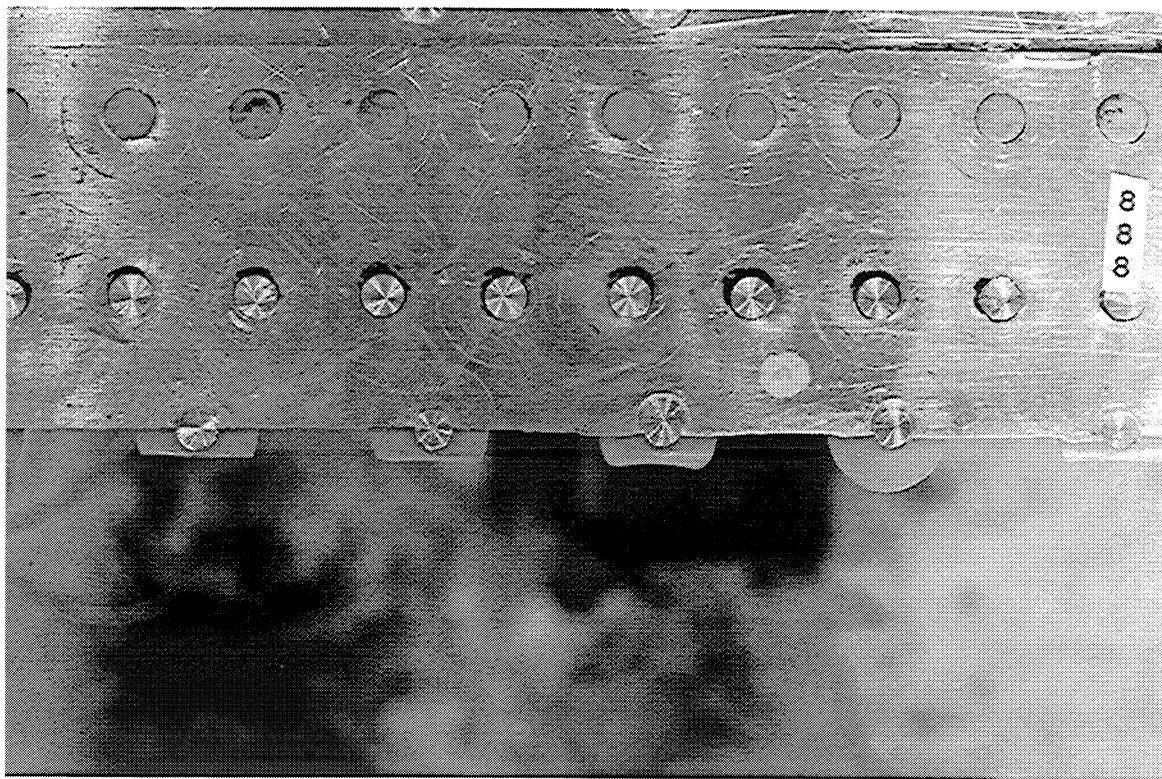
Figure 39
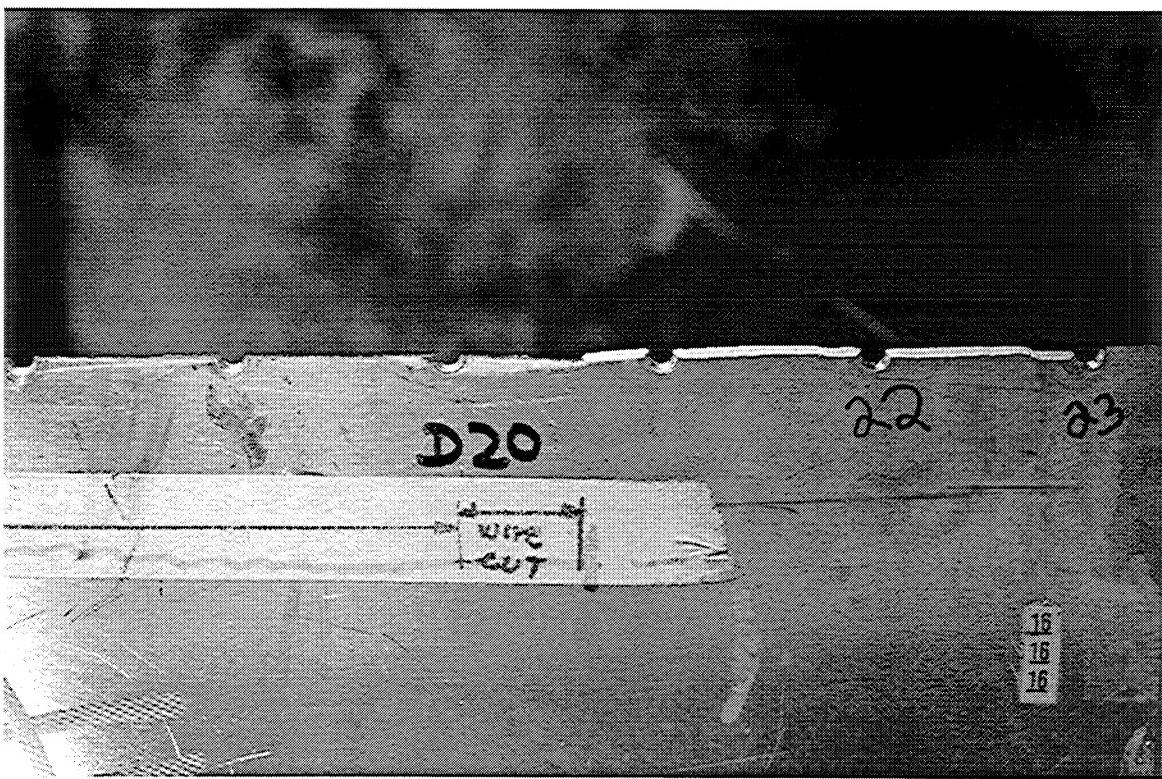

Figure 40
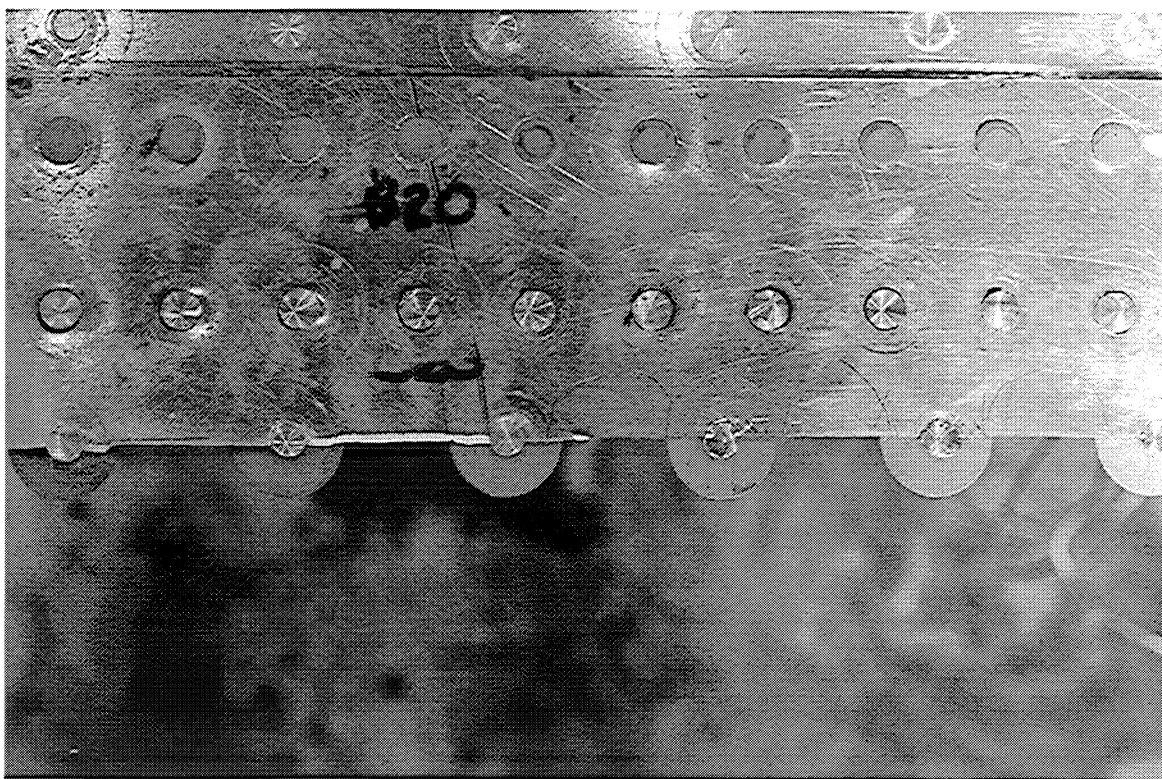
Figure 41
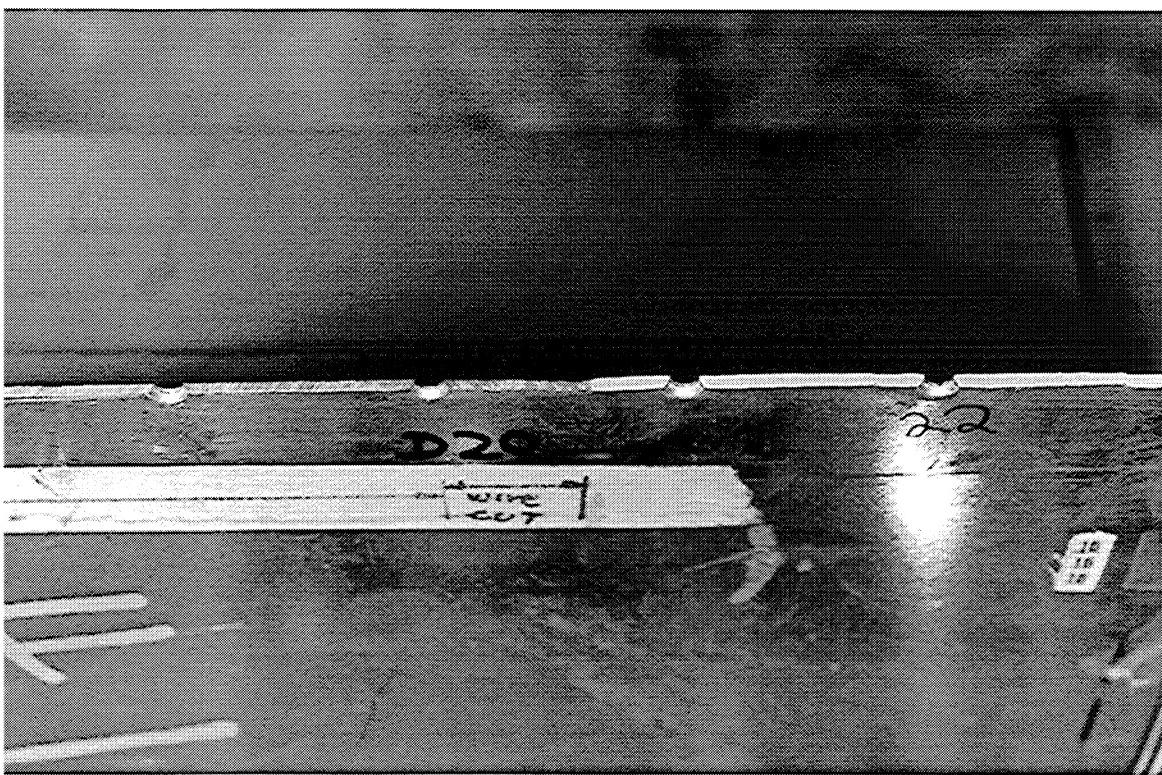
Figure 42

Figure 43
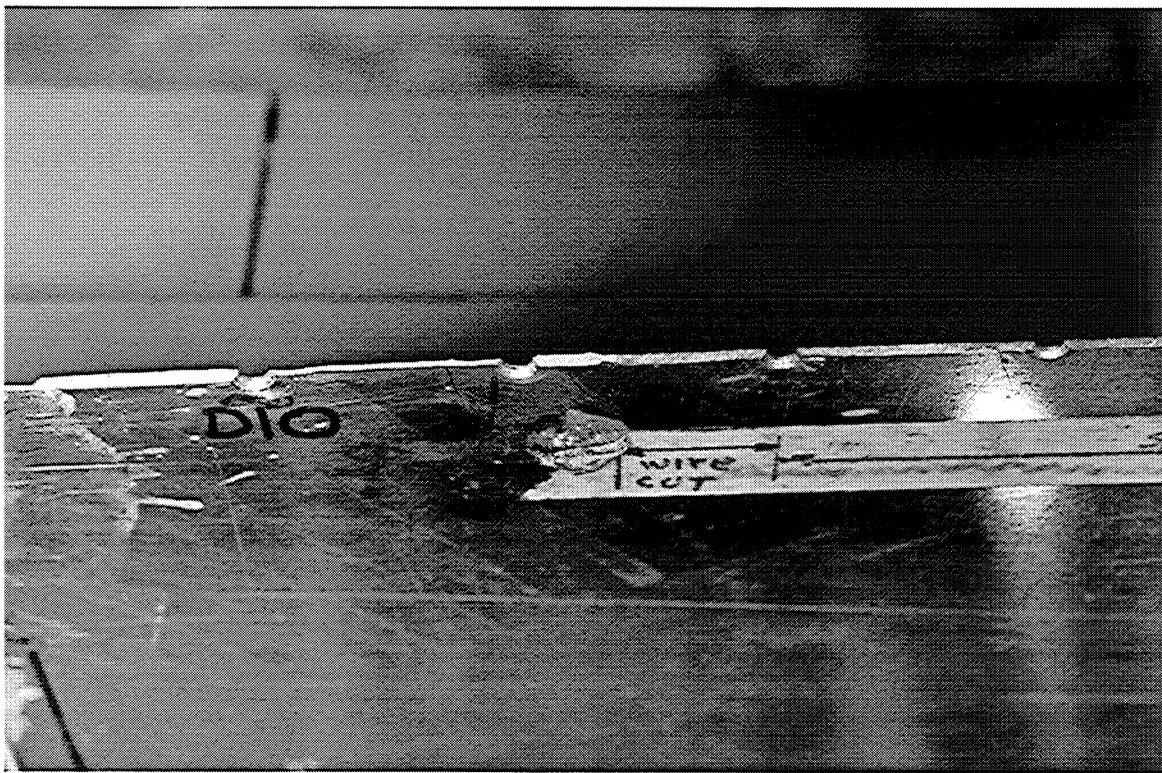

Figure 44
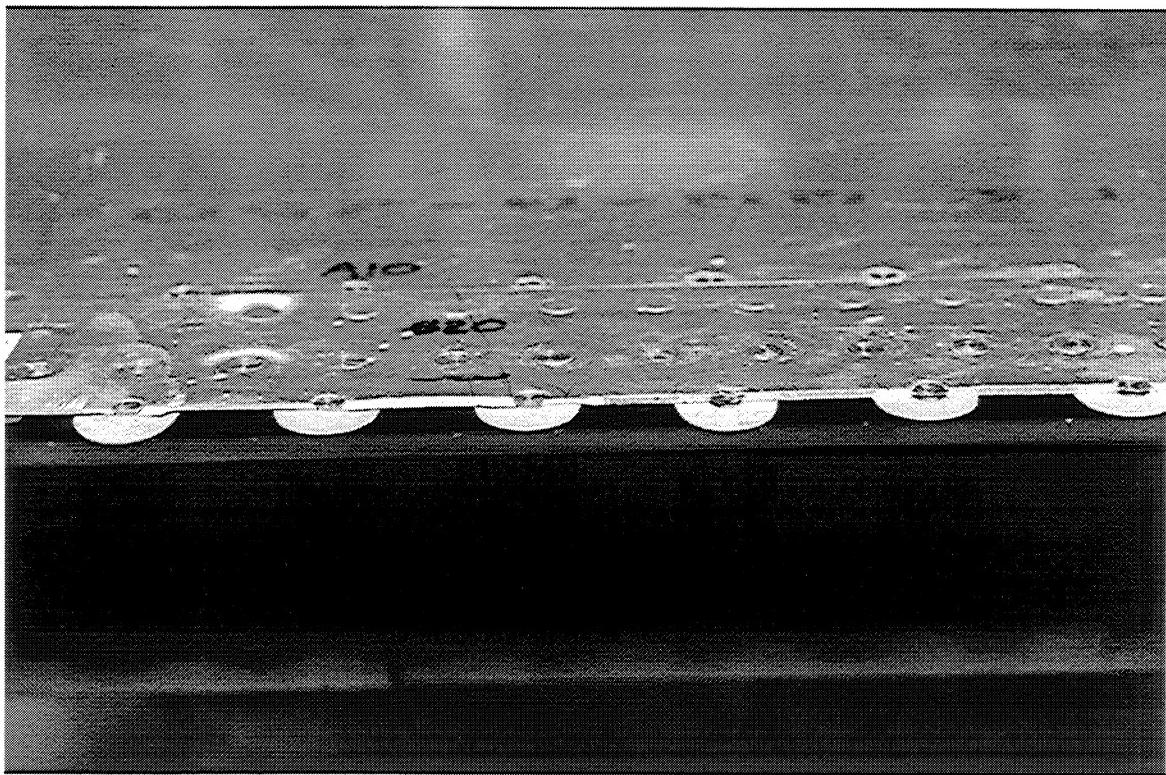
Figure 45
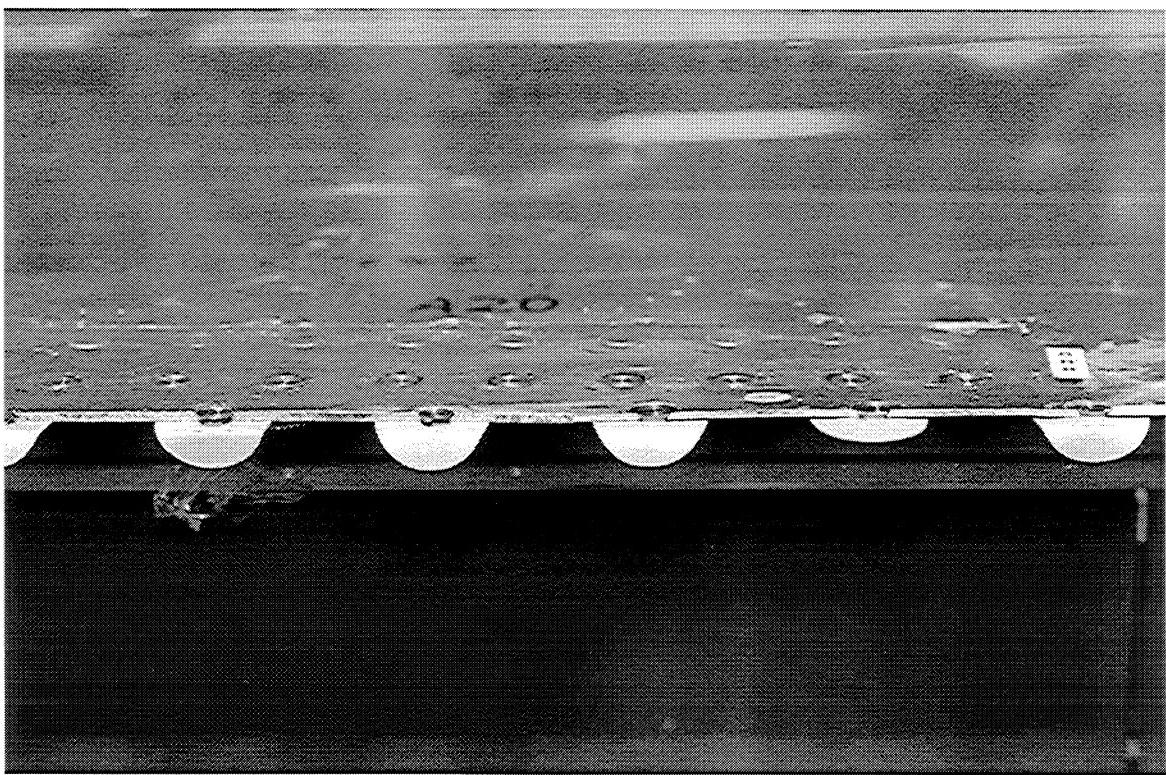
Figure 46
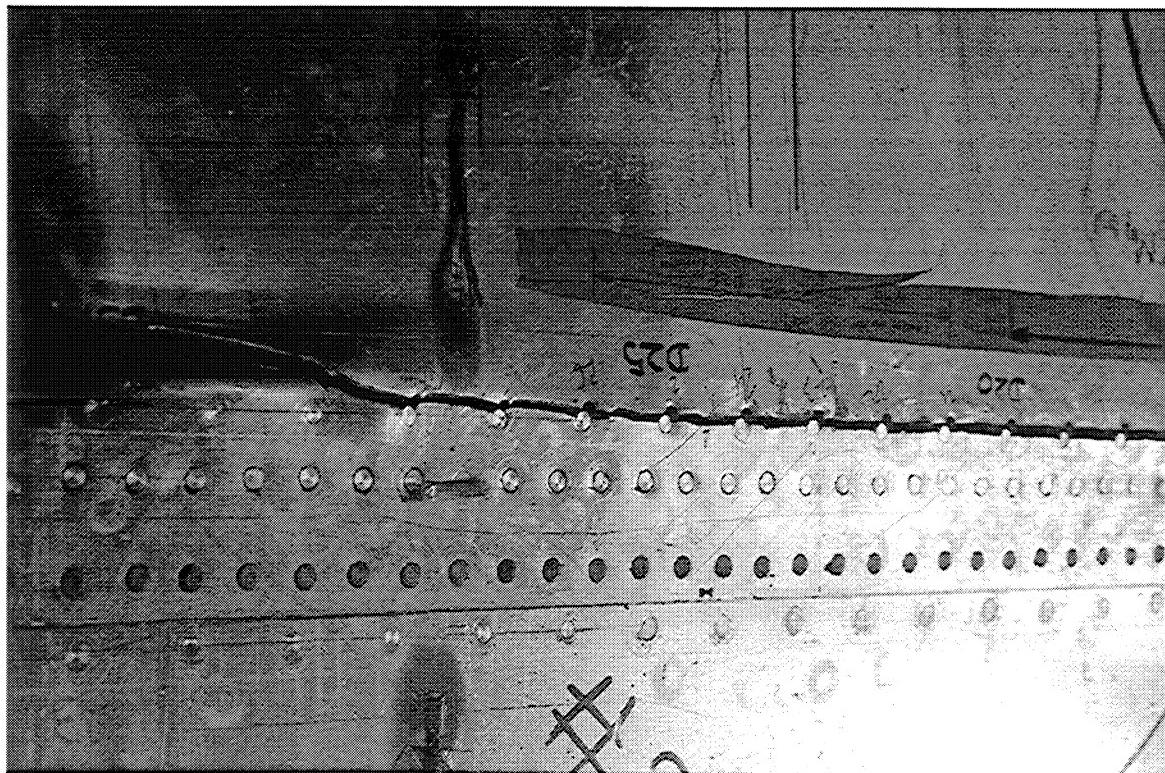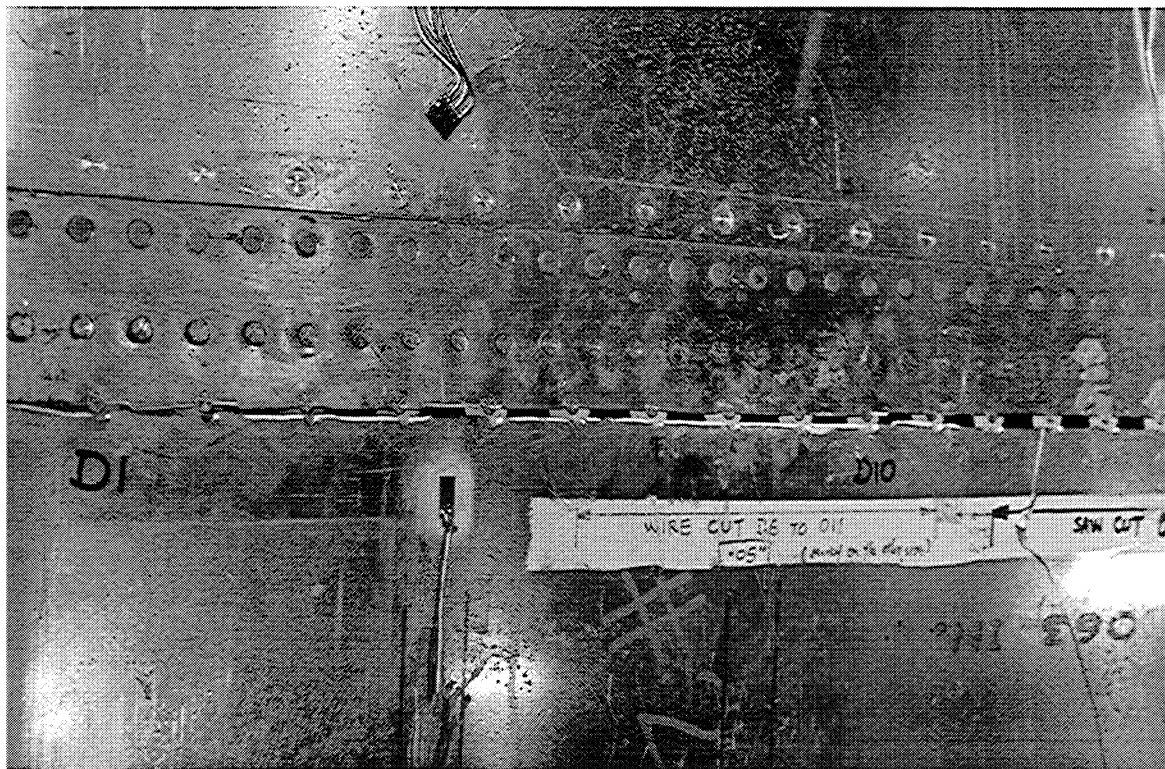
Figure 47

Figure 48
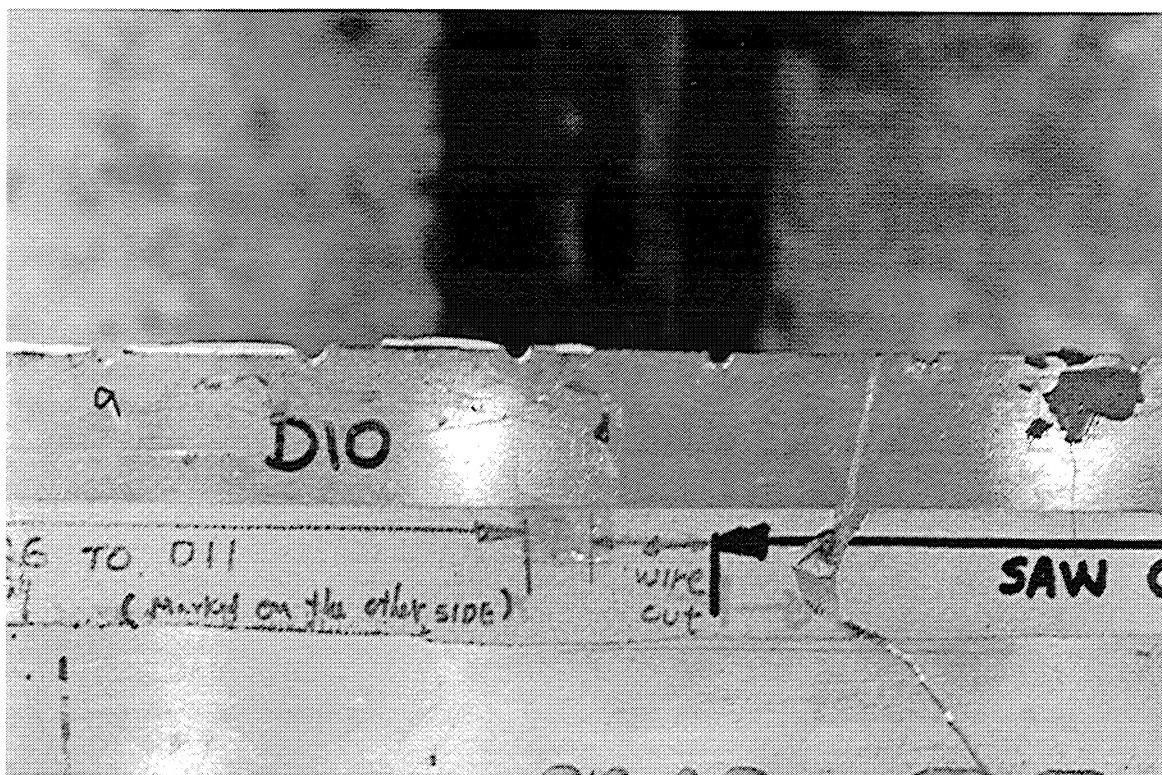
Figure 49
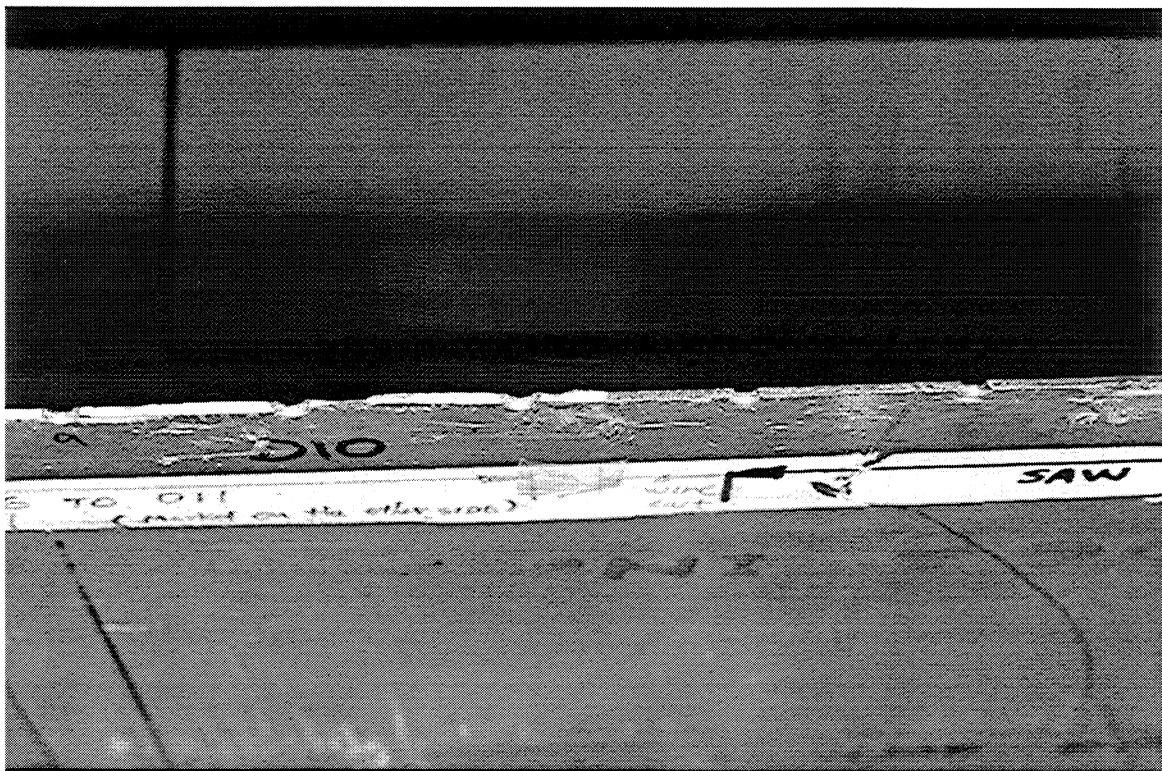
Figure 50
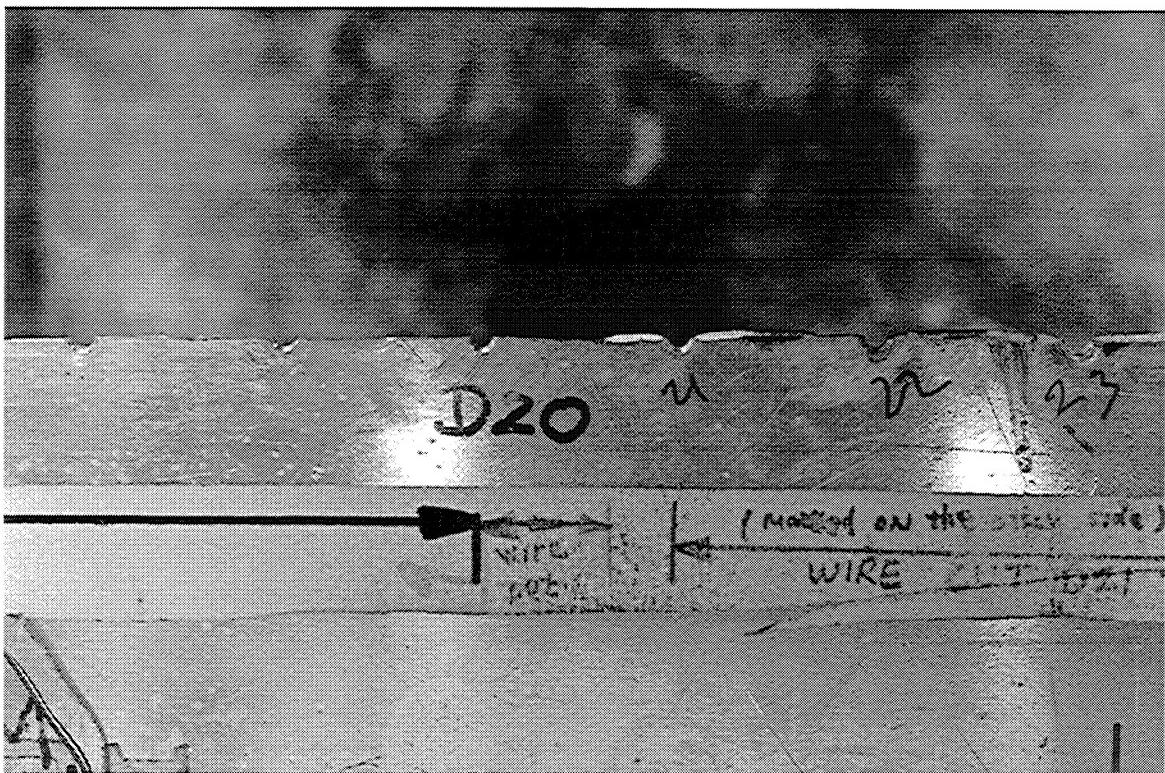
Figure 51

Figure 52
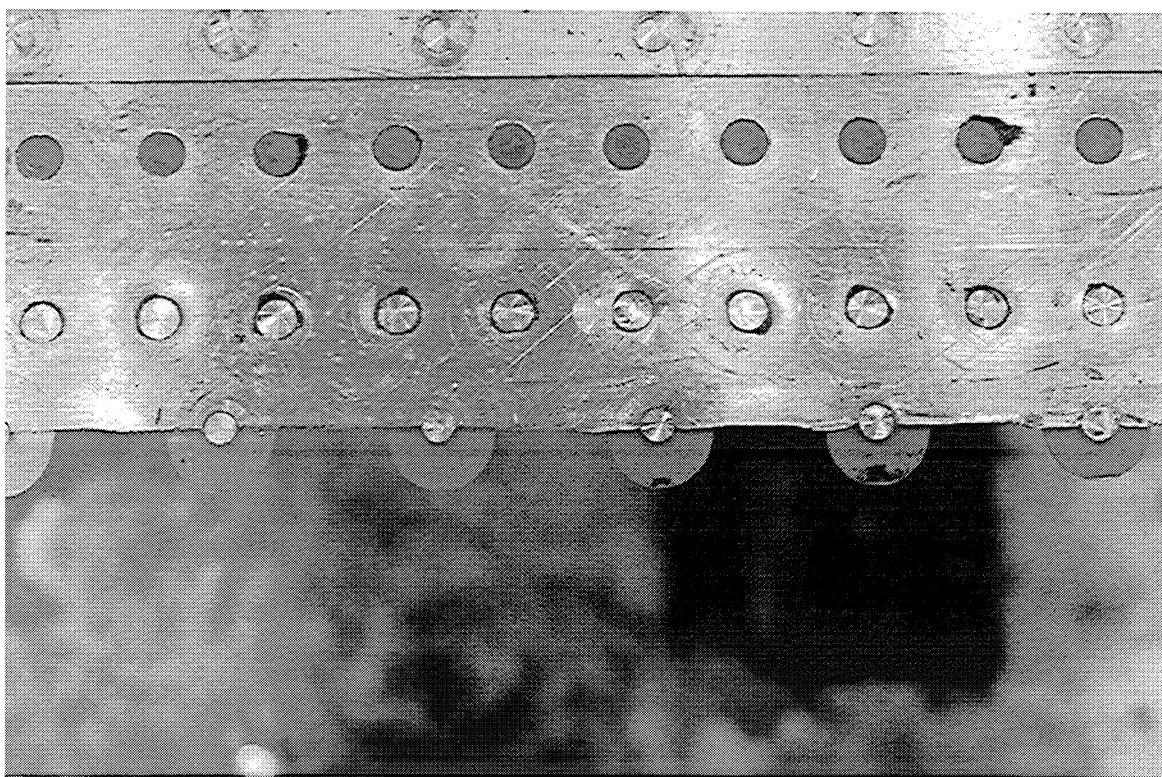
Figure 53
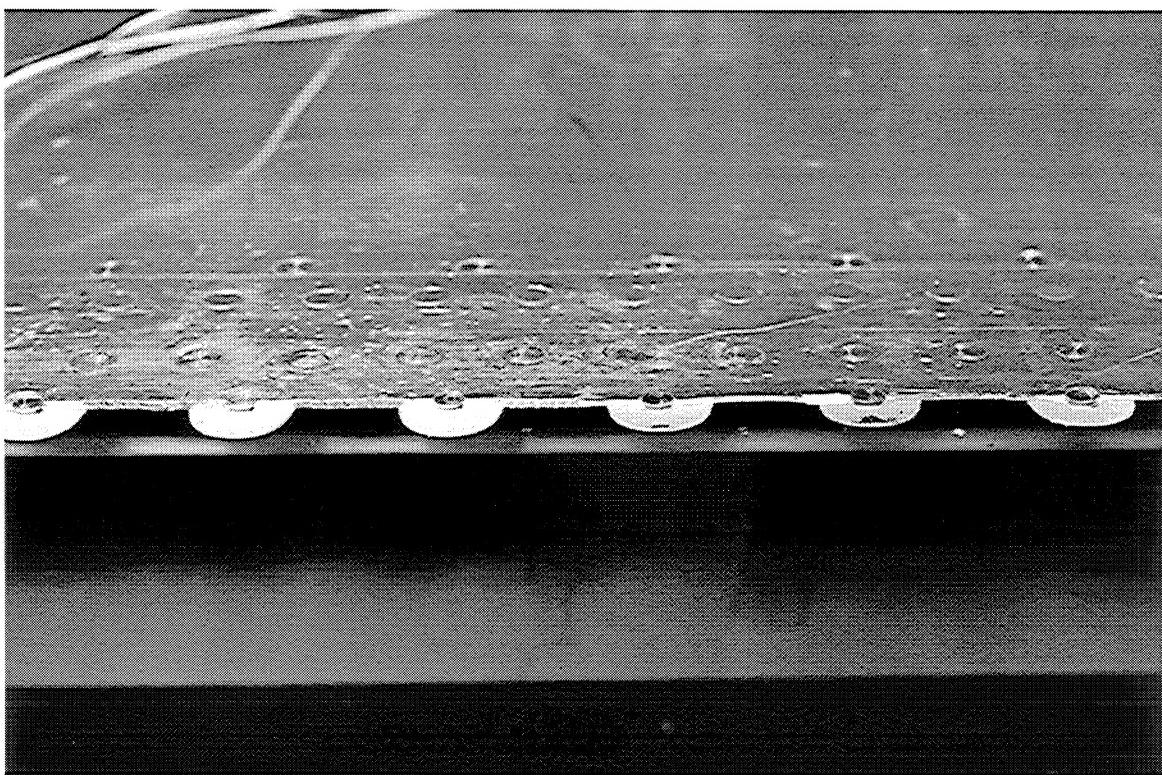
Figure 54
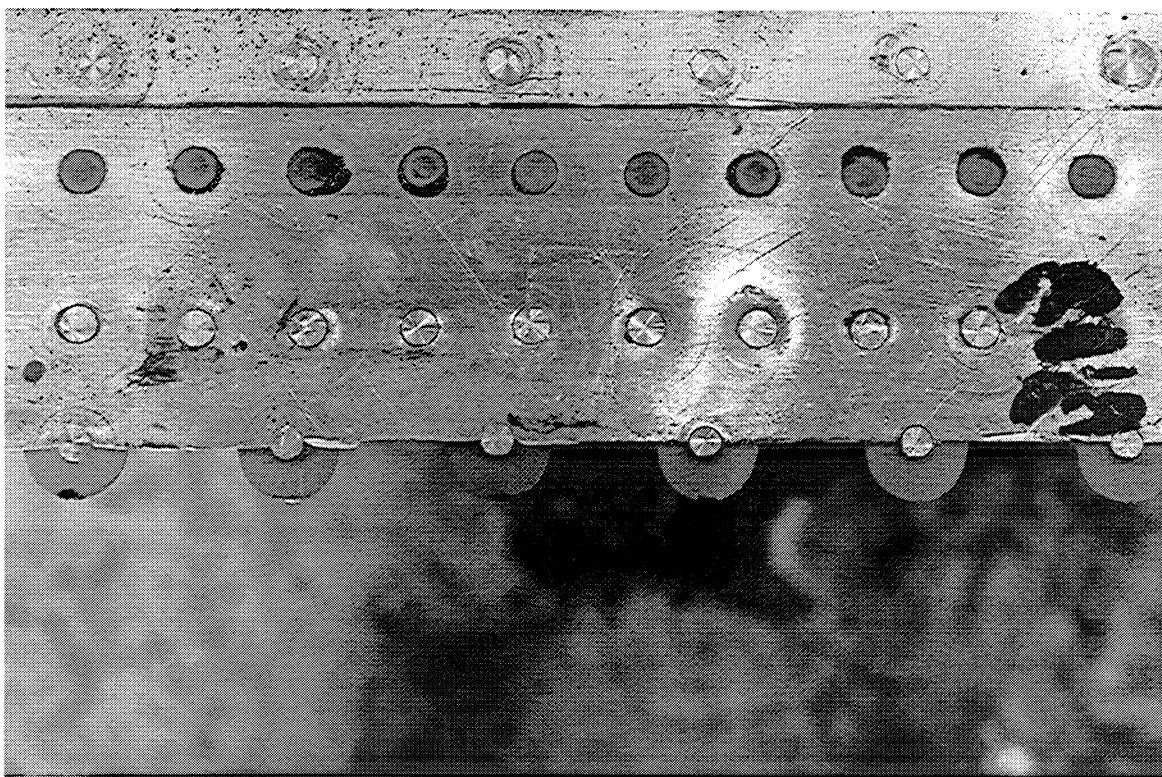
Figure 55
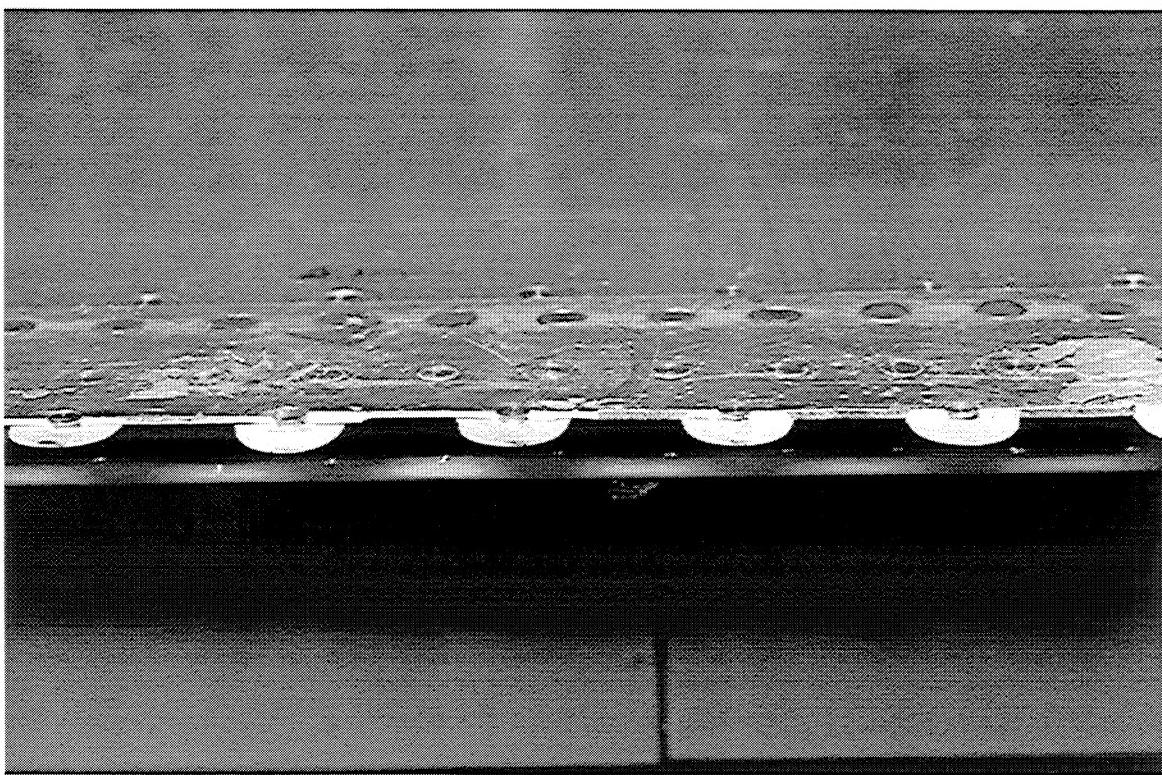
Figure 56
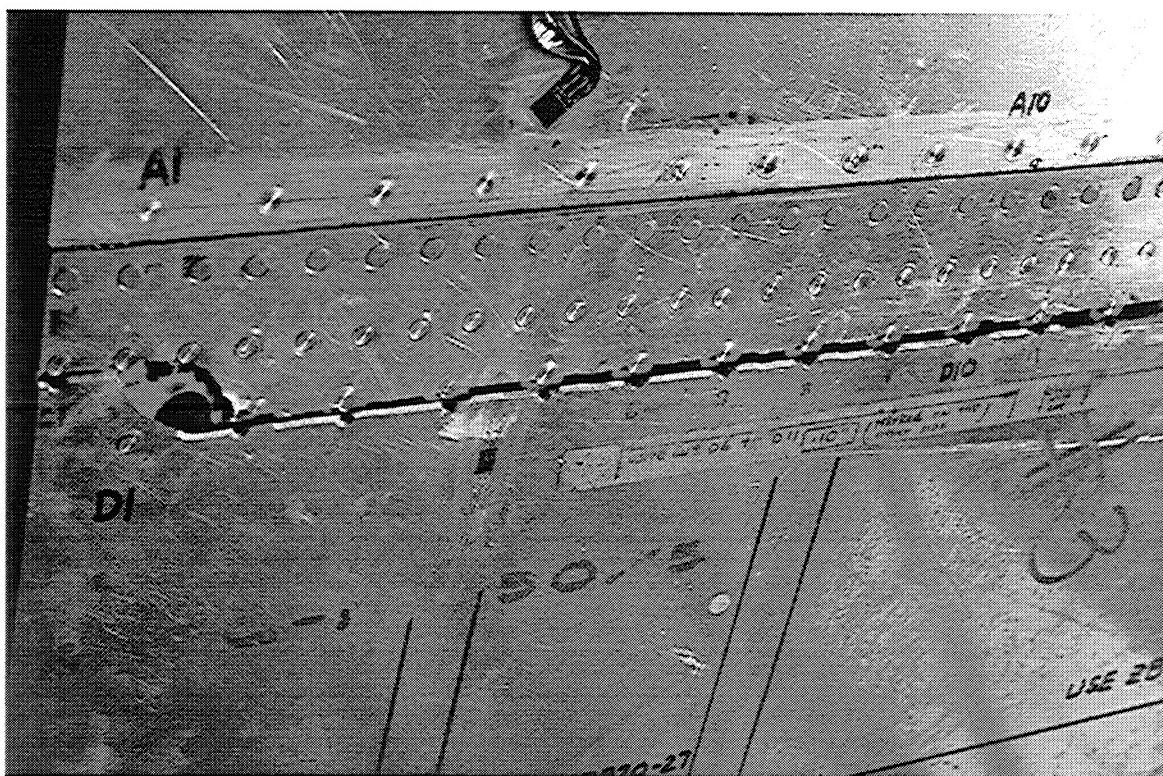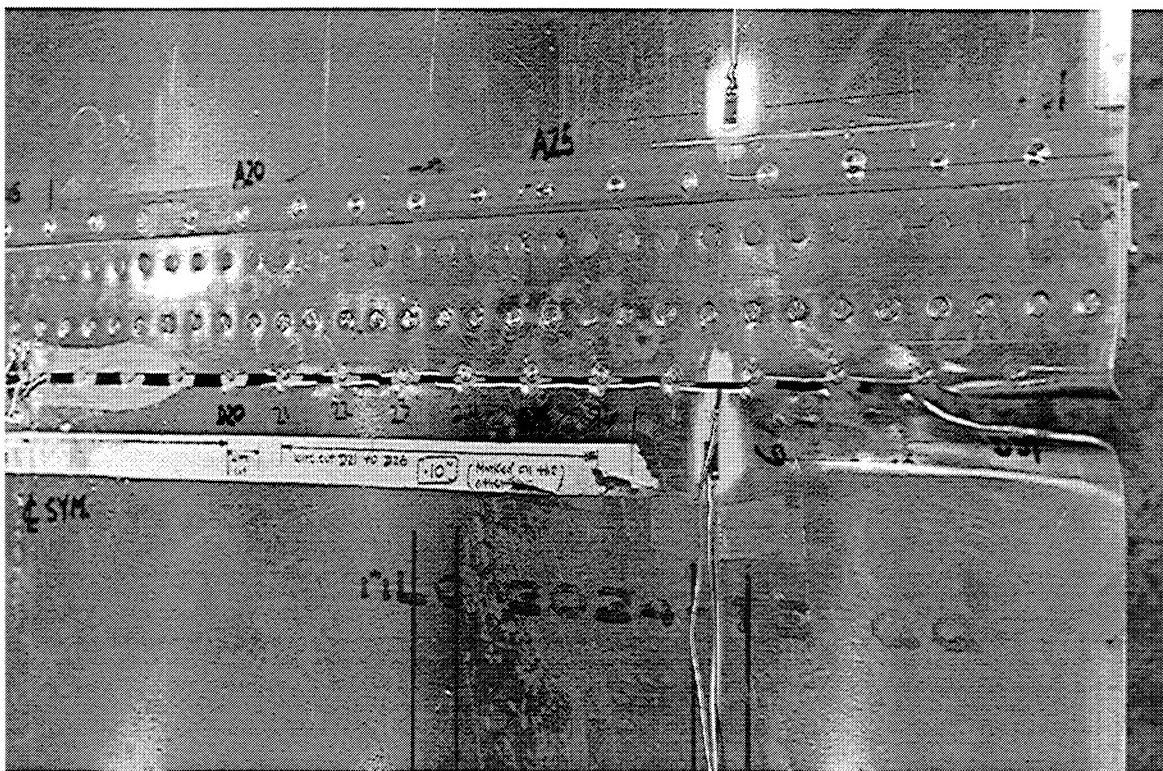
Figure 57

Figure 58

Figure 59
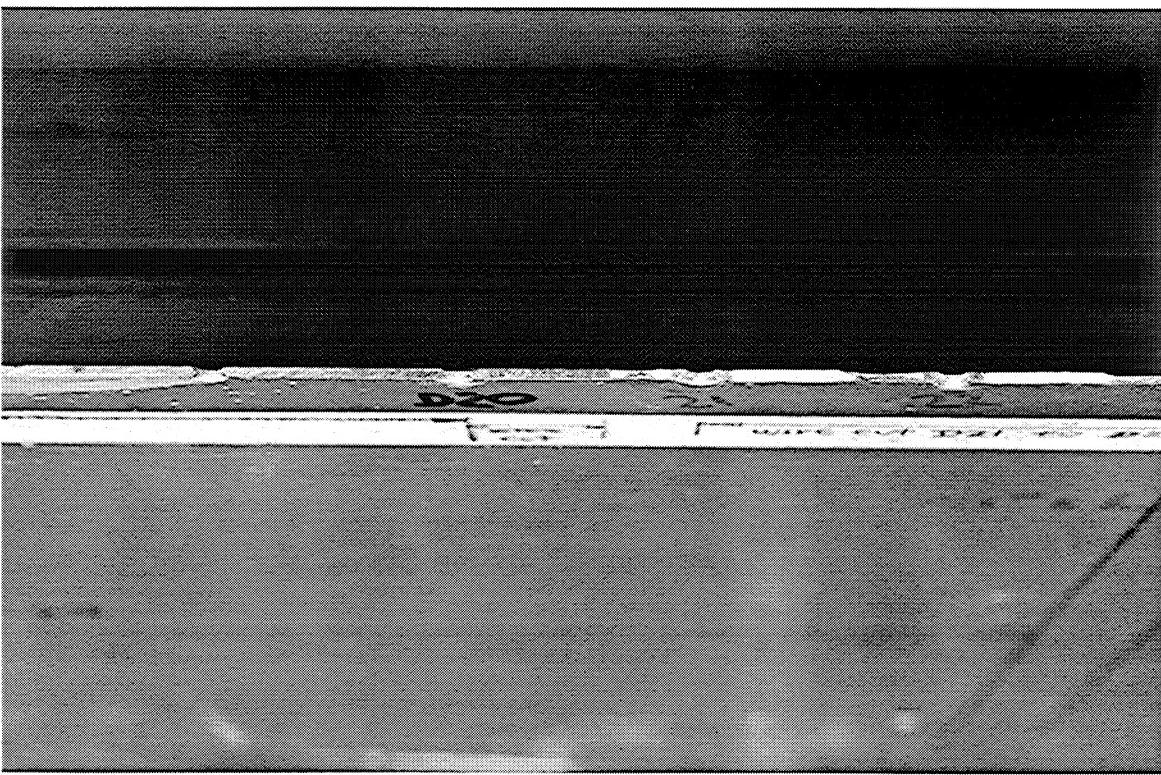
Figure 60
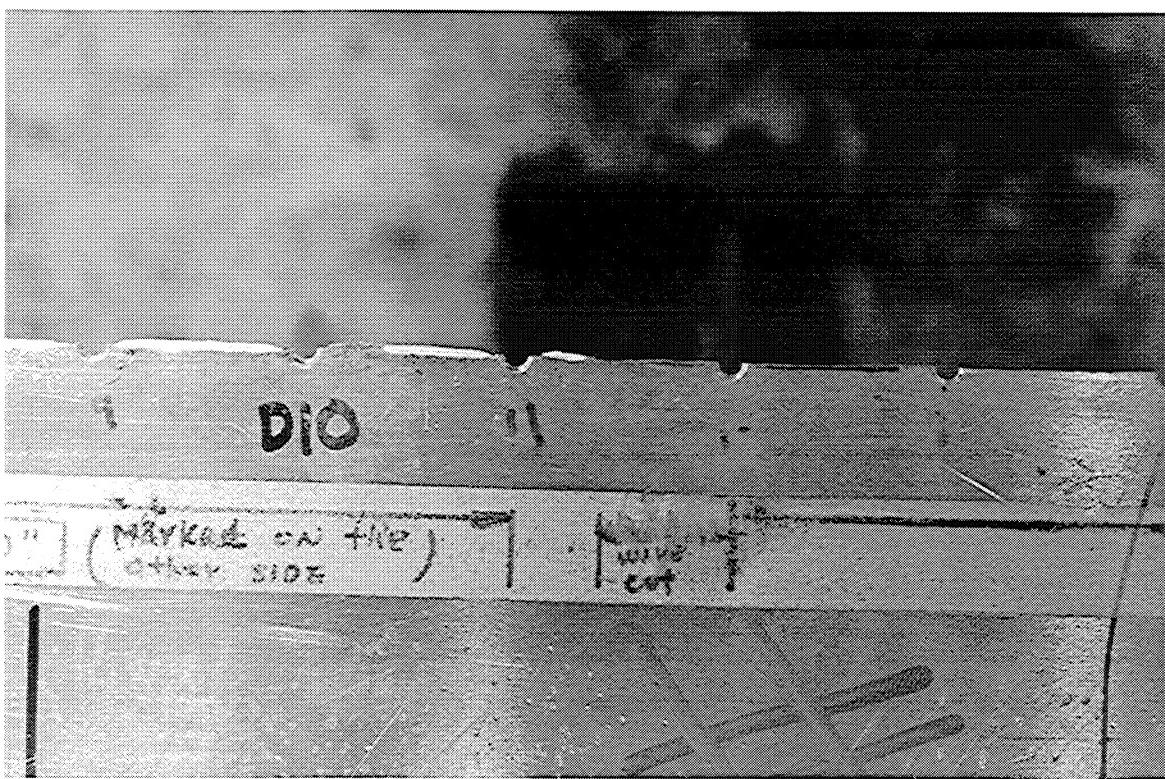
Figure 61

Figure 62
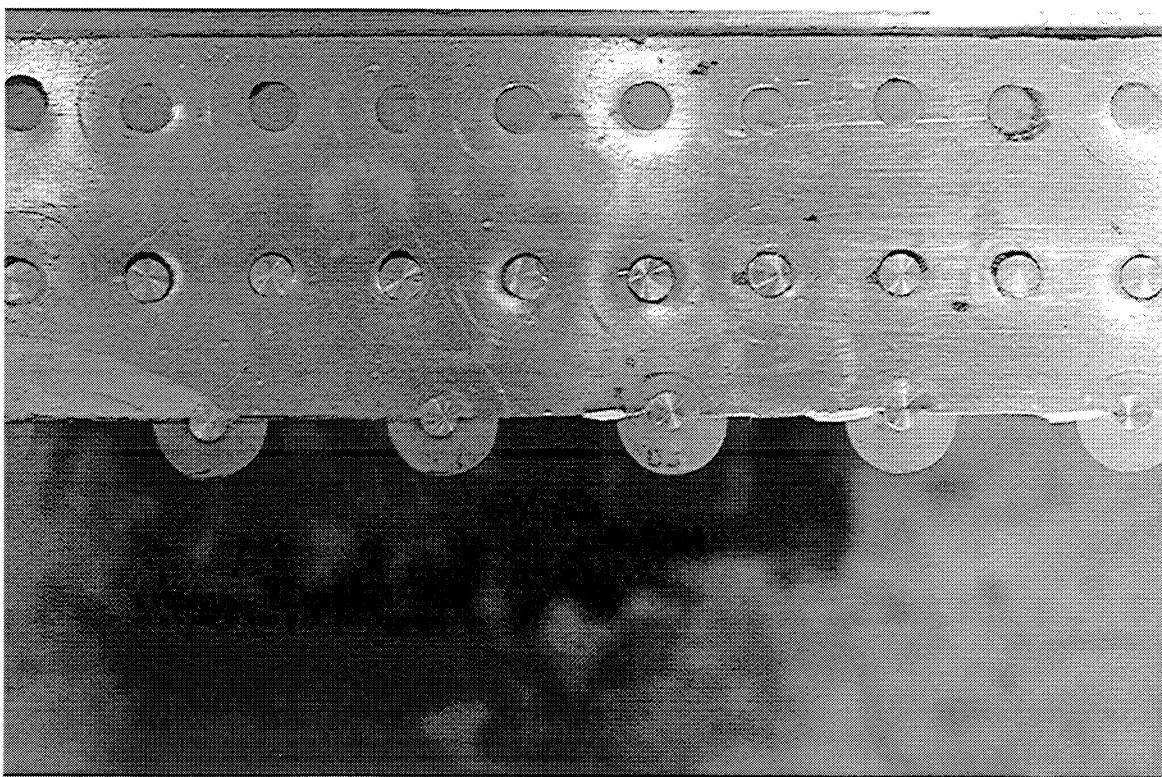
Figure 63

Figure 64

Figure 65

Figure 66

54
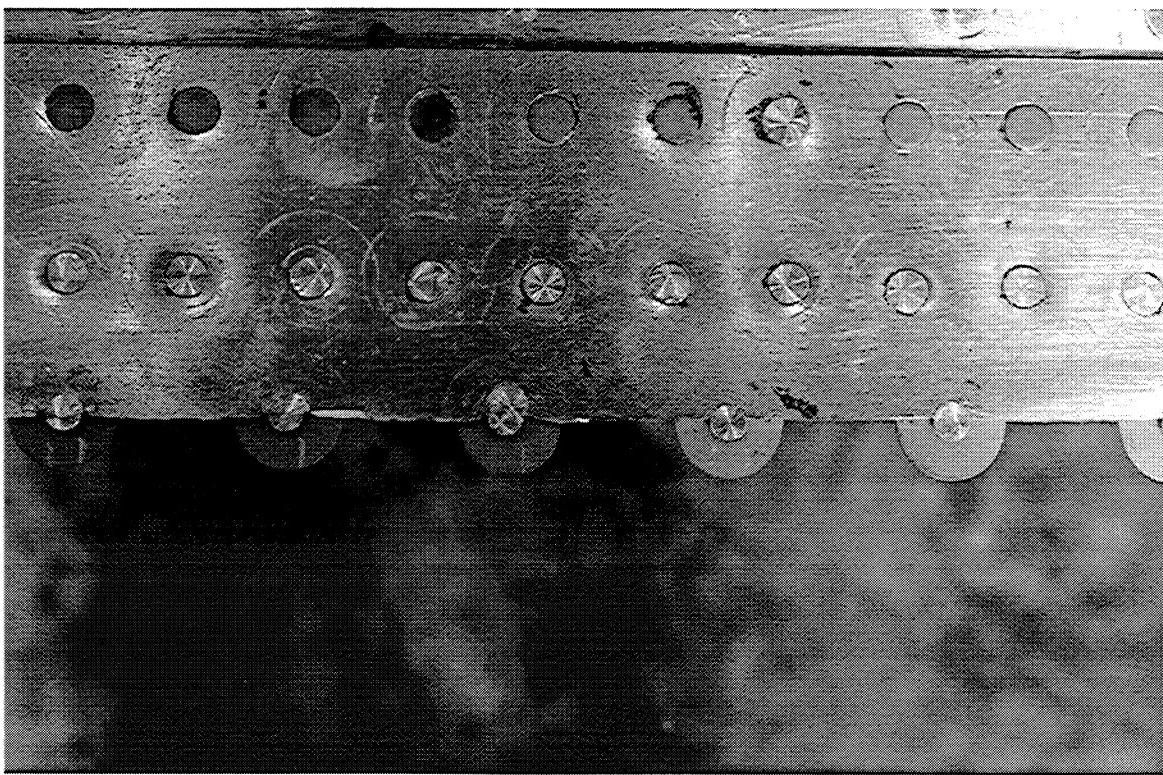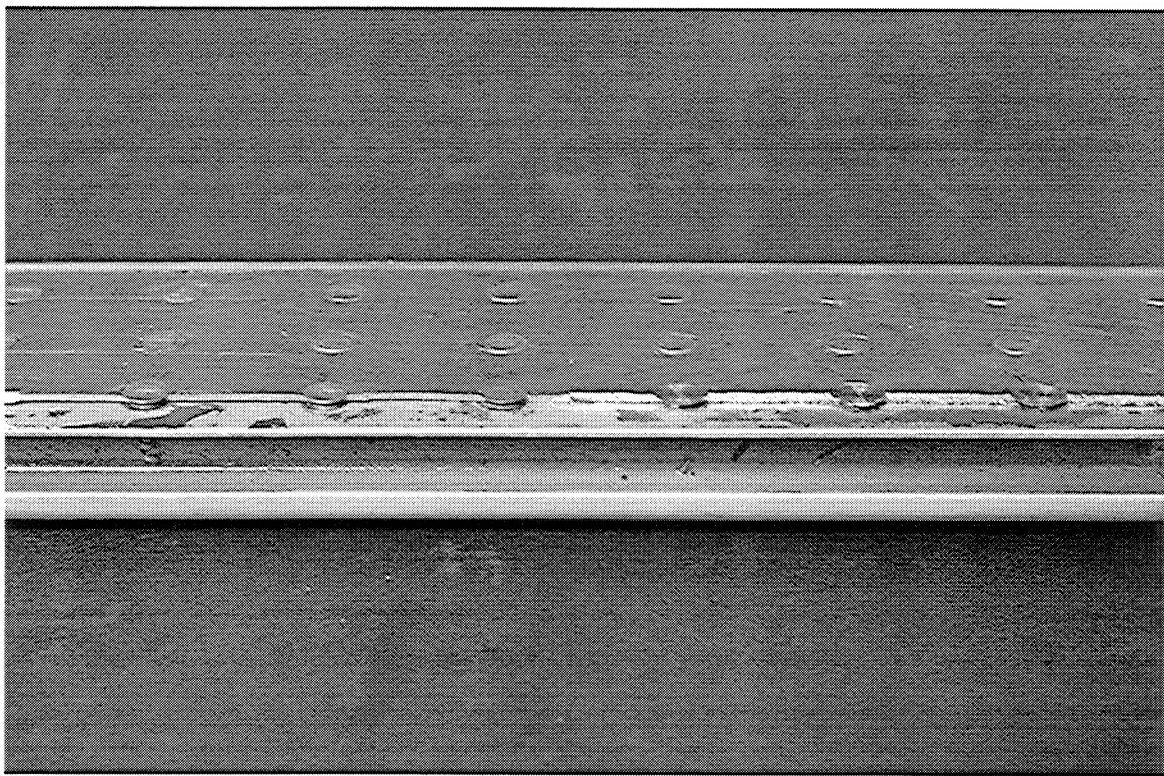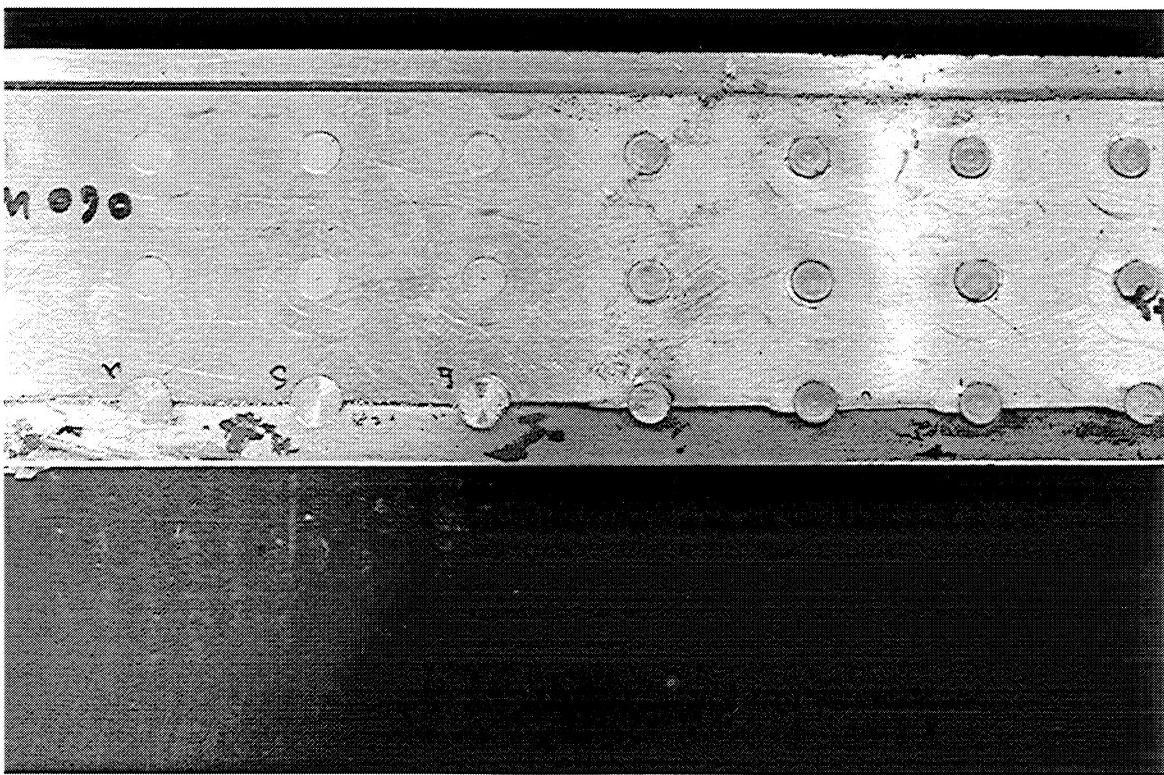
Figure 67

Figure 68
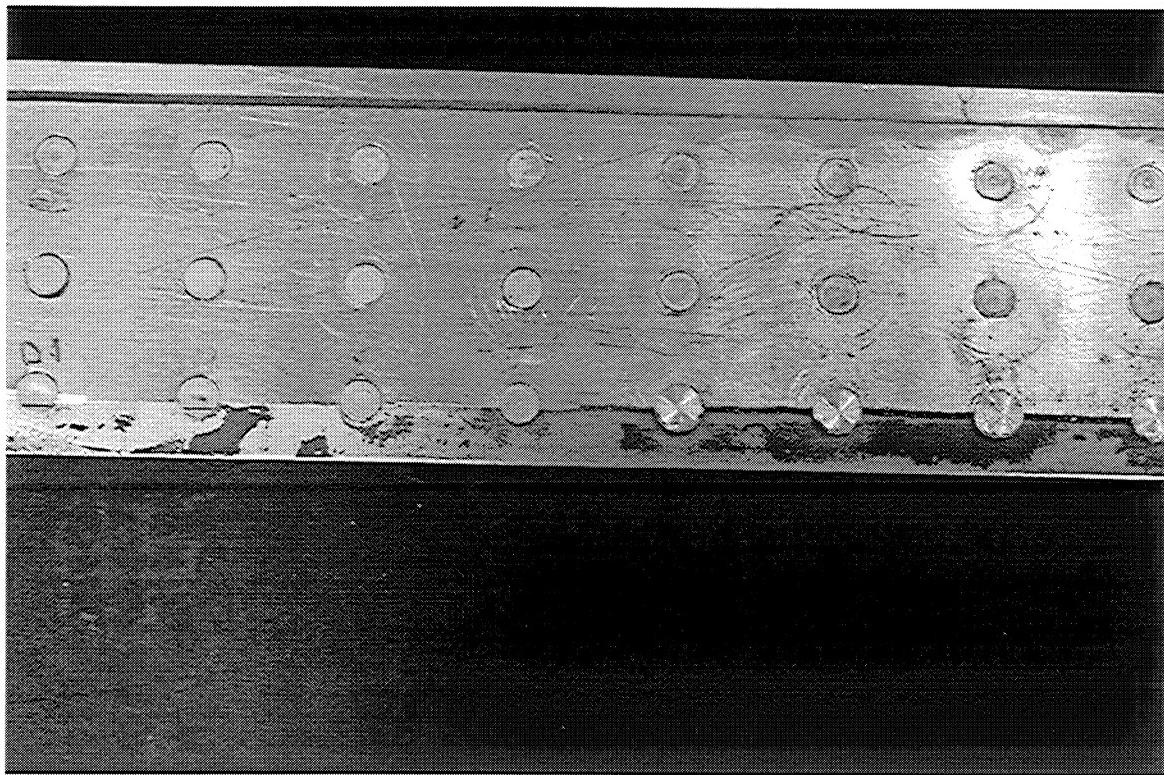
Figure 69
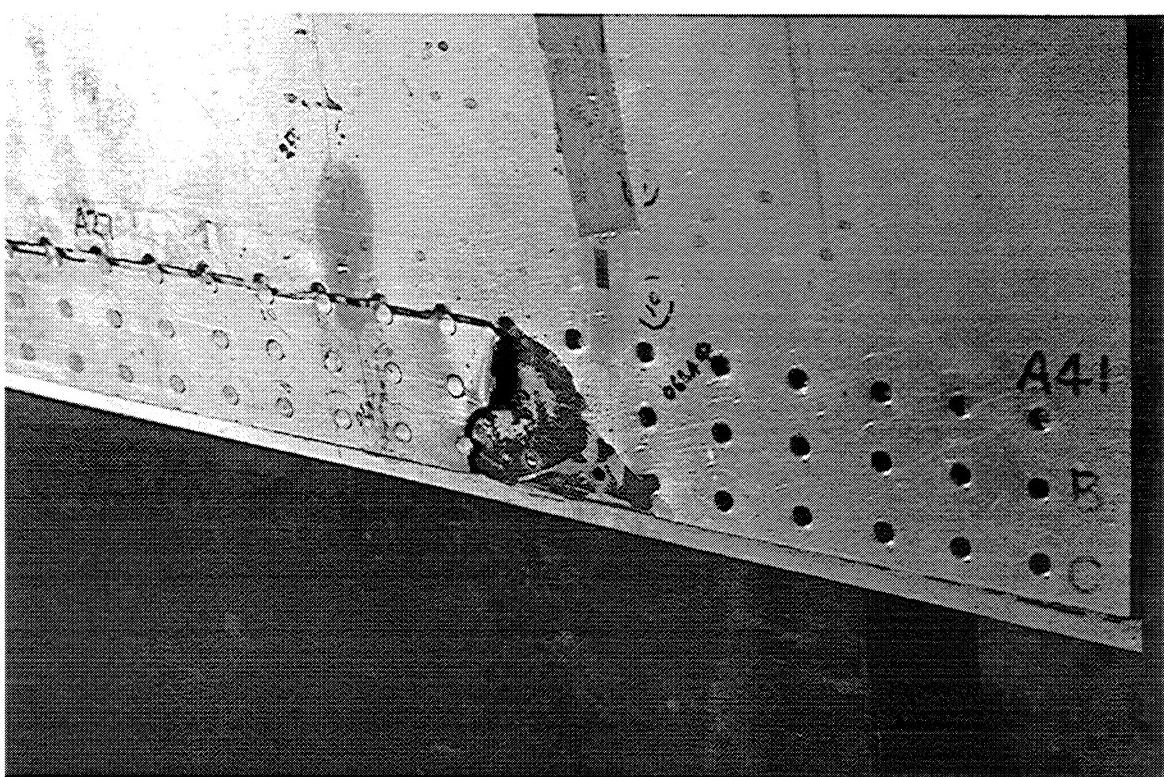
Figure 70
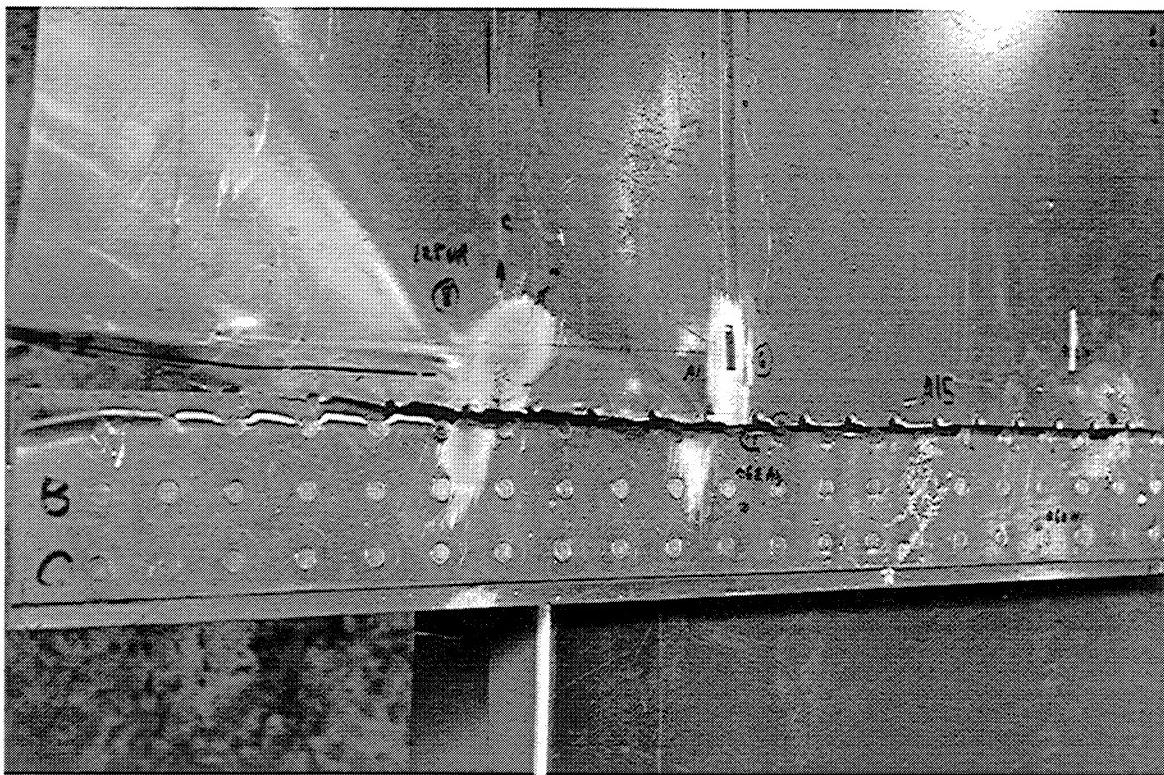
Figure 71
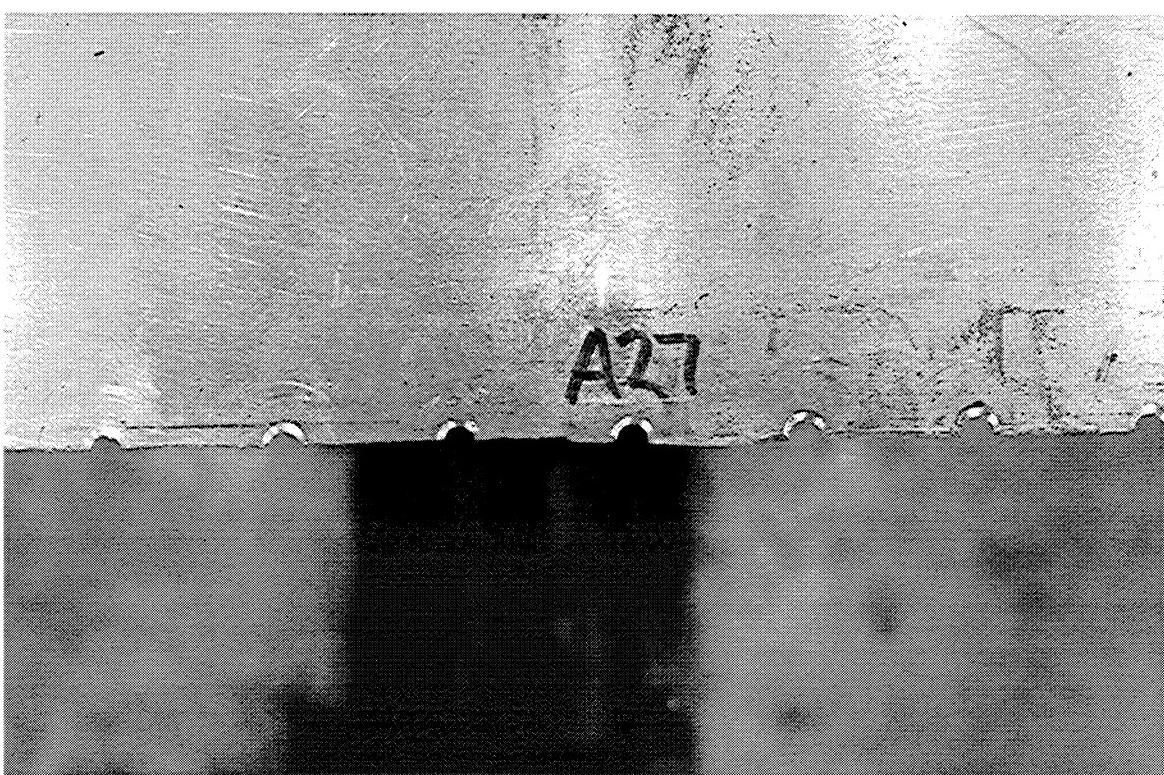
Figure 72
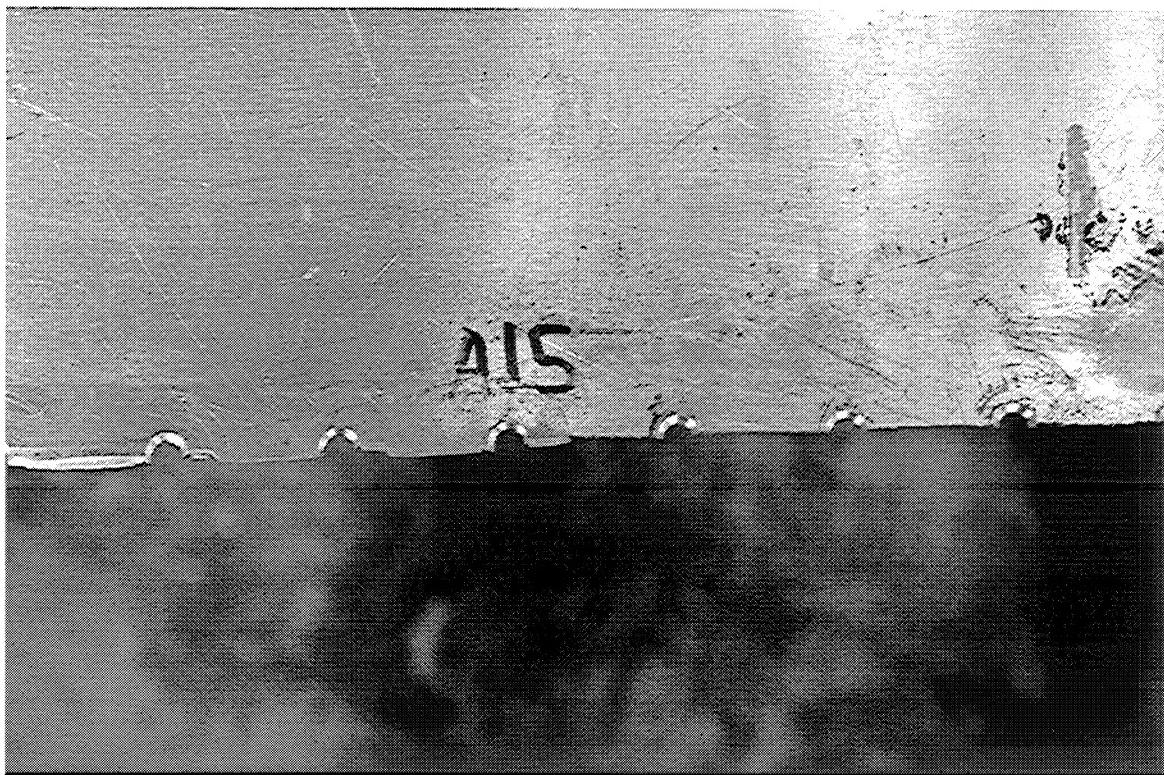
Figure 73
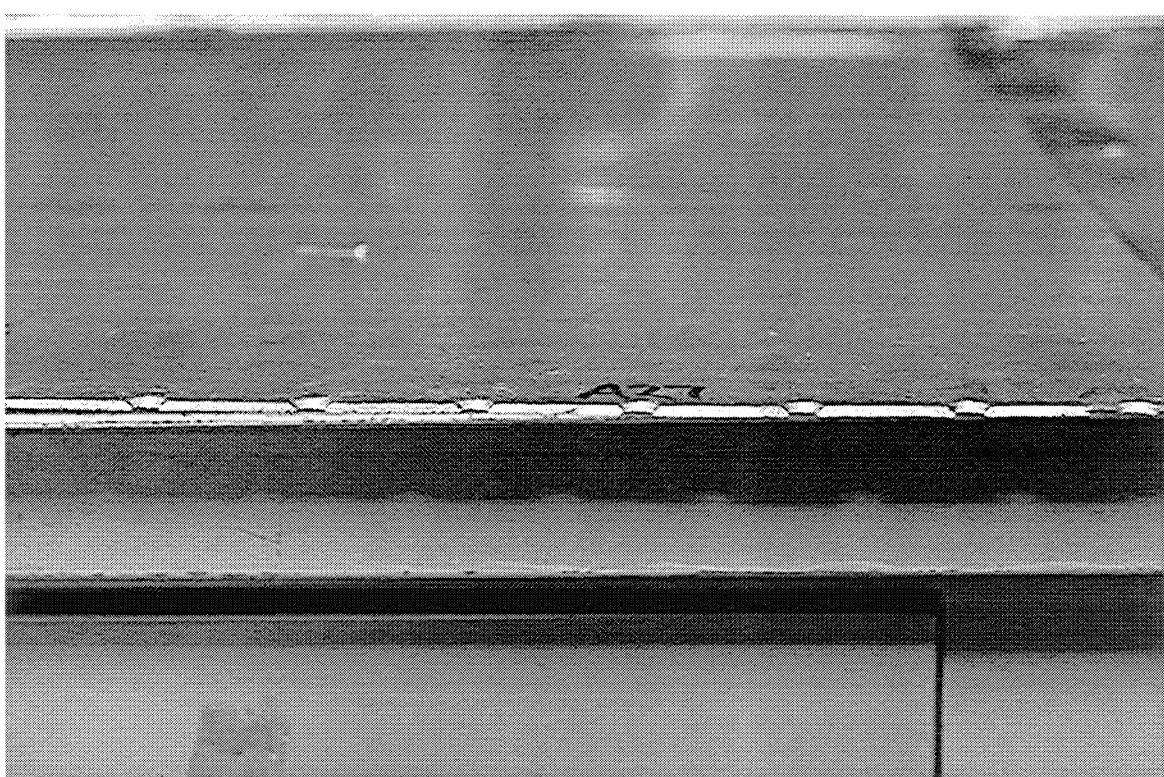
Figure 74

Figure 75
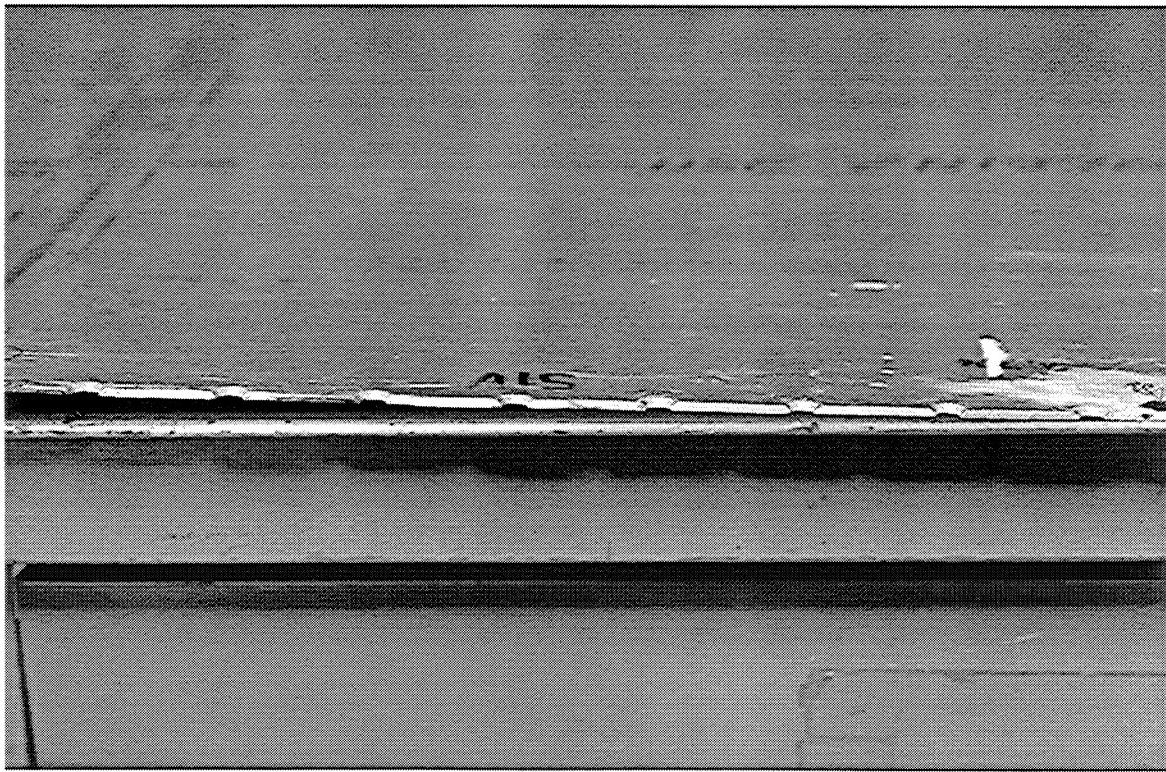
Figure 76
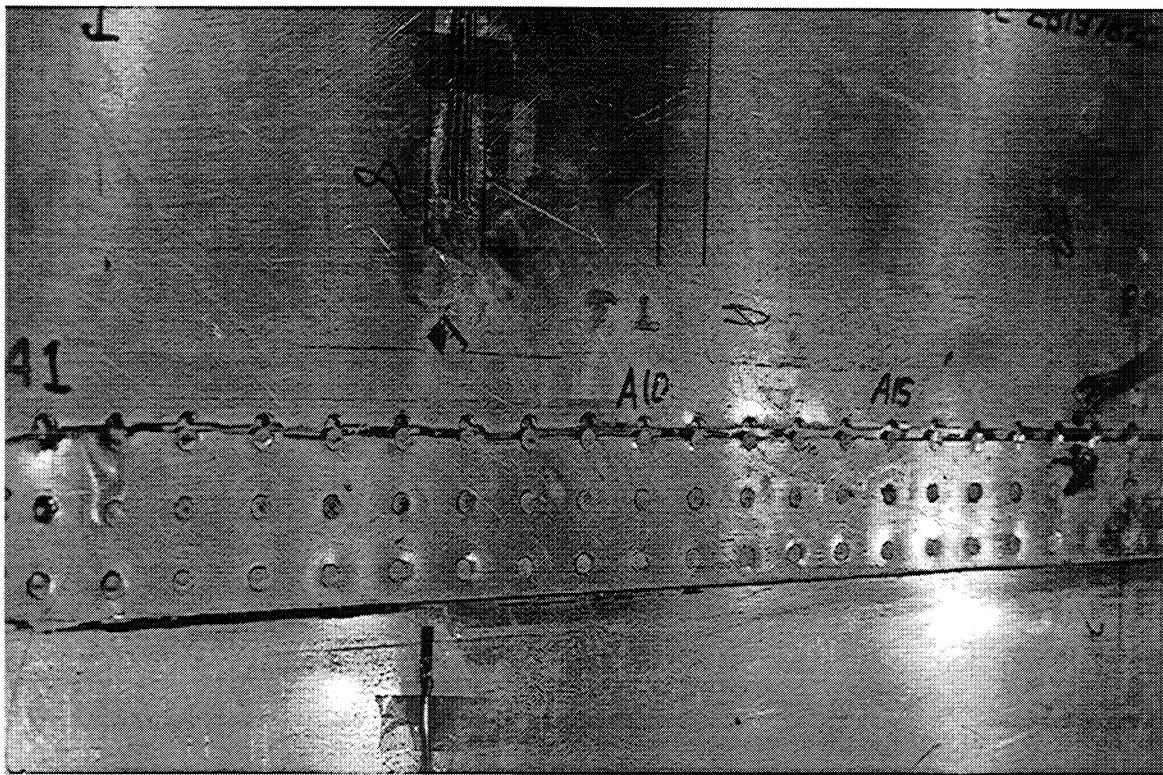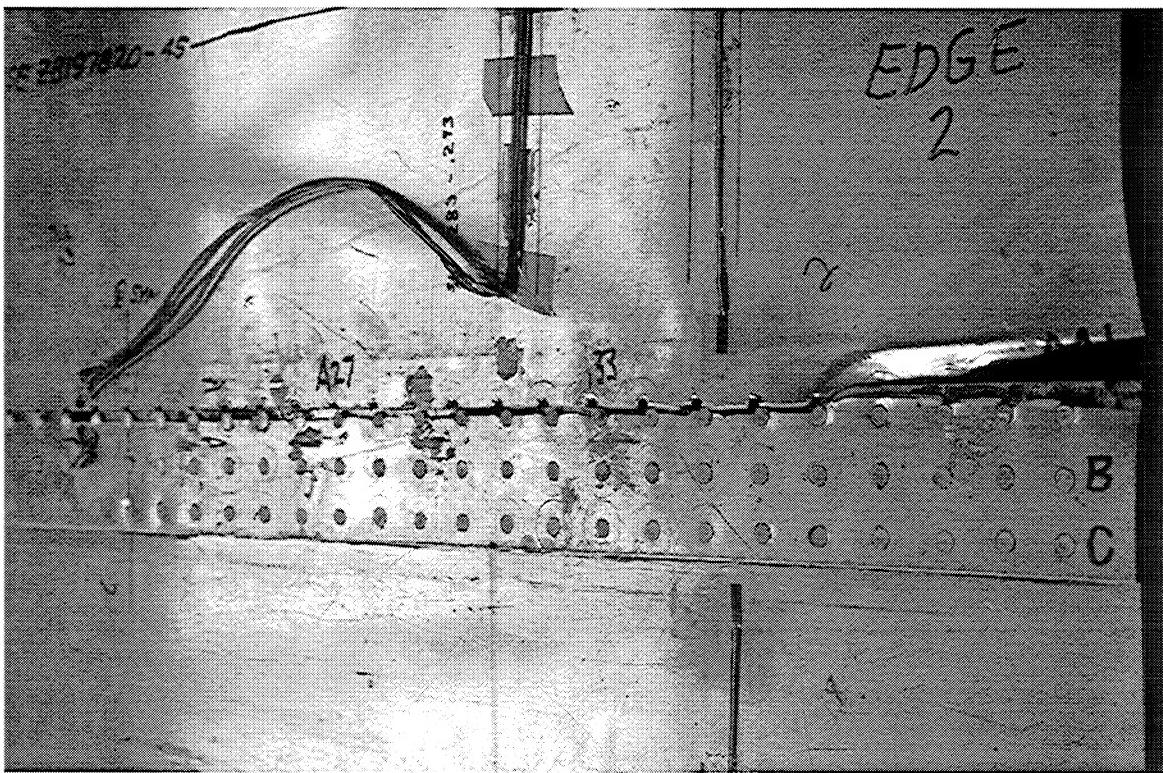
Figure 77

Figure 78
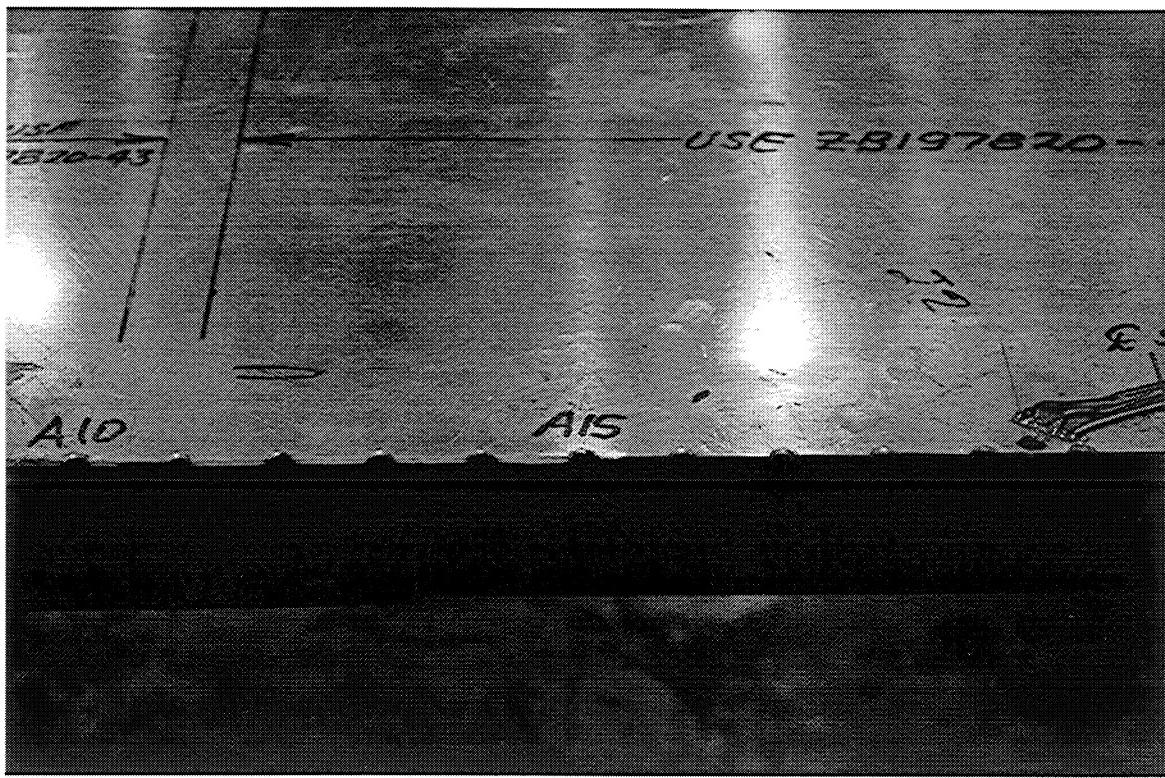
Figure 79

Figure 80

Figure 81
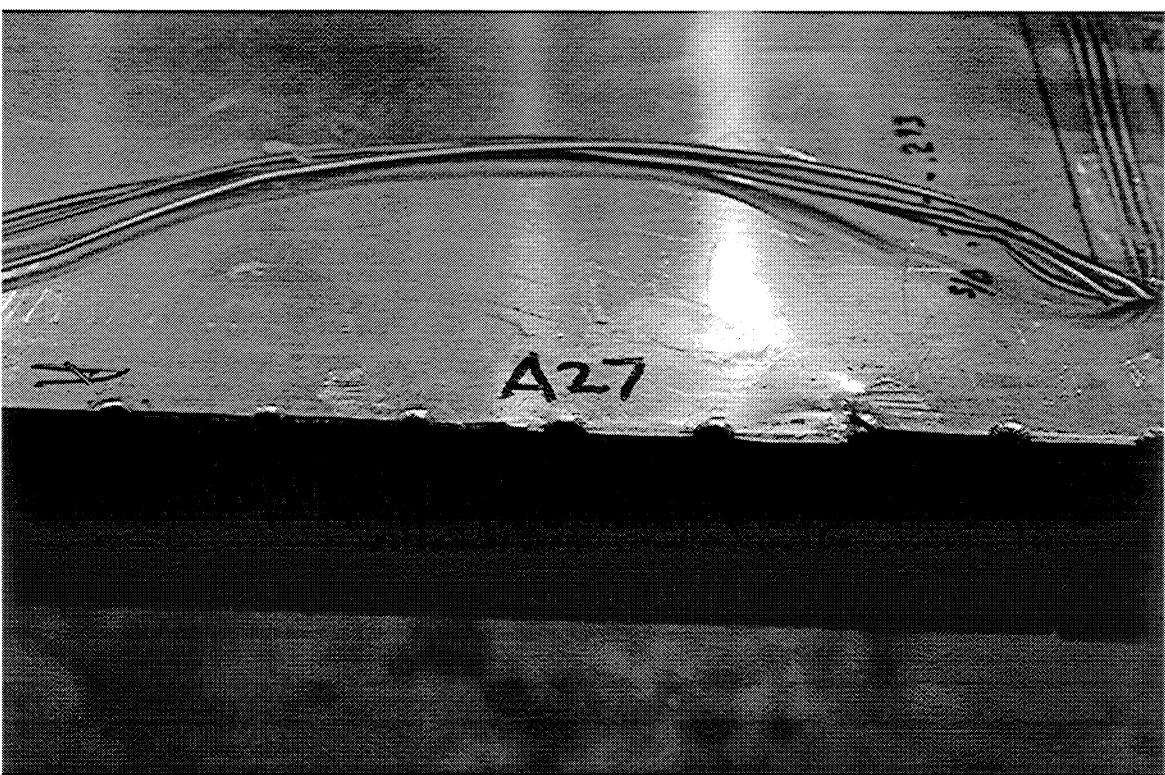
Figure 82
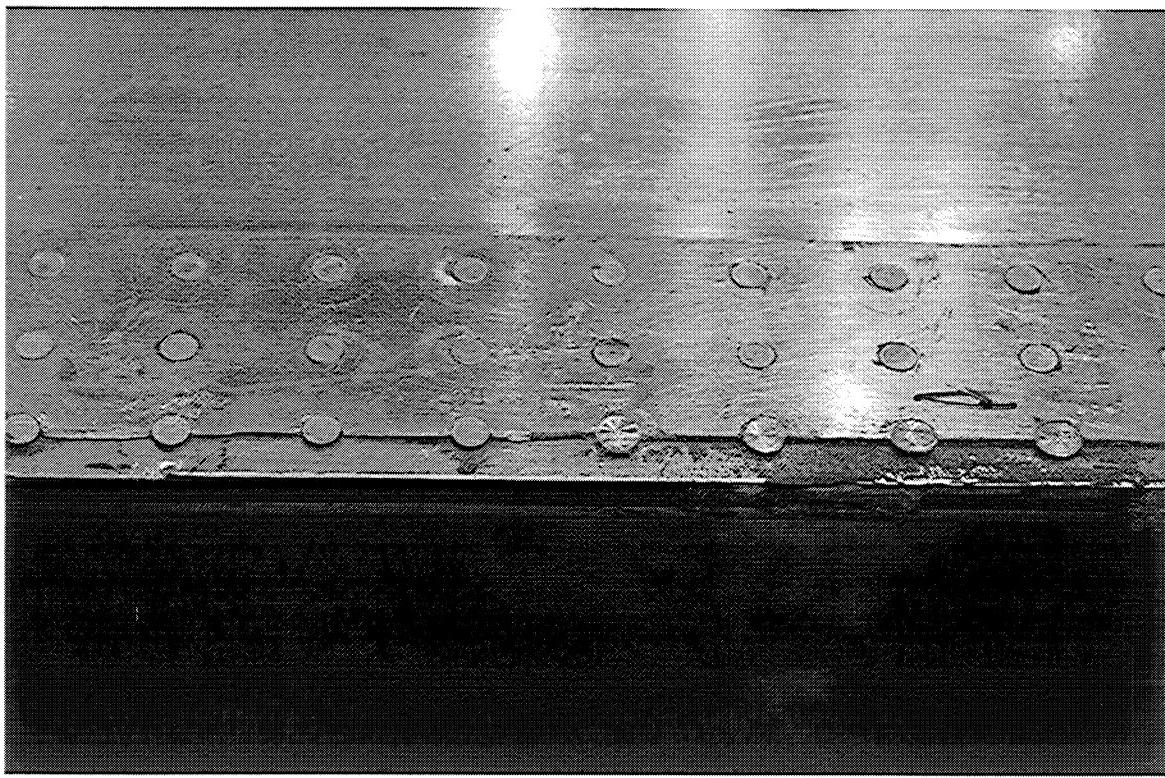
Figure 83
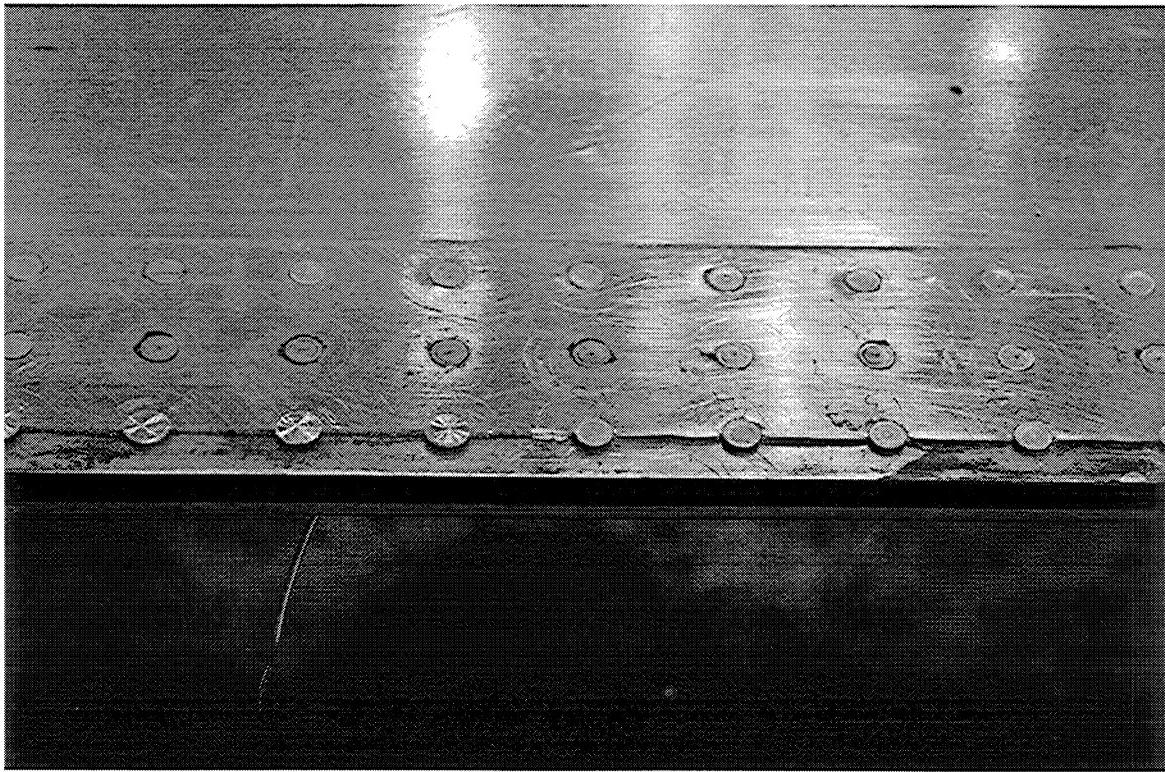
Figure 84
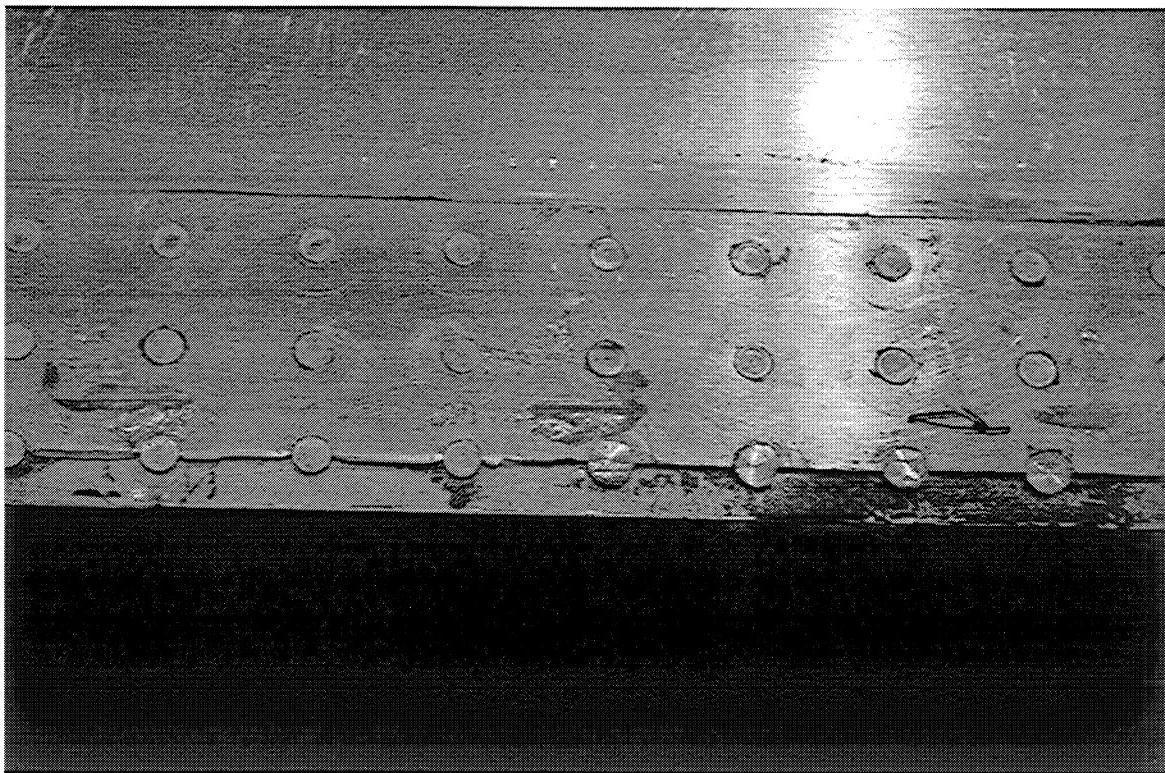
Figure 85
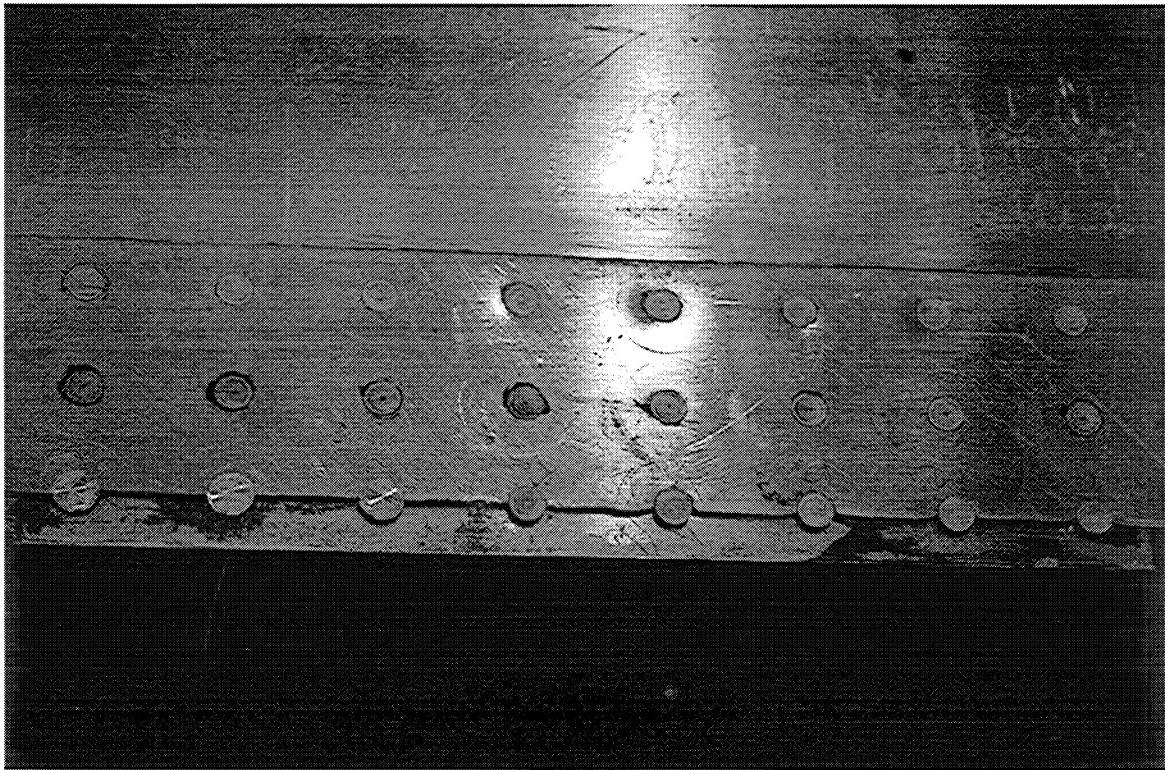
Figure 86
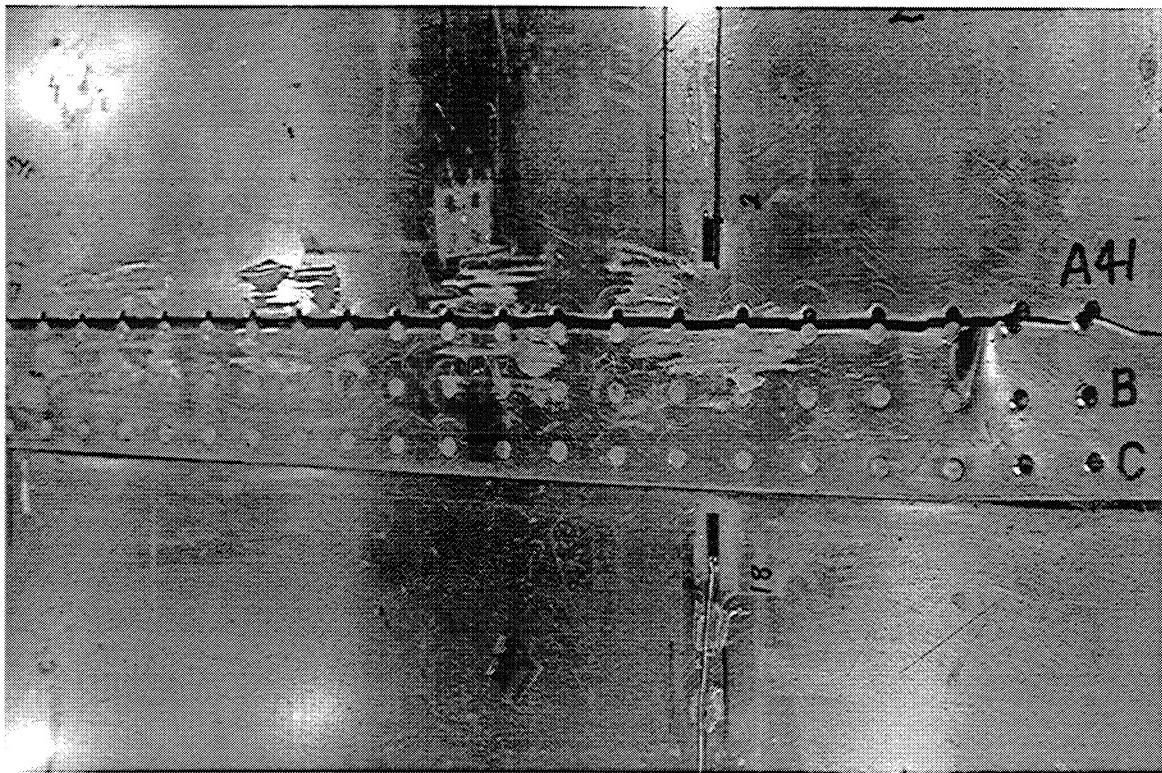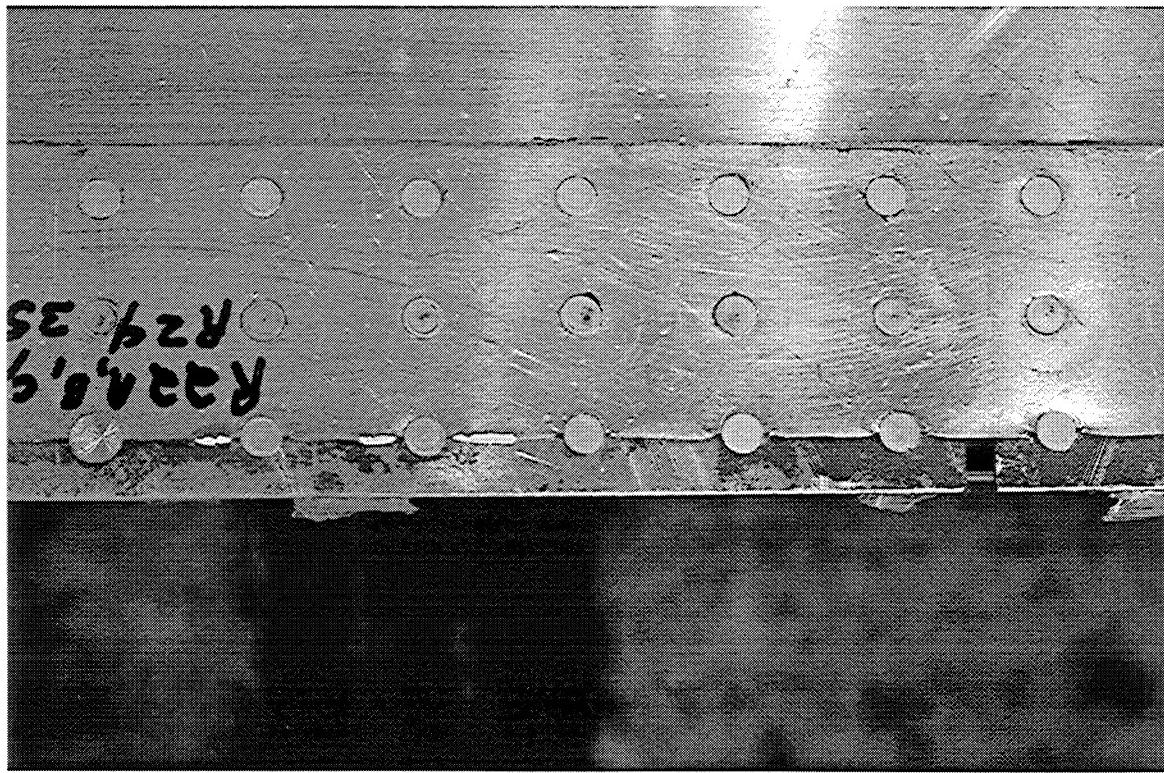
Figure 87

Figure 88

Figure 89
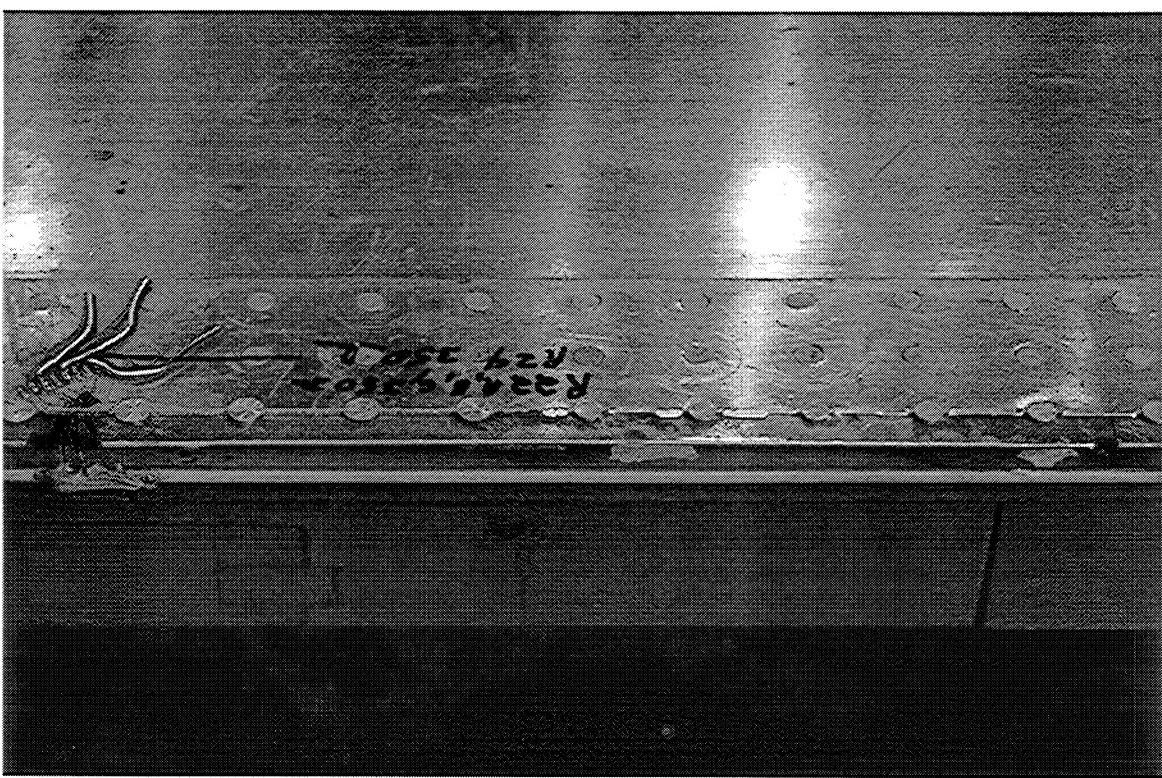
Figure 90

Figure 91
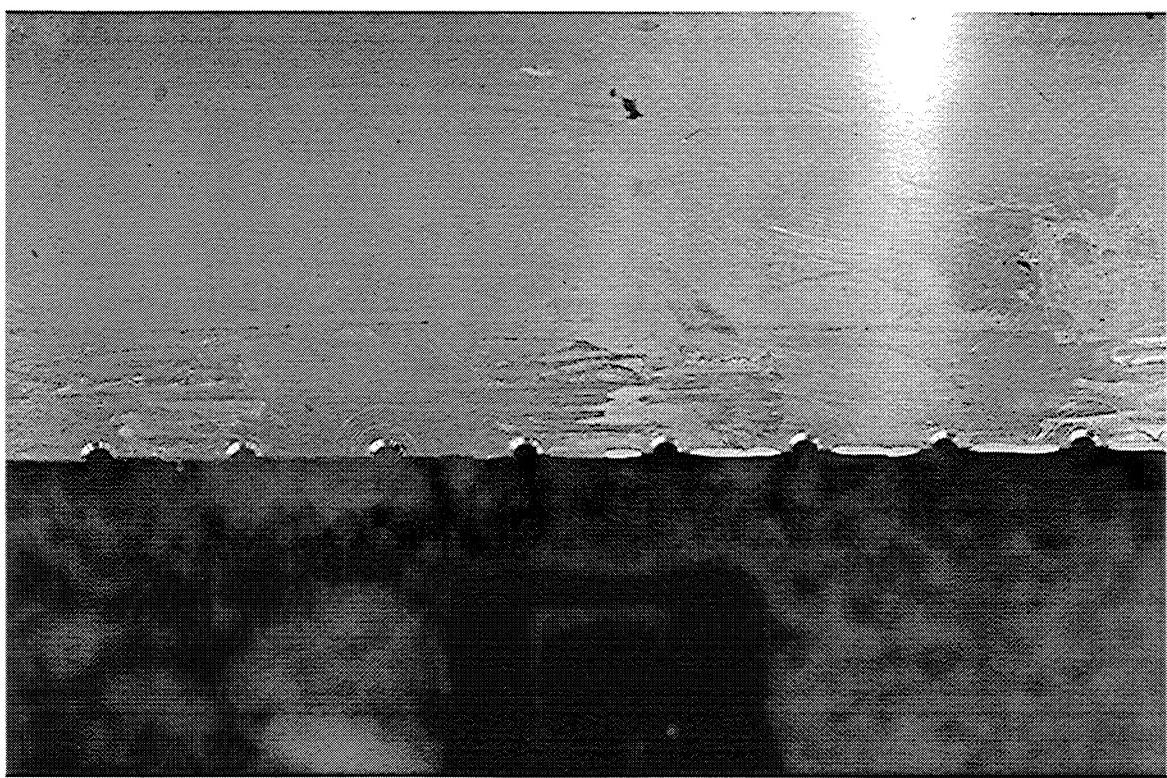
Figure 92
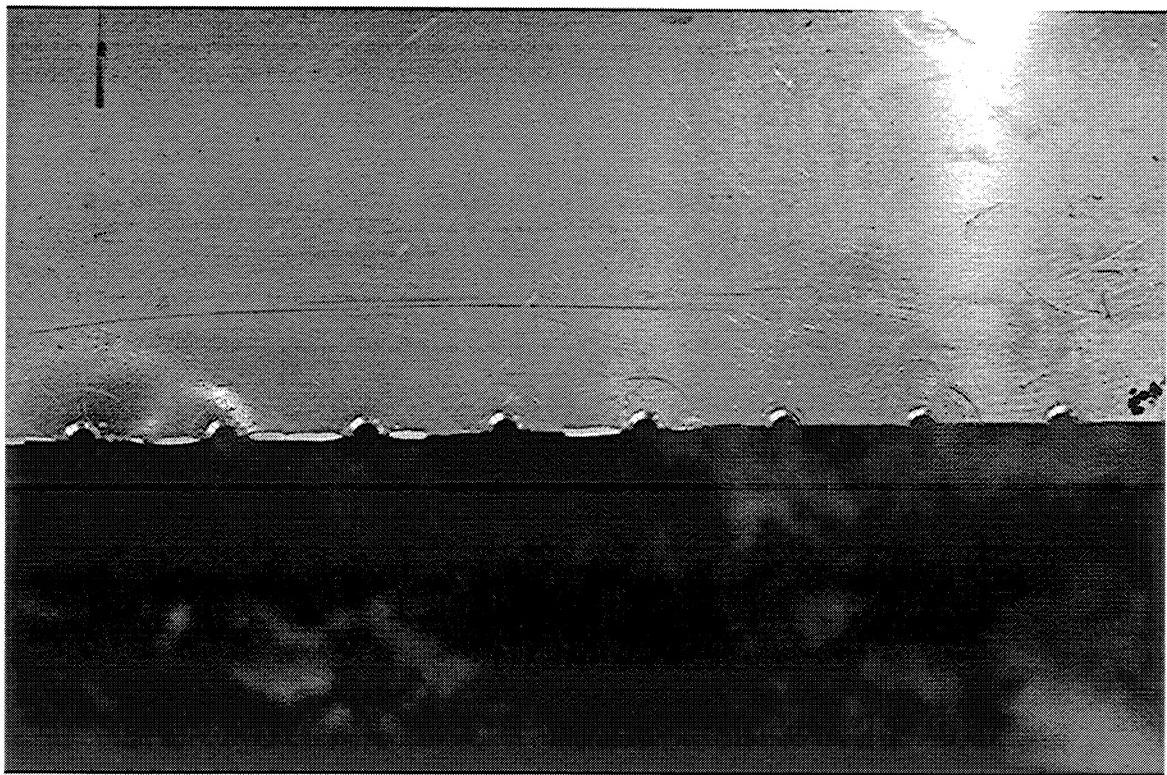
Figure 93
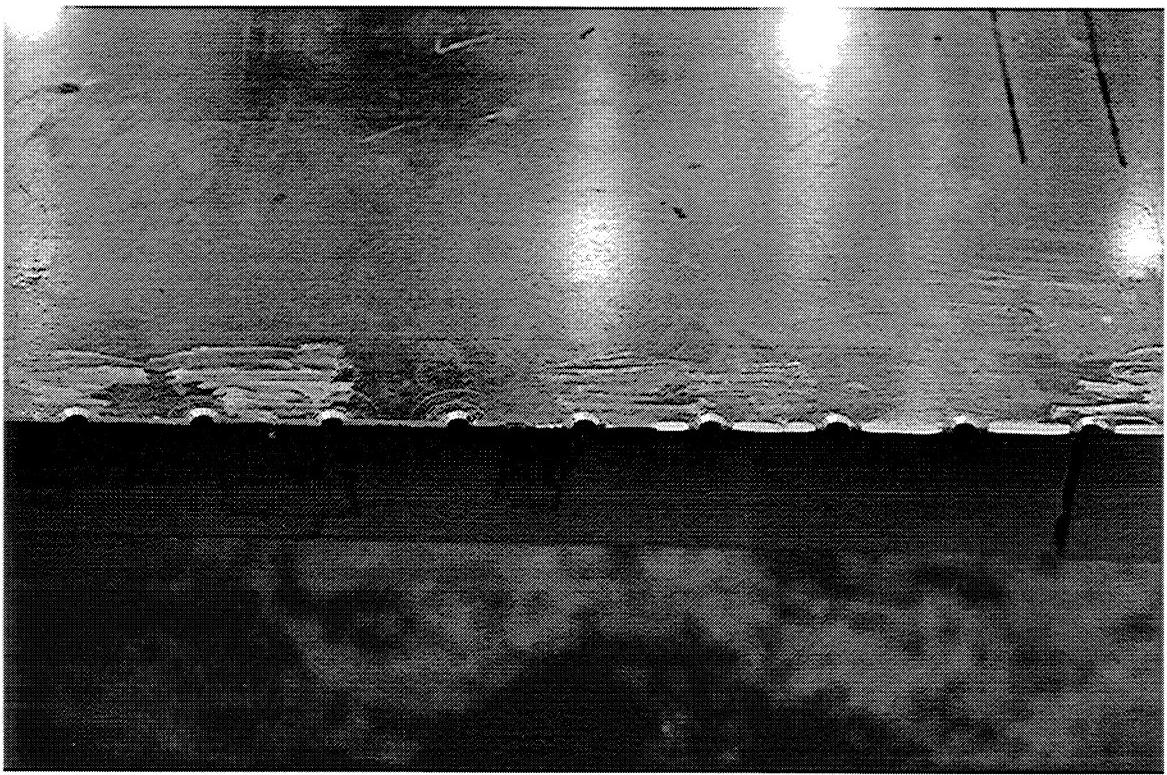
Figure 94
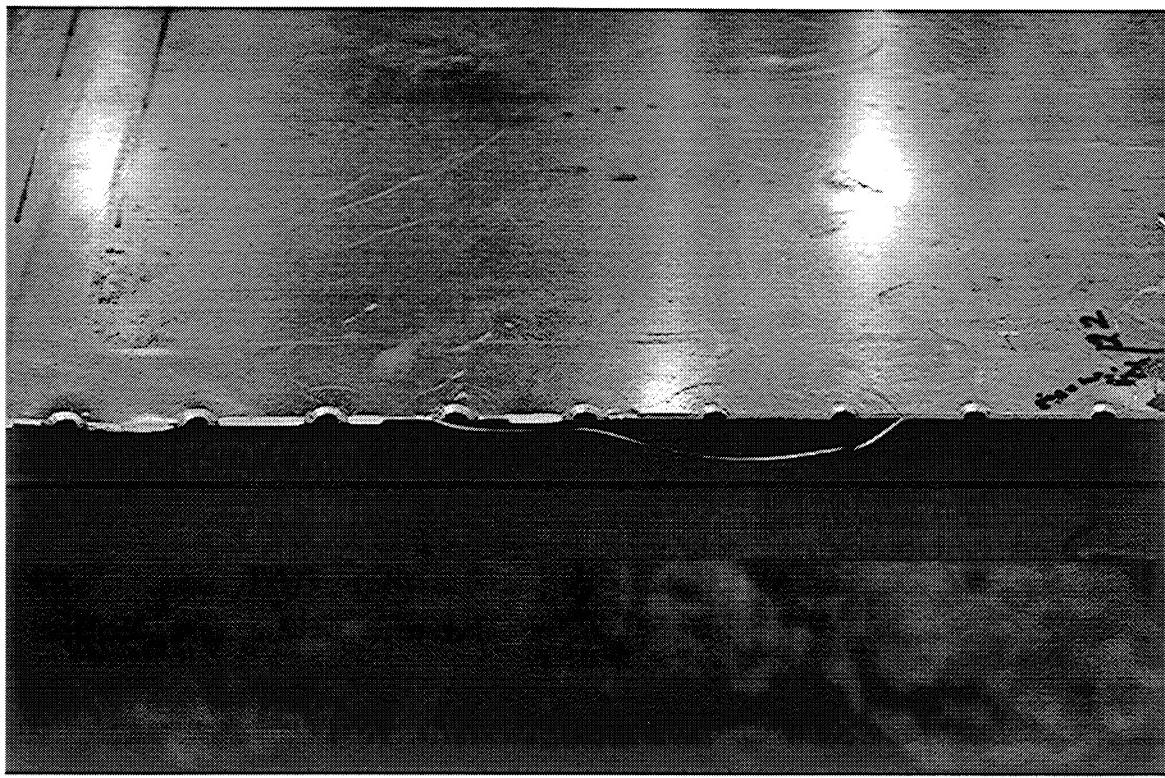
Figure 95
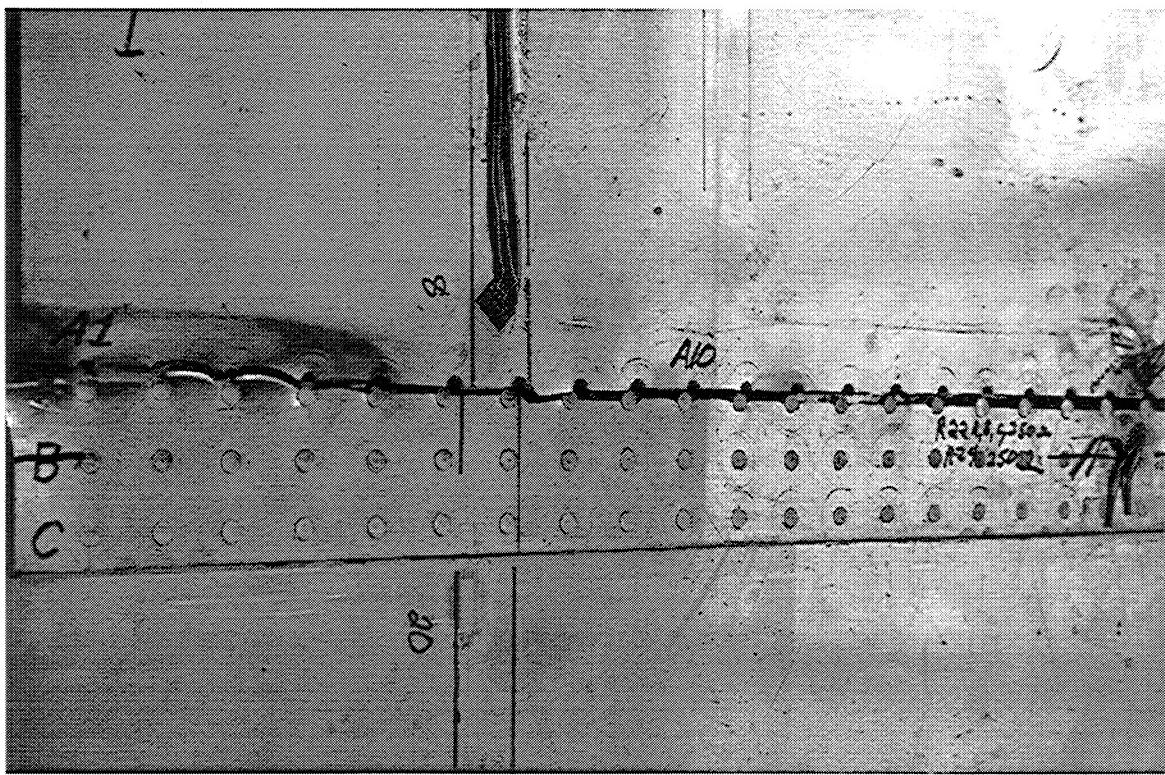
Figure 96
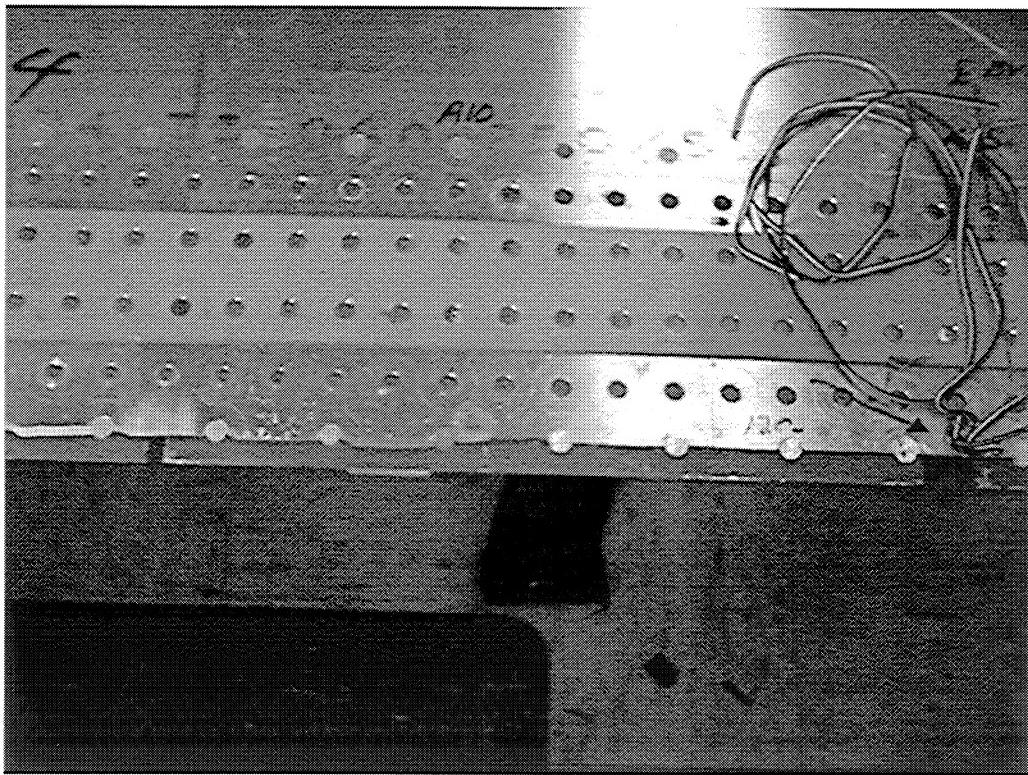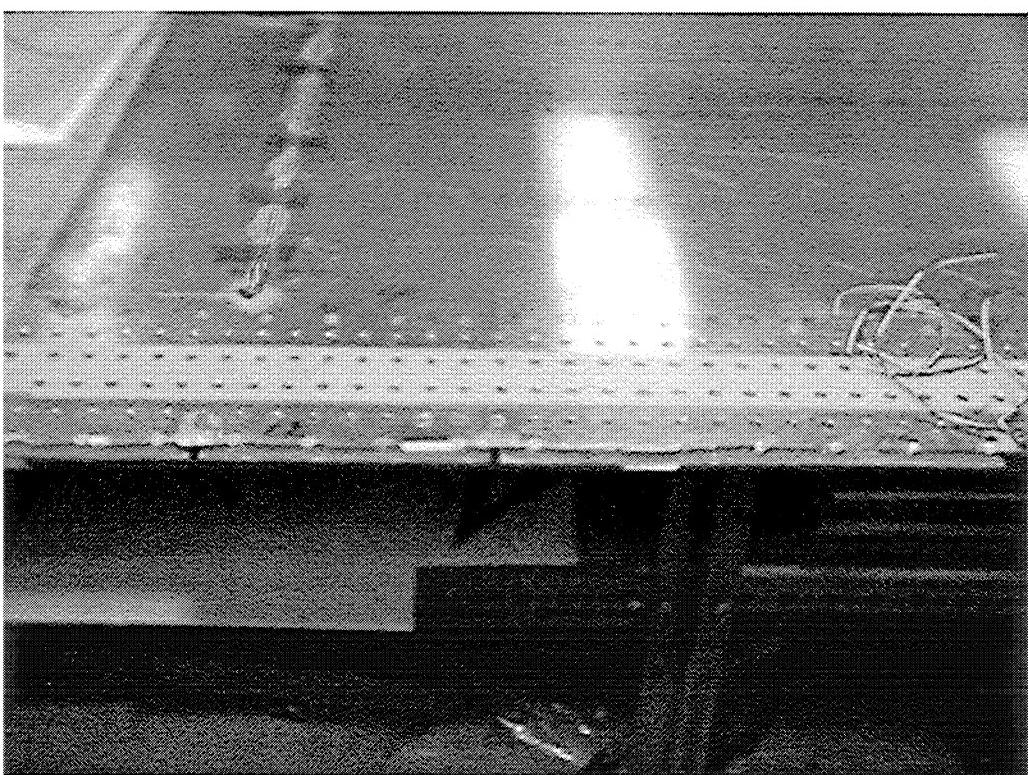
Figure 97

Figure 98
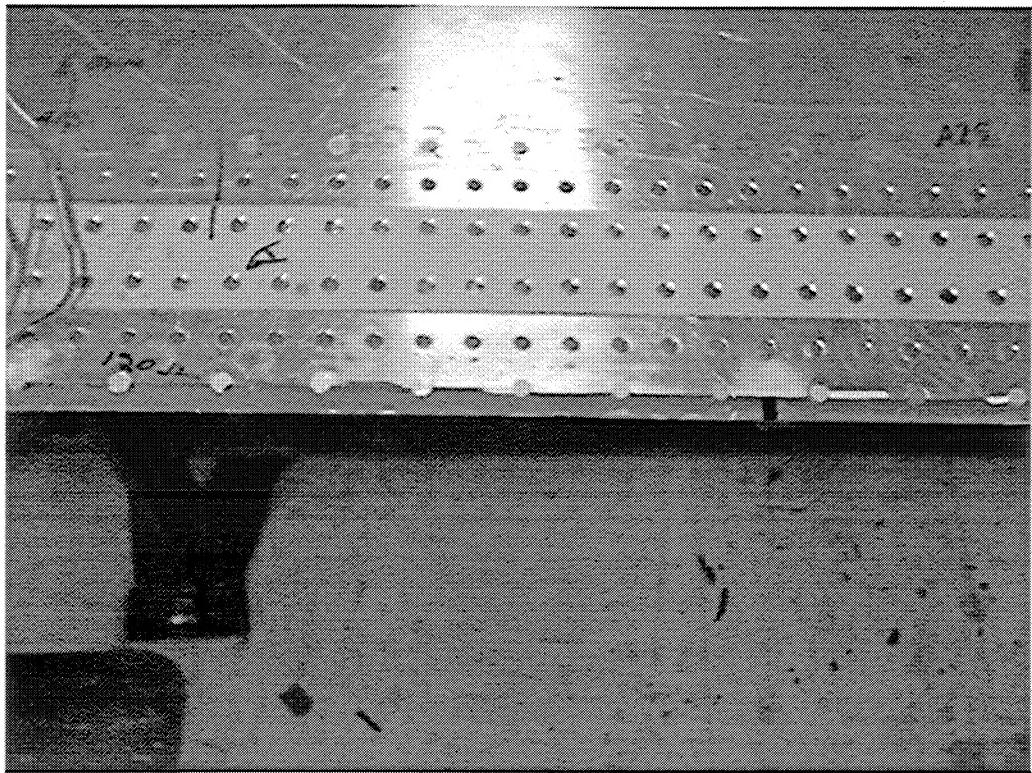
Figure 99
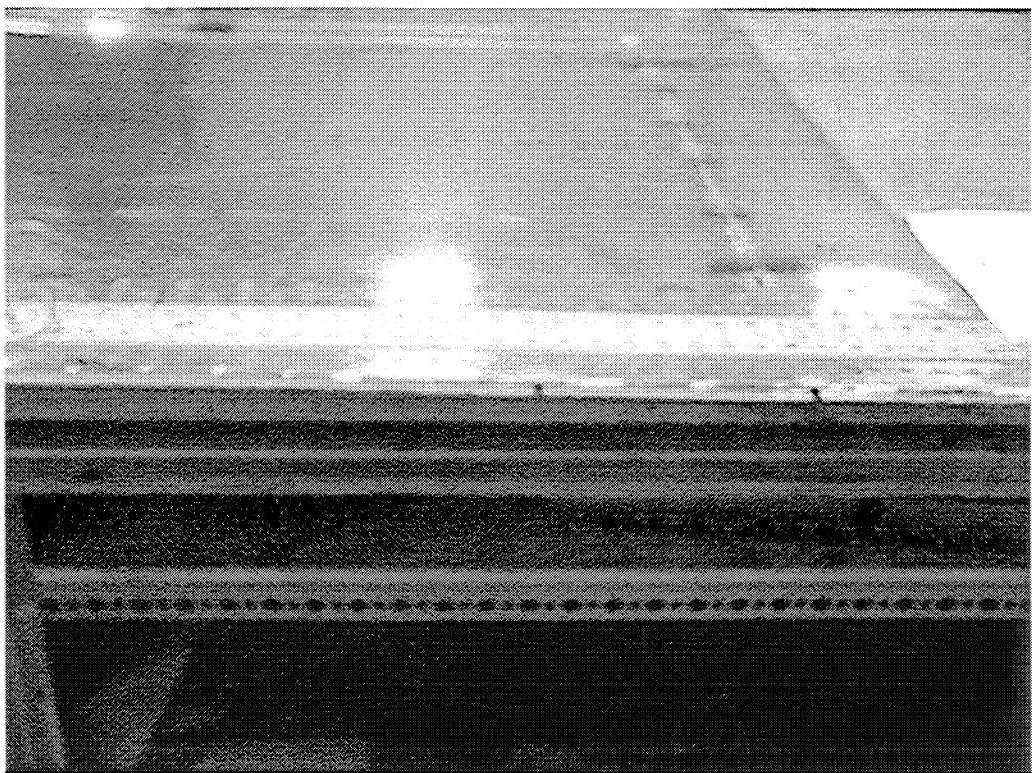
Figure 100
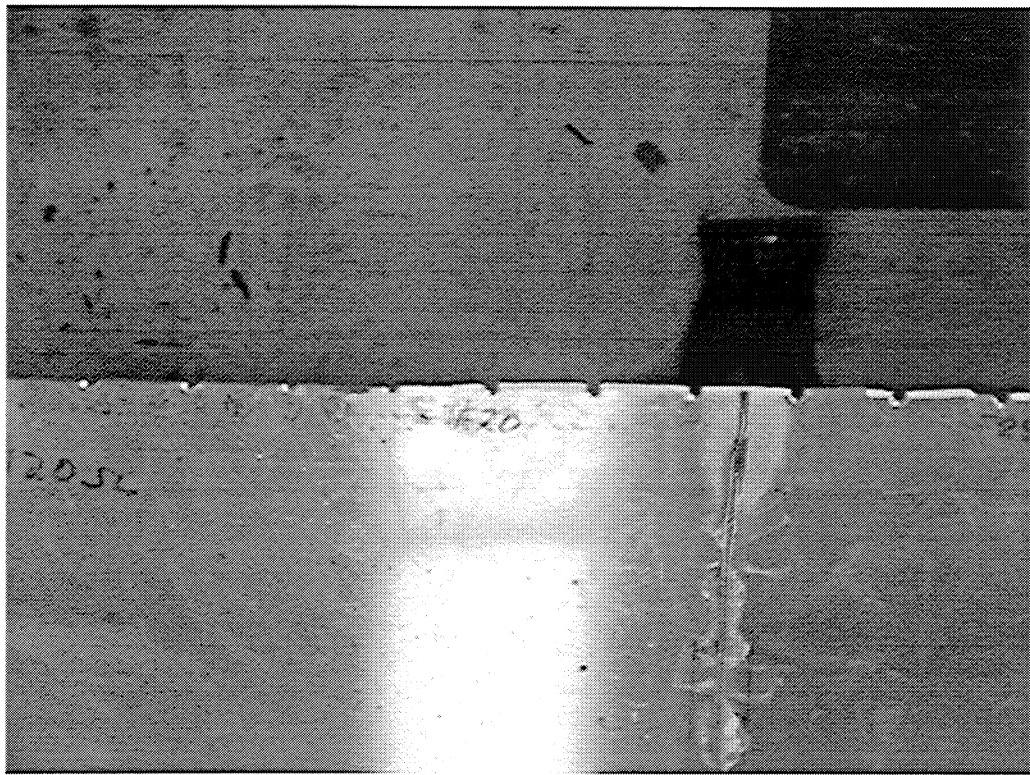
Figure 101
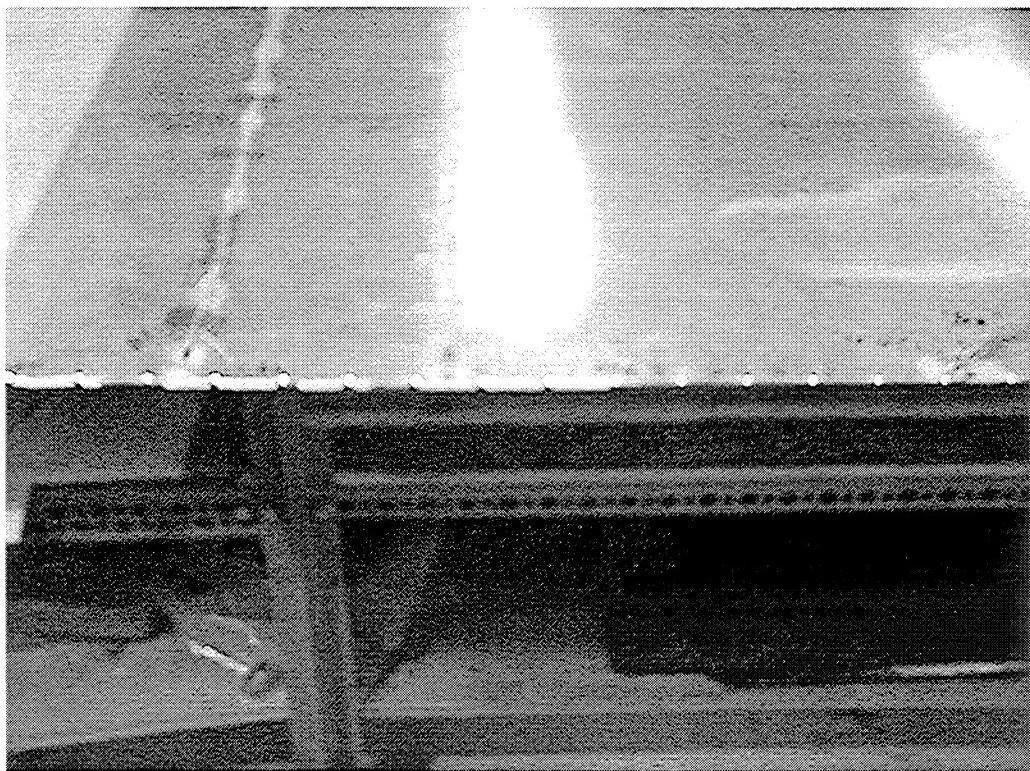
Figure 102
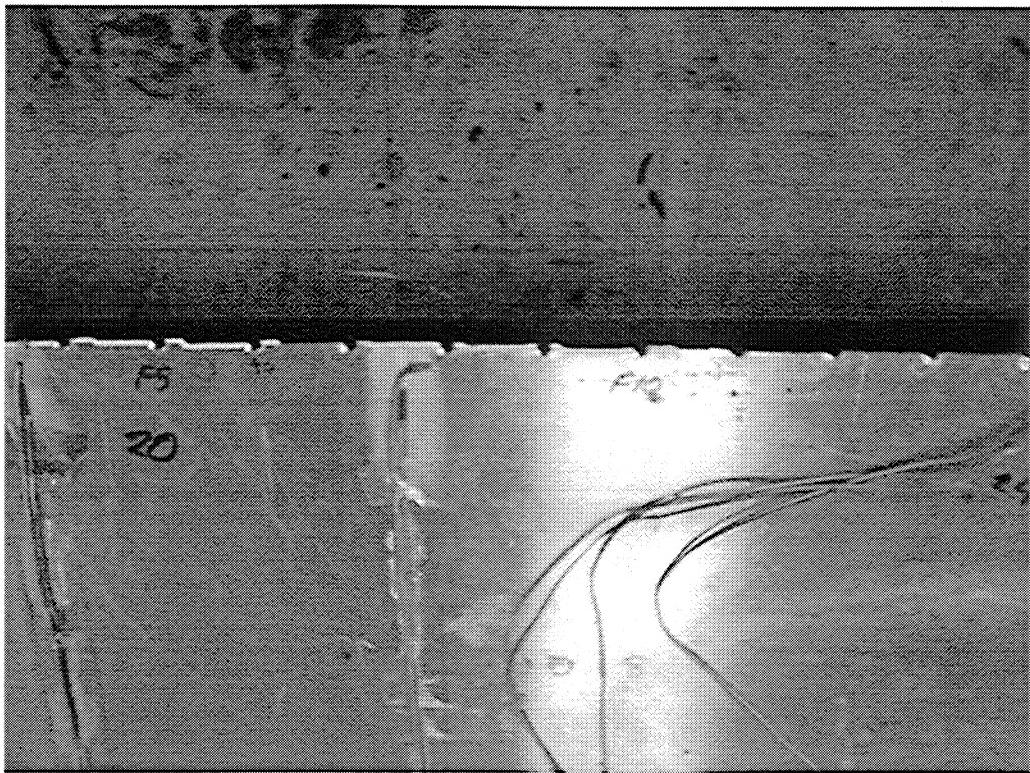
Figure 103
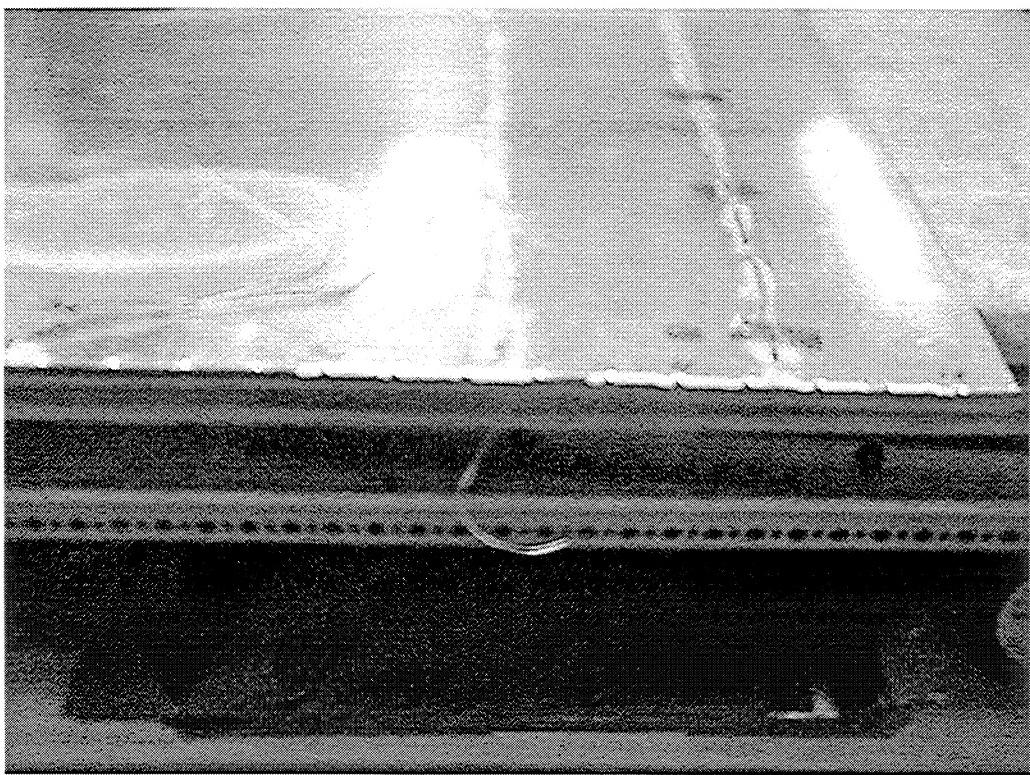
Figure 104
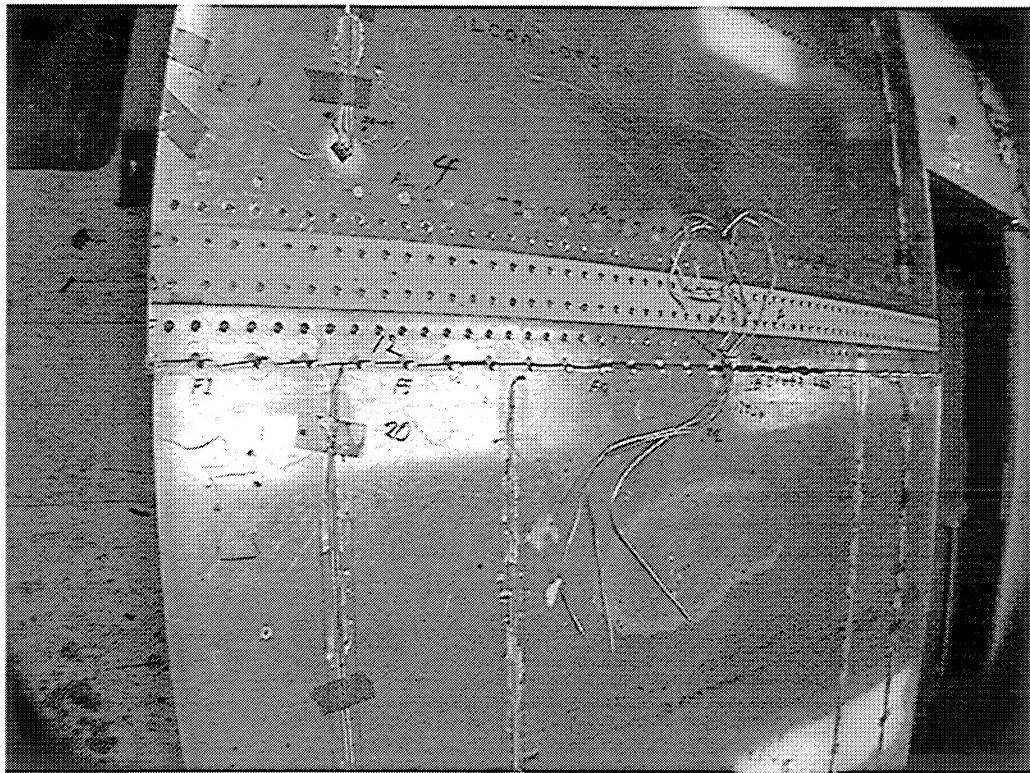
Figure 105
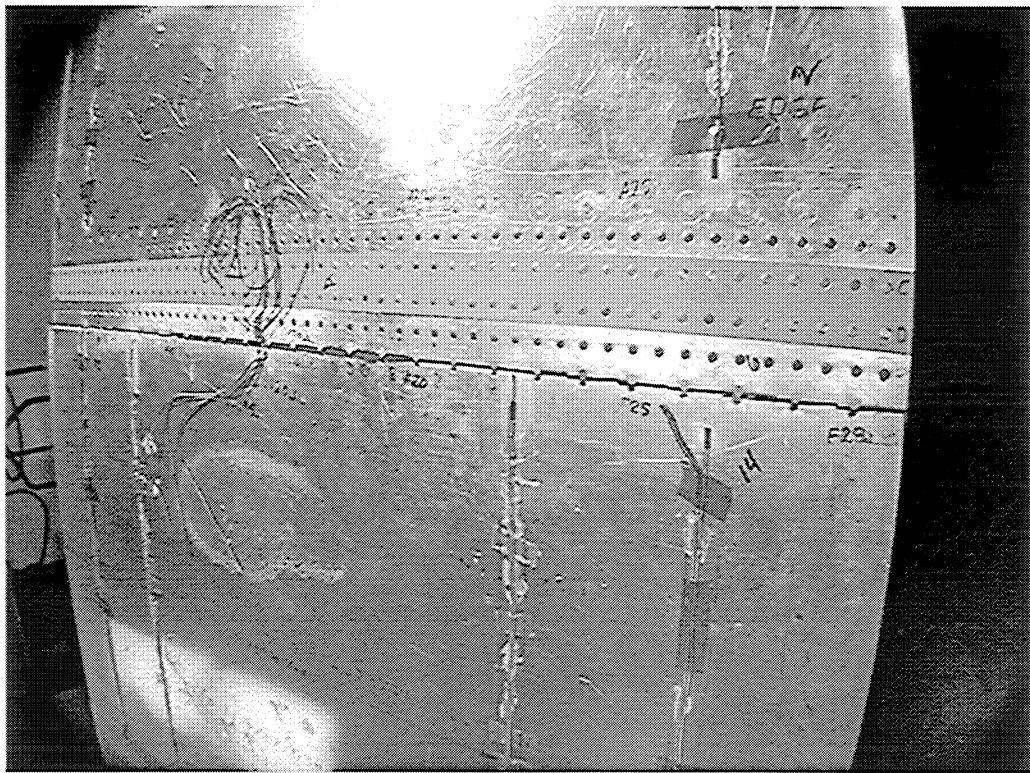
Figure 106
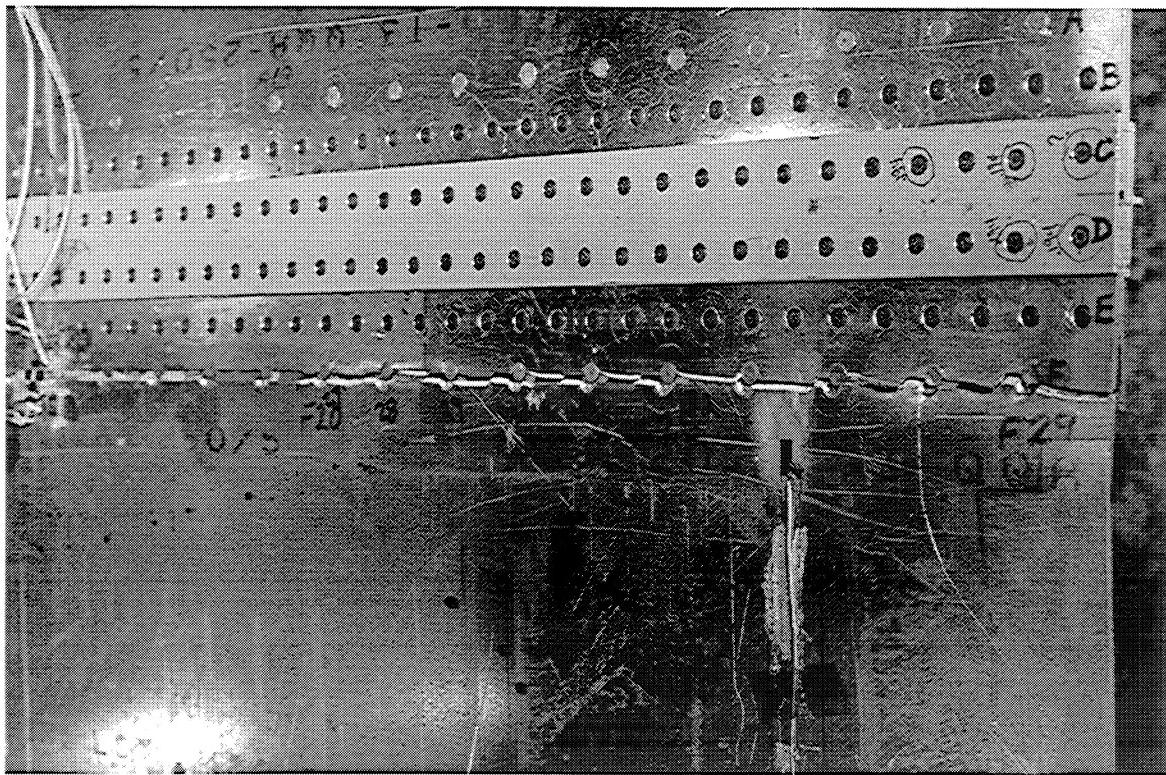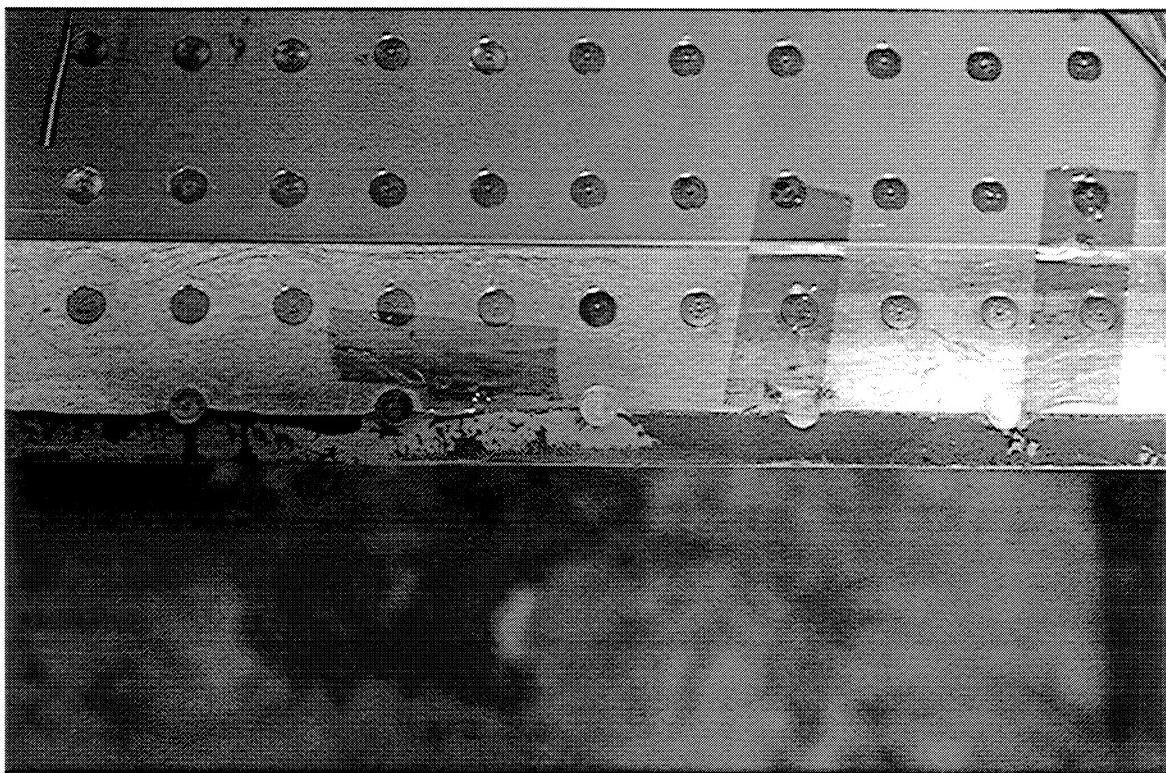
Figure 107

Figure 108
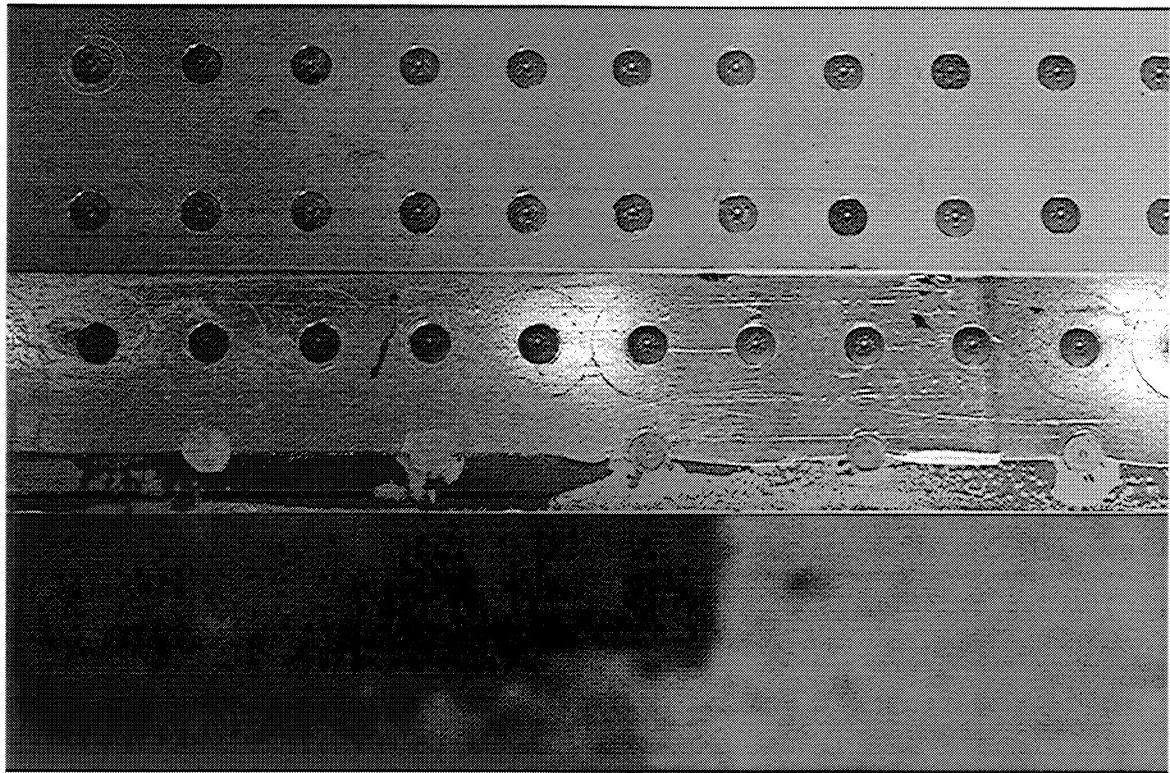
Figure 109

Figure 110

76
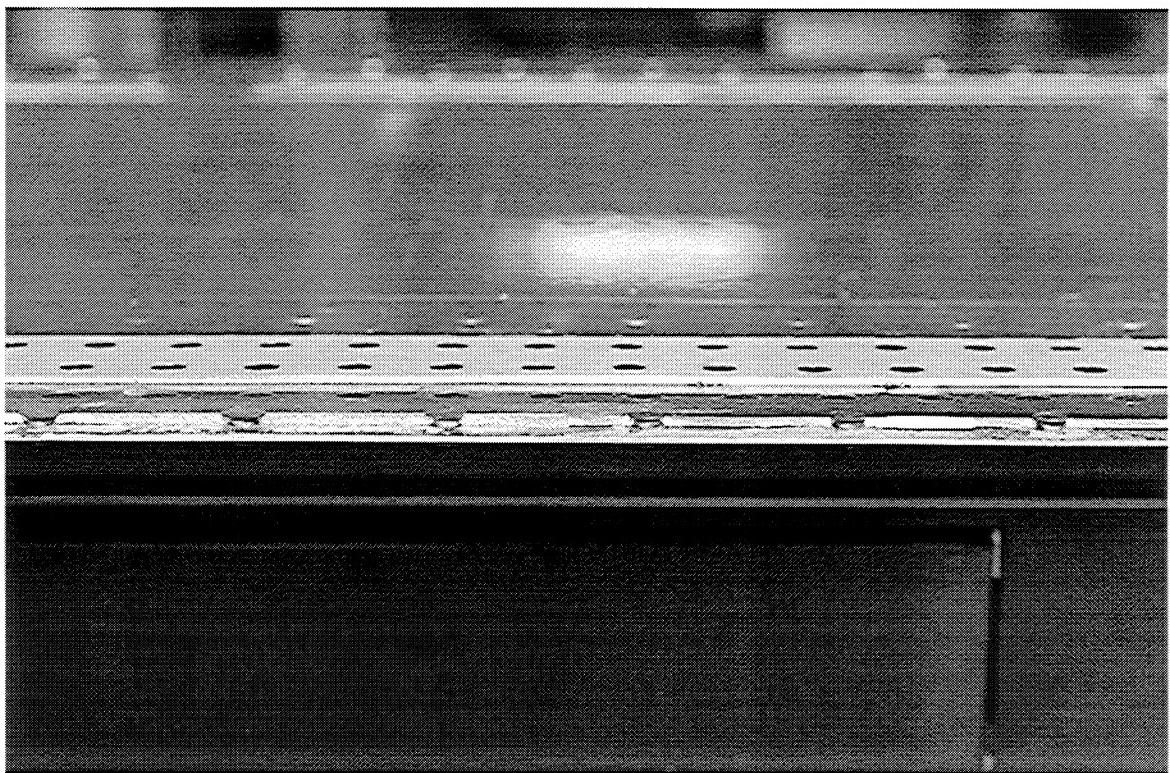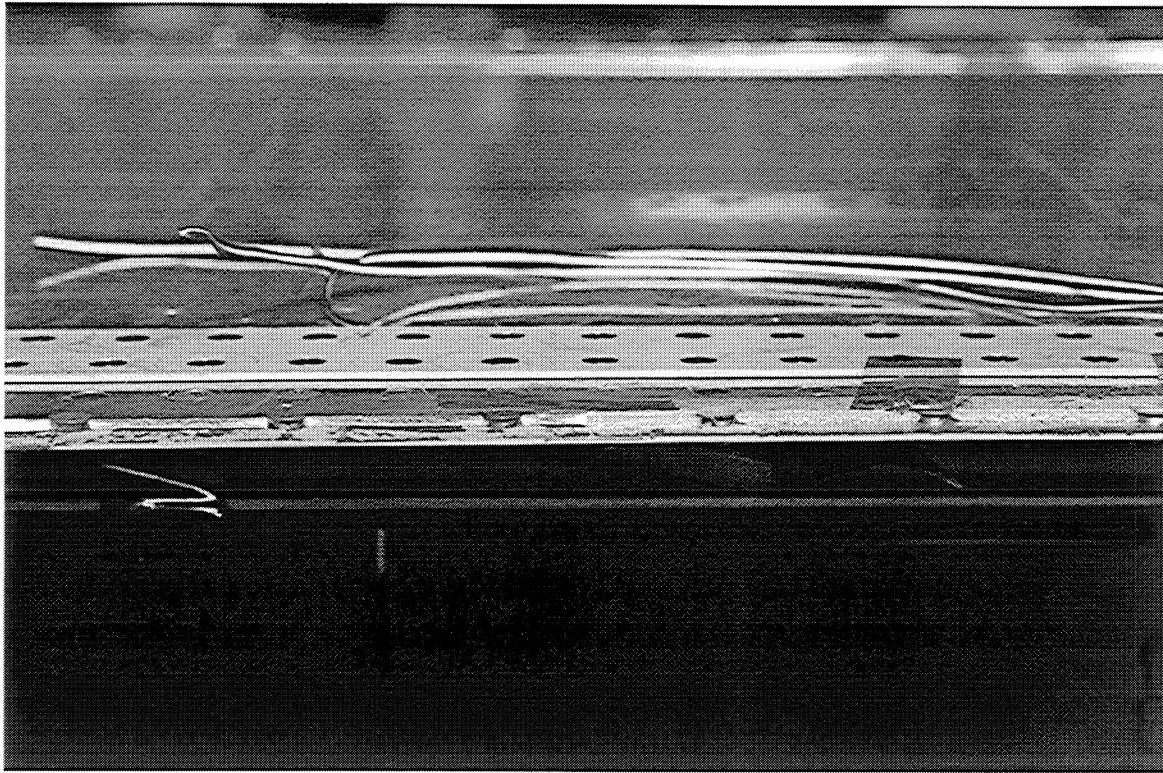
Figure 111

Figure 112
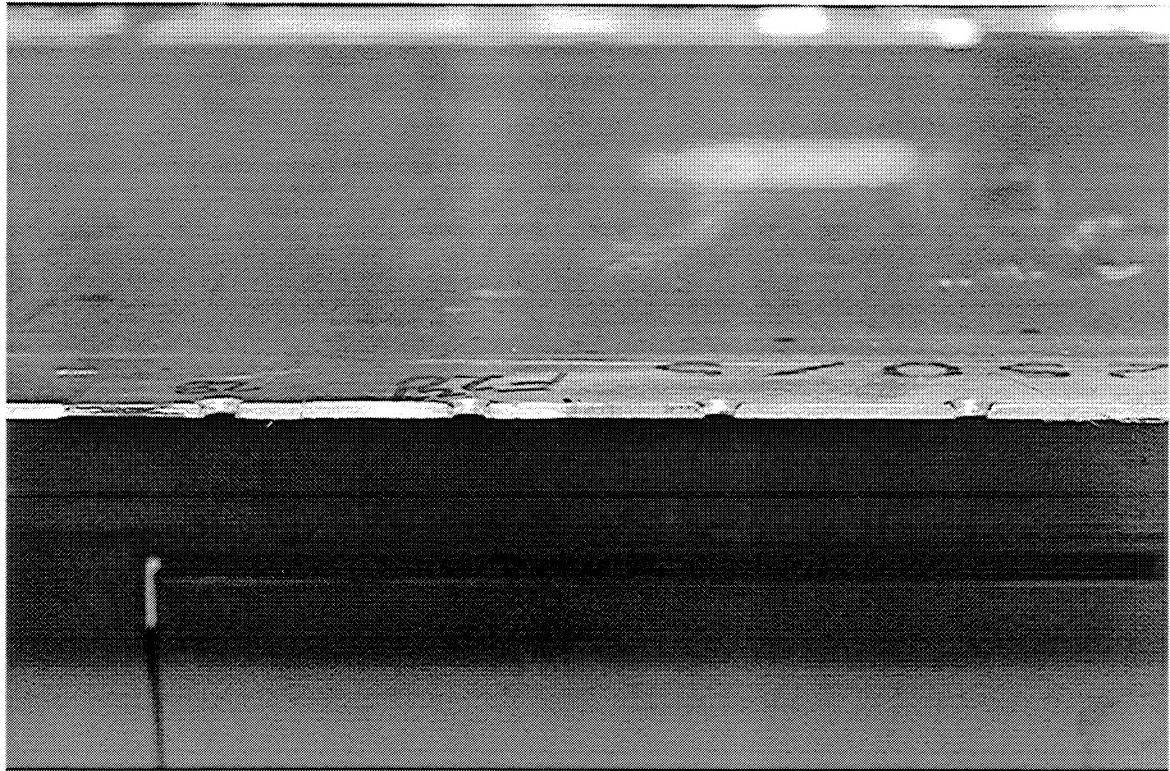
Figure 113
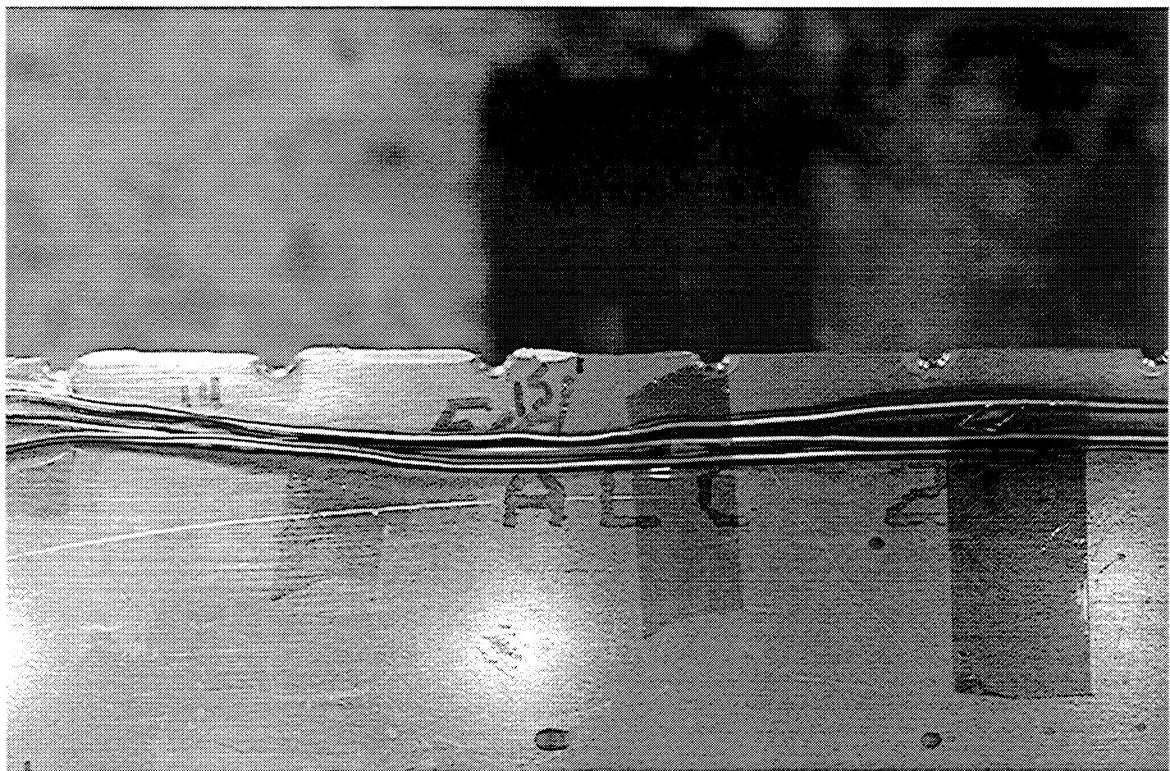
Figure 114

Figure 115

MSD 503-3
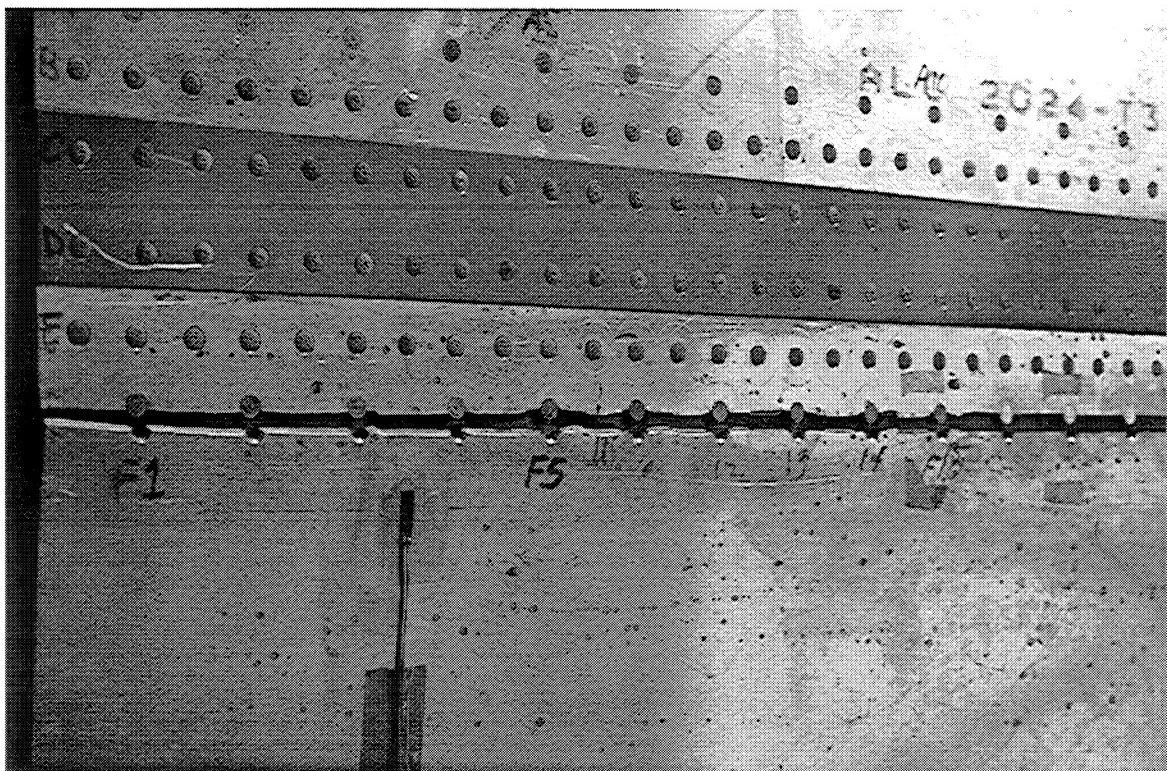
Figure 116
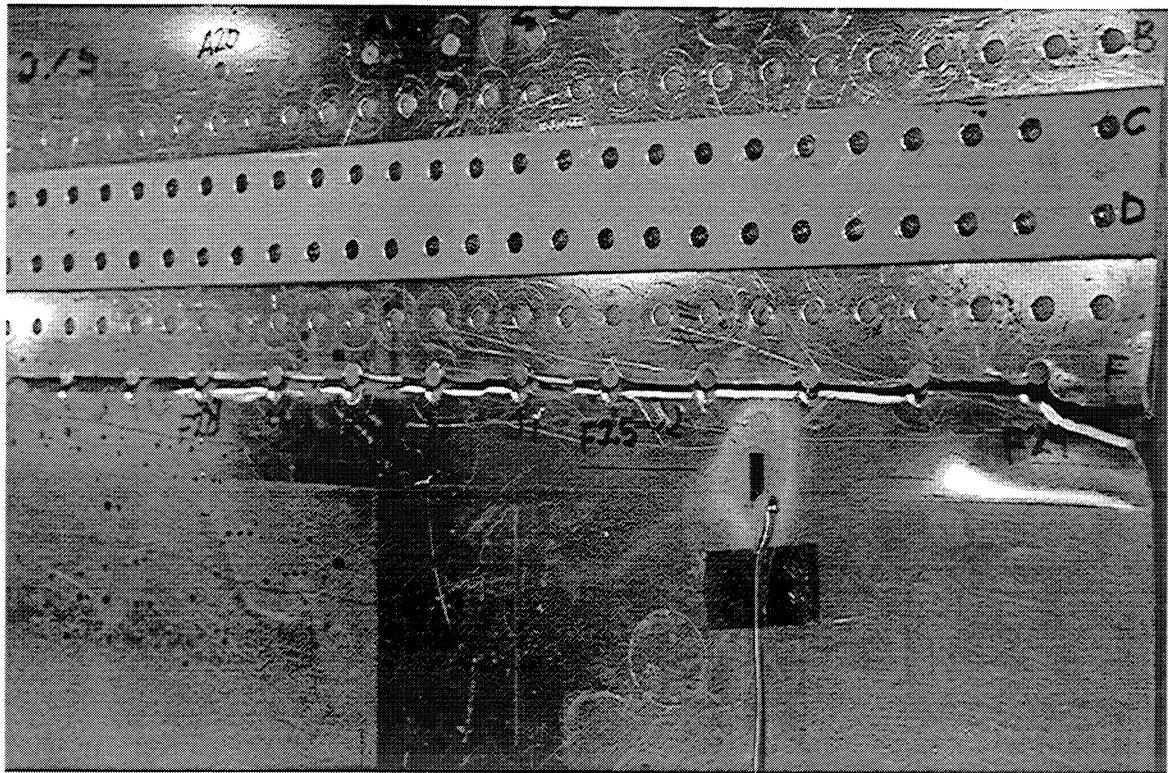
Figure 117
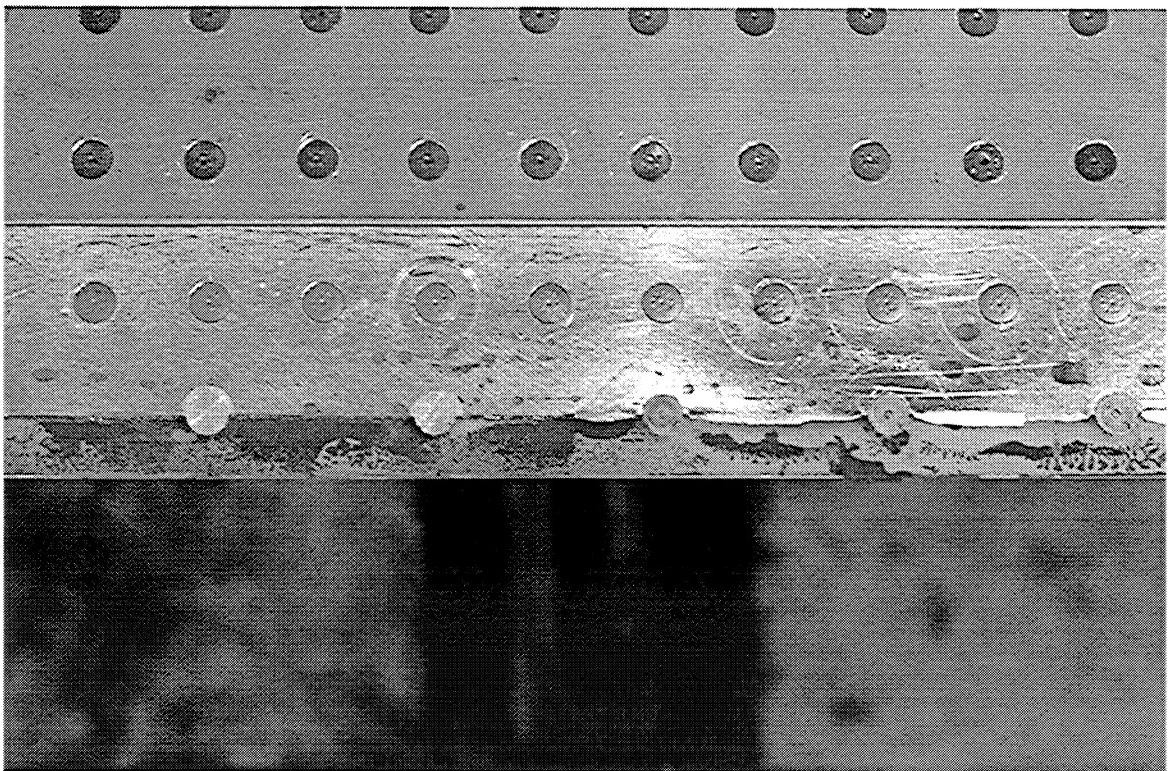
Figure 118
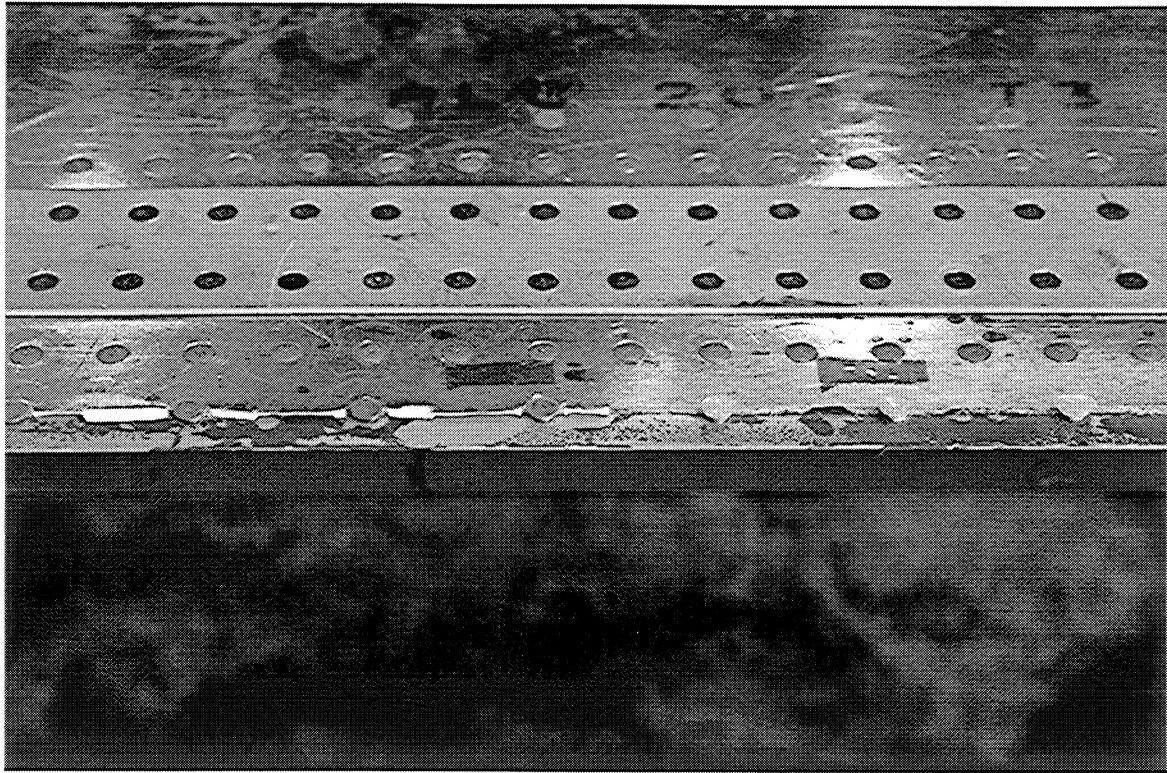
Figure 119
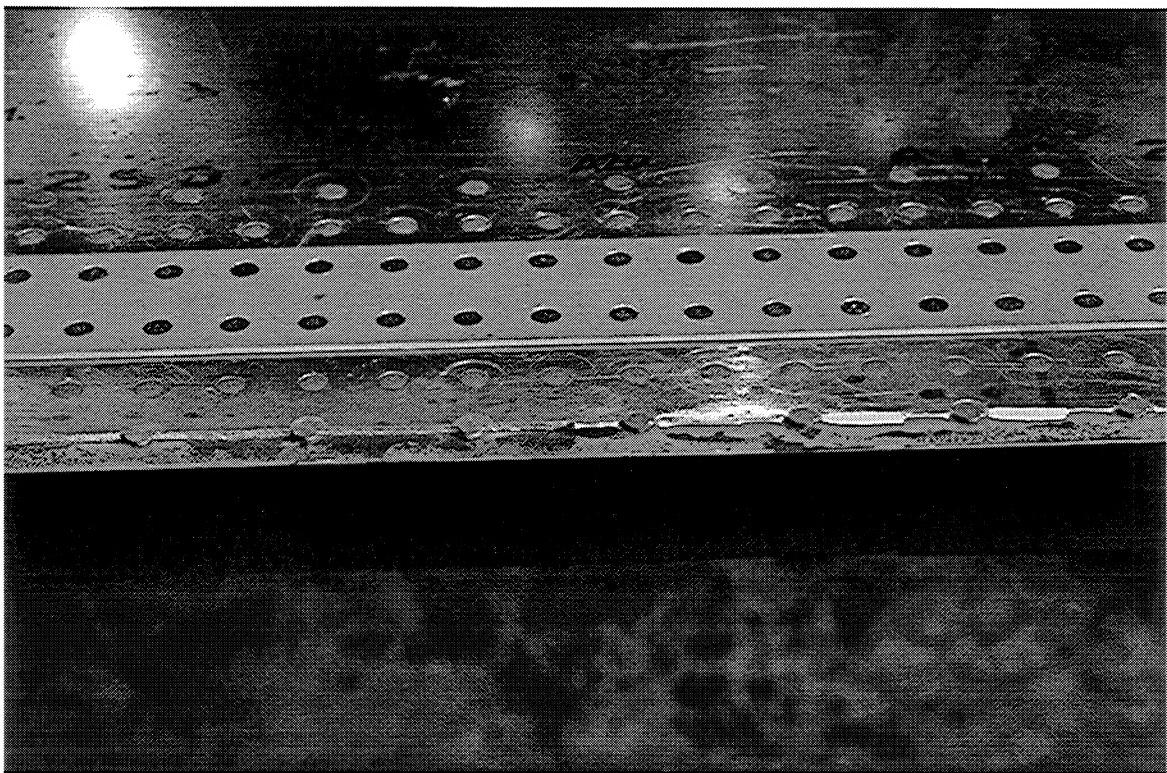
Figure 120
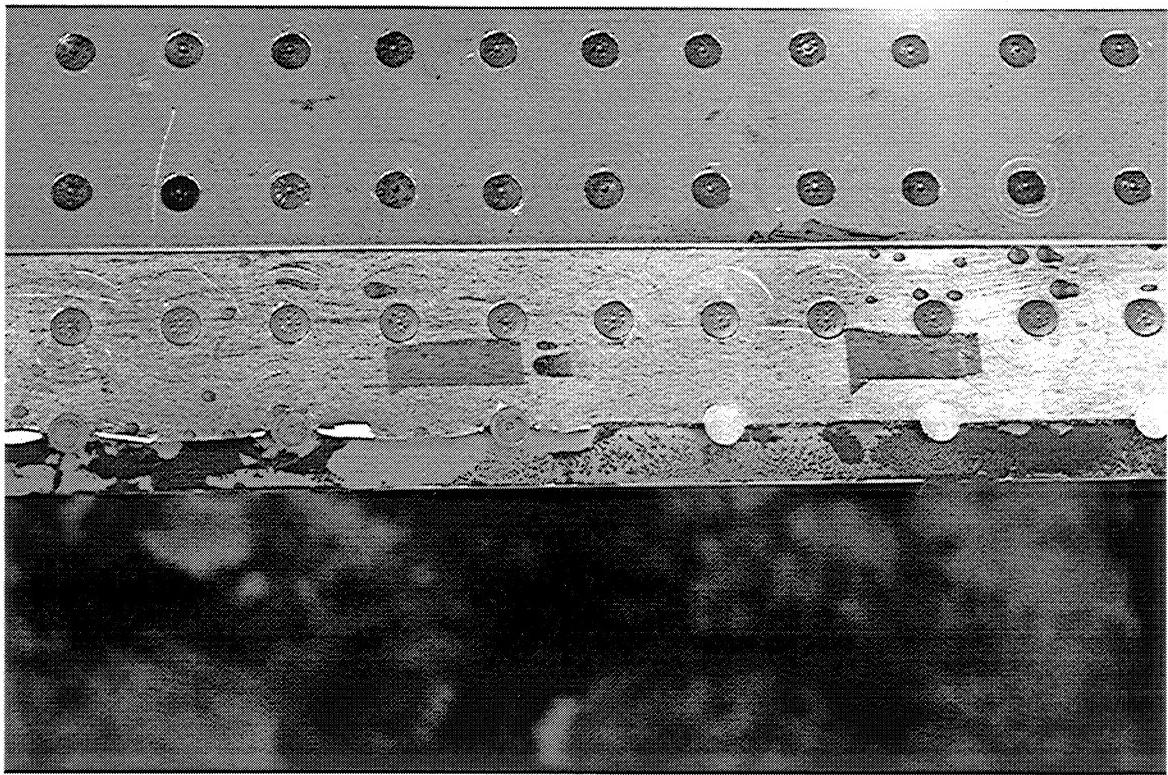
Figure 121
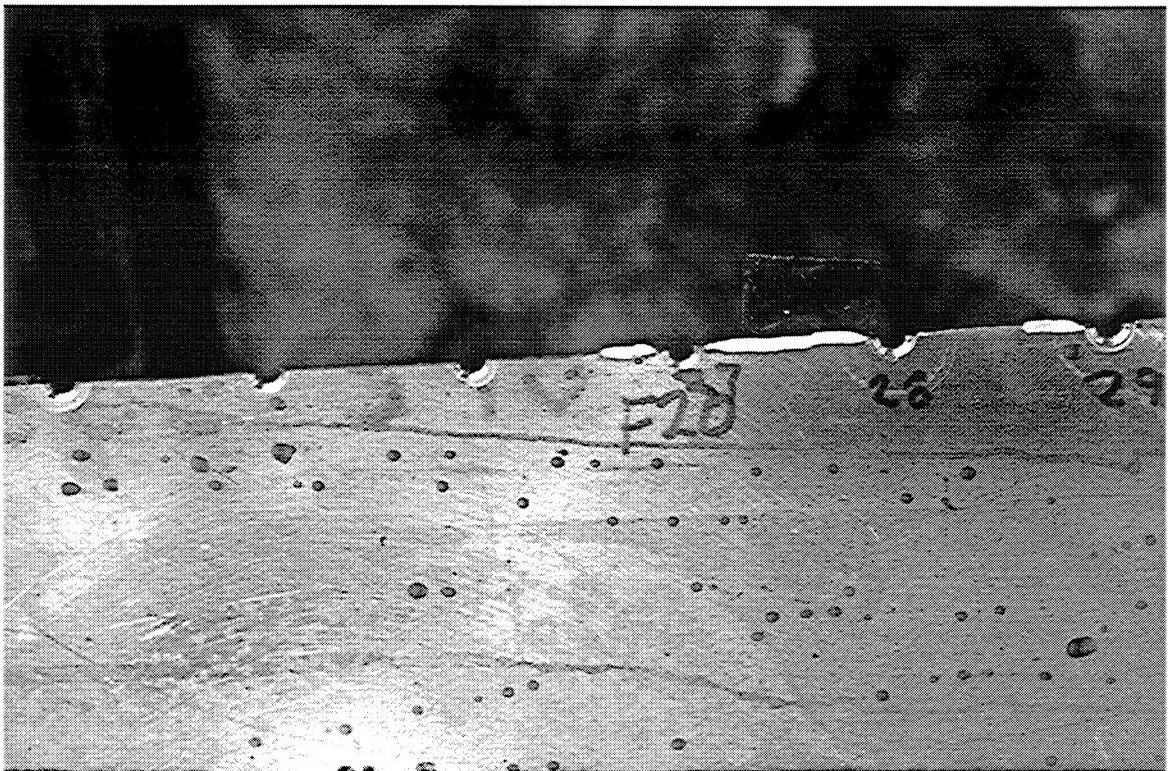
Figure 122

Figure 123
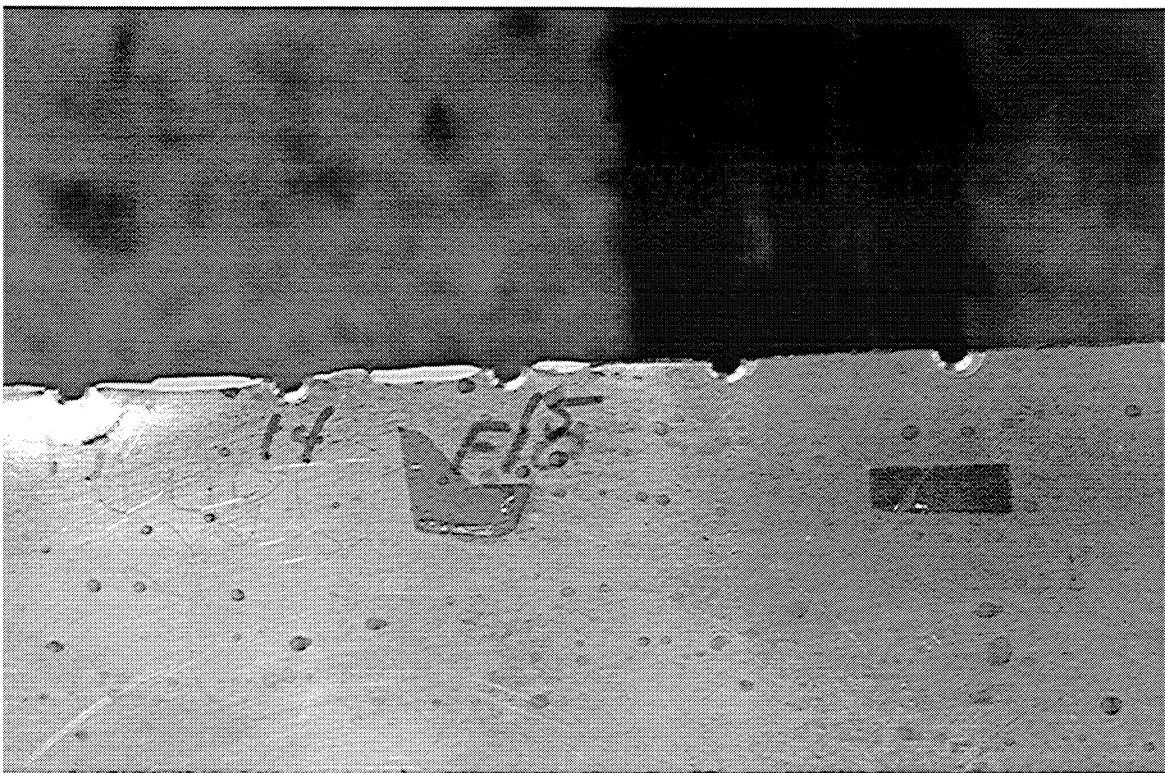
Figure 124
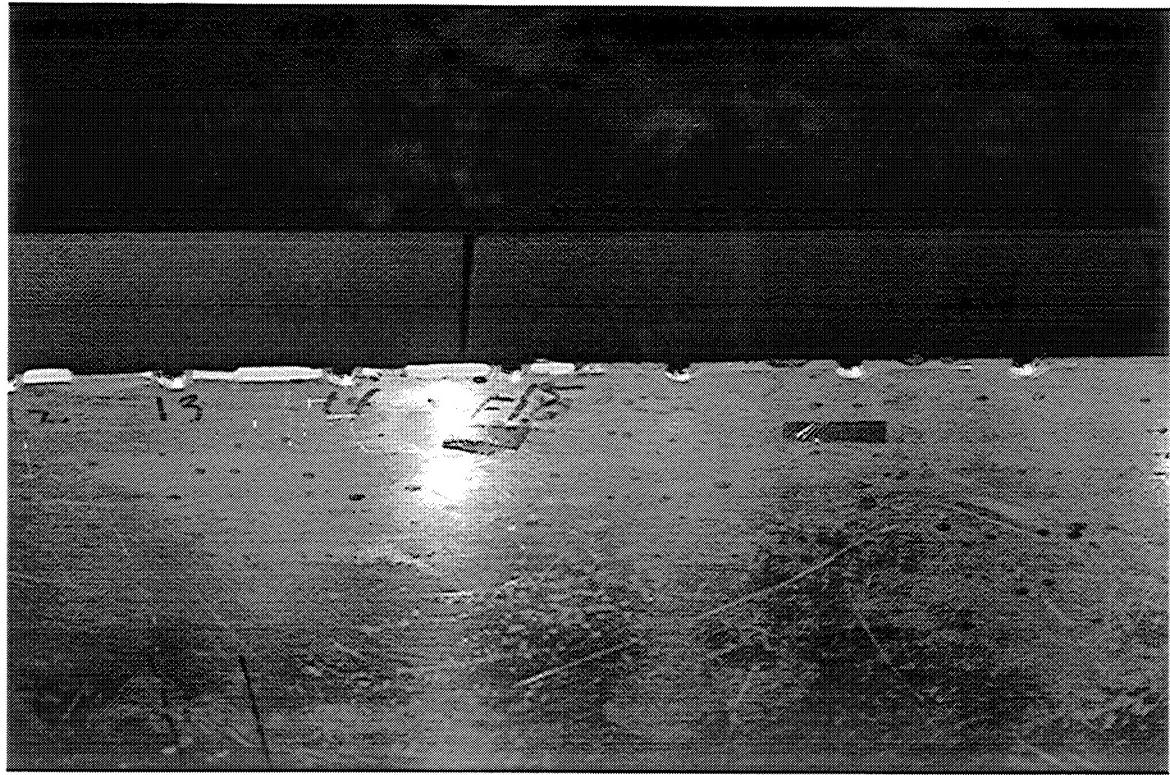
Figure 125
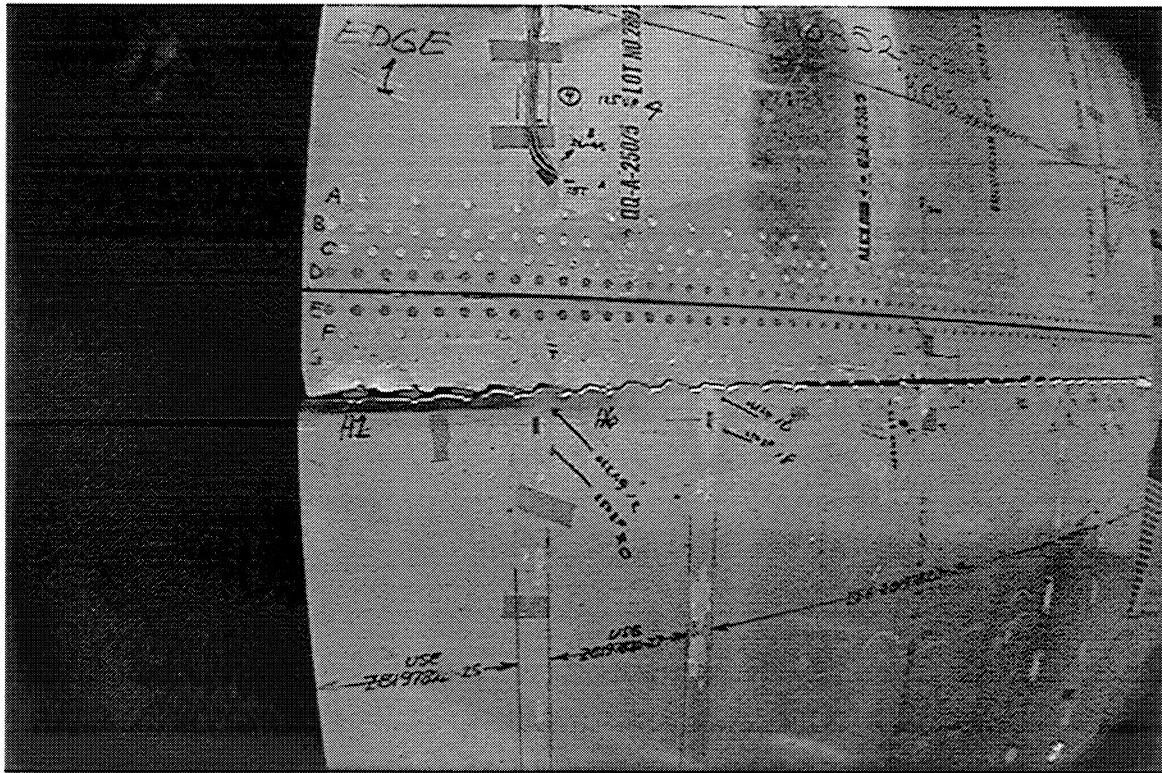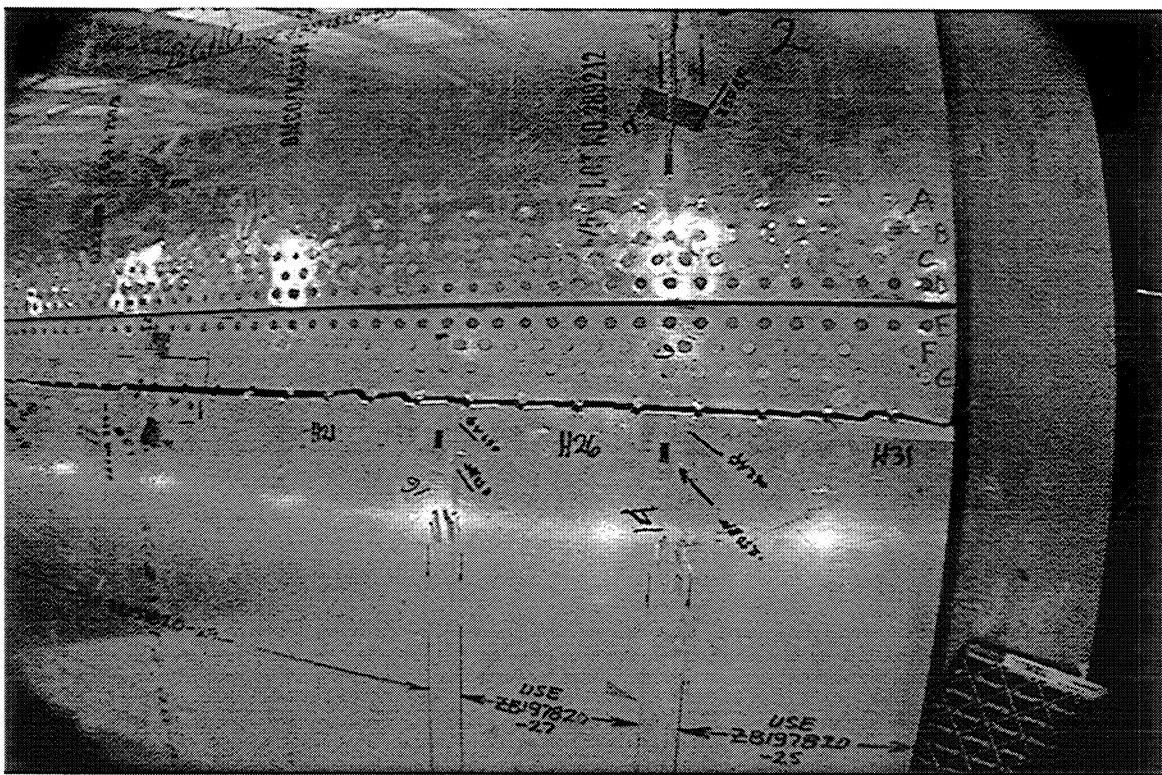
Figure 126

Figure 127
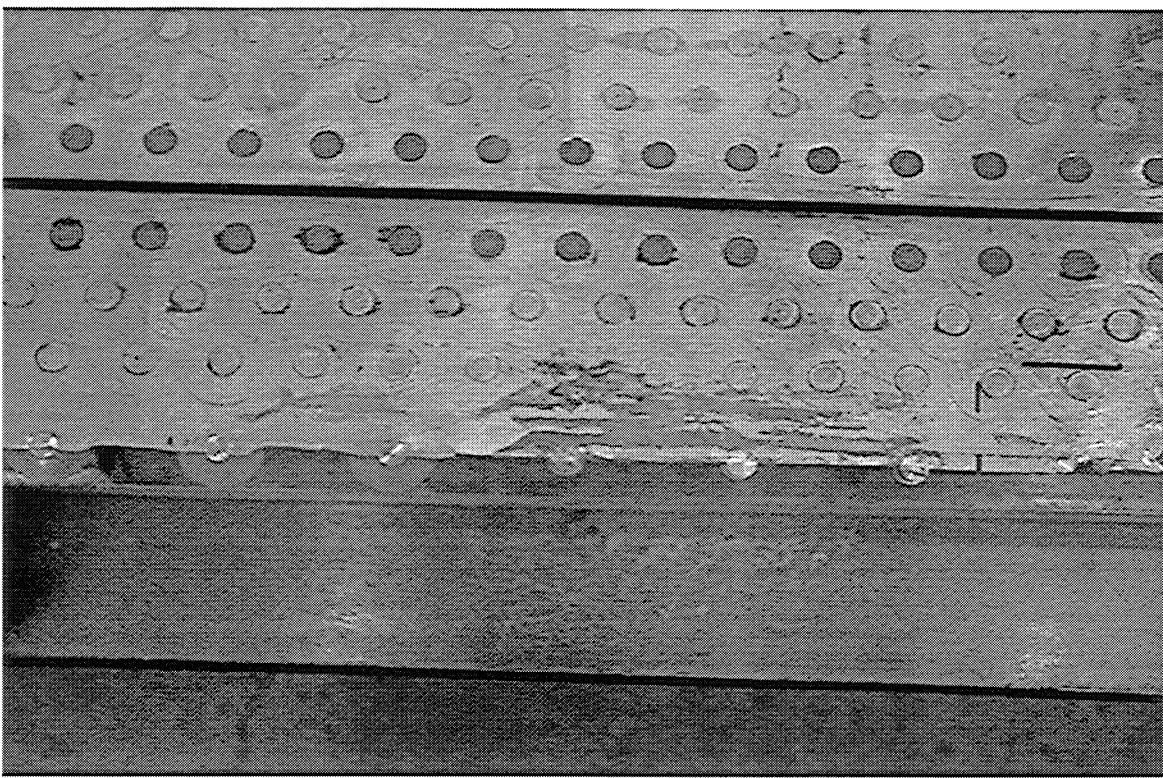
Figure 128
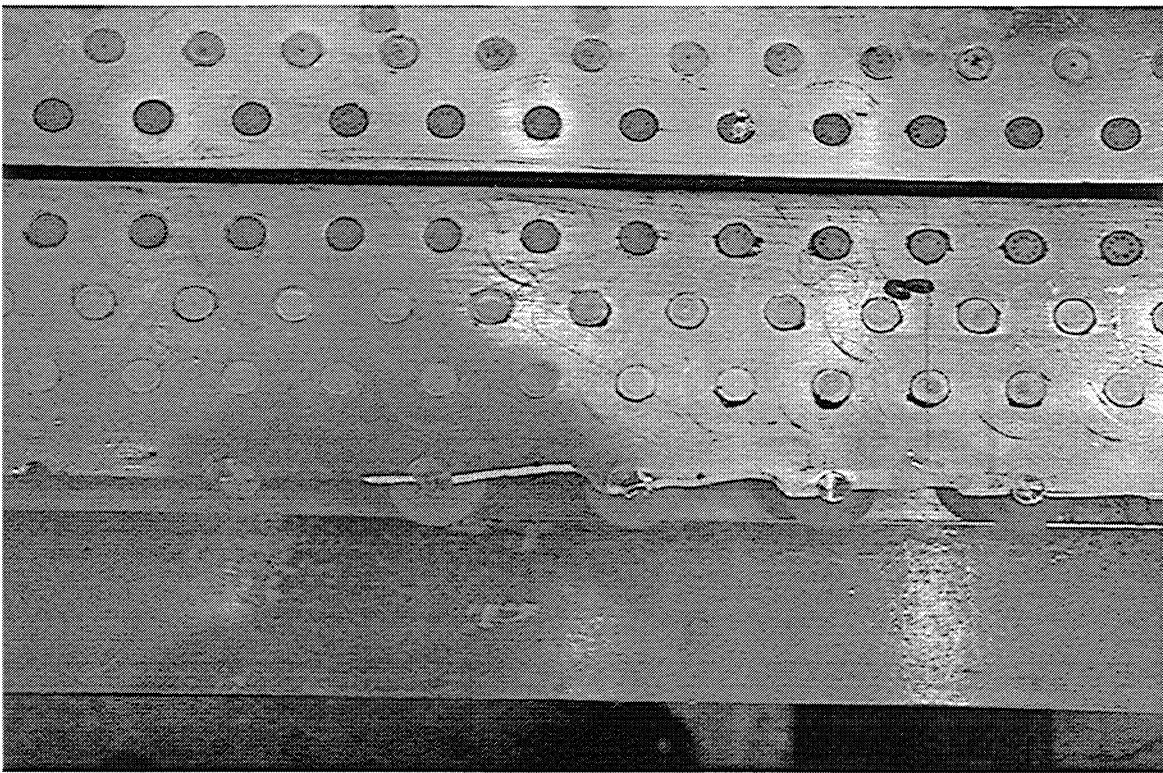
Figure 129
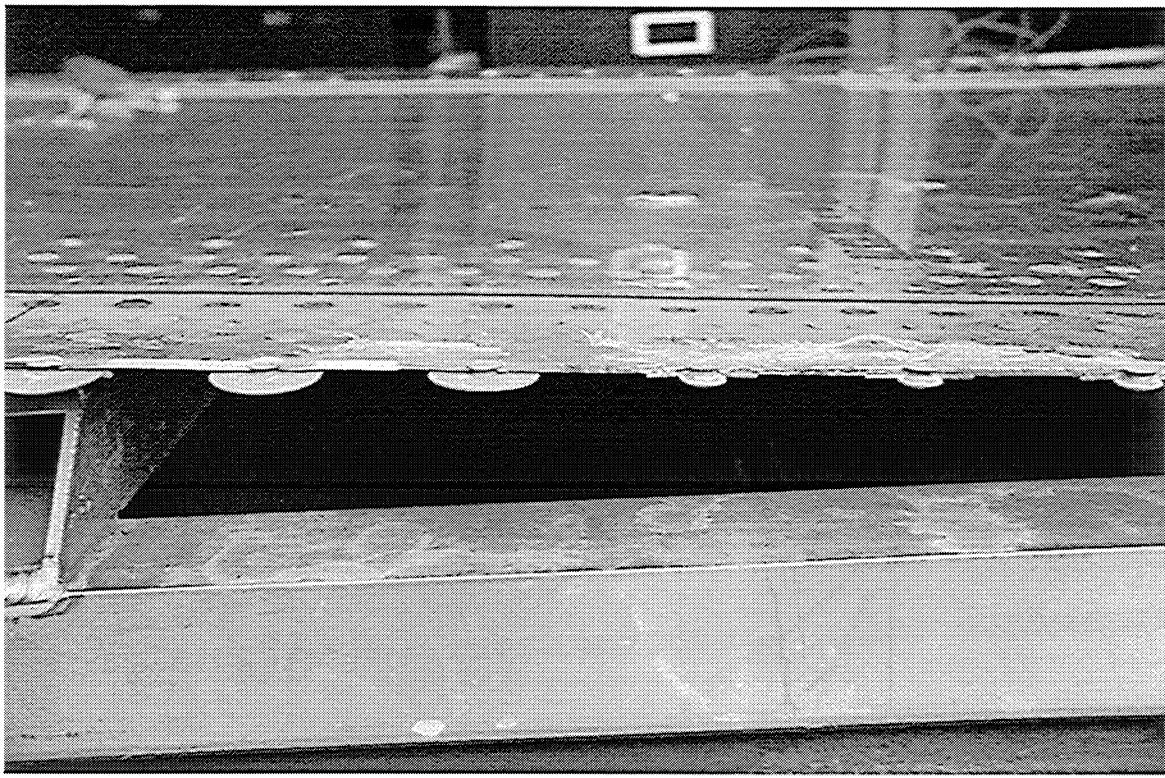
Figure 130
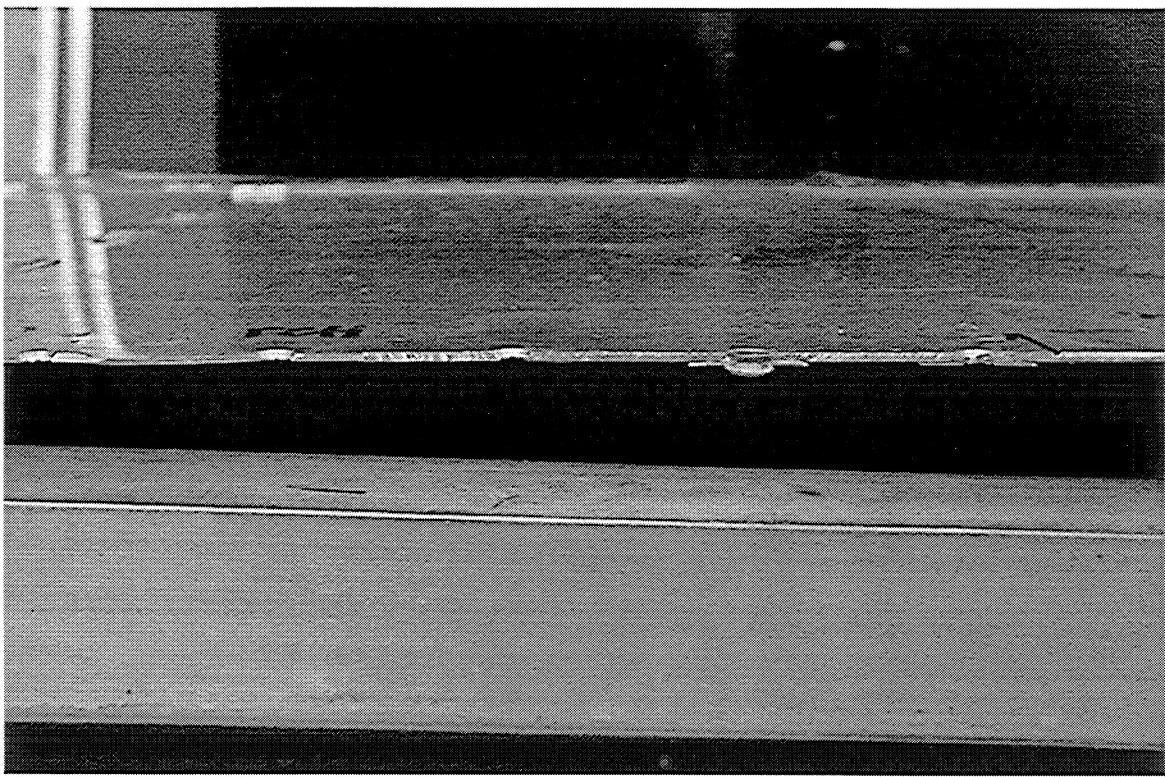
Figure 131

Figure 132
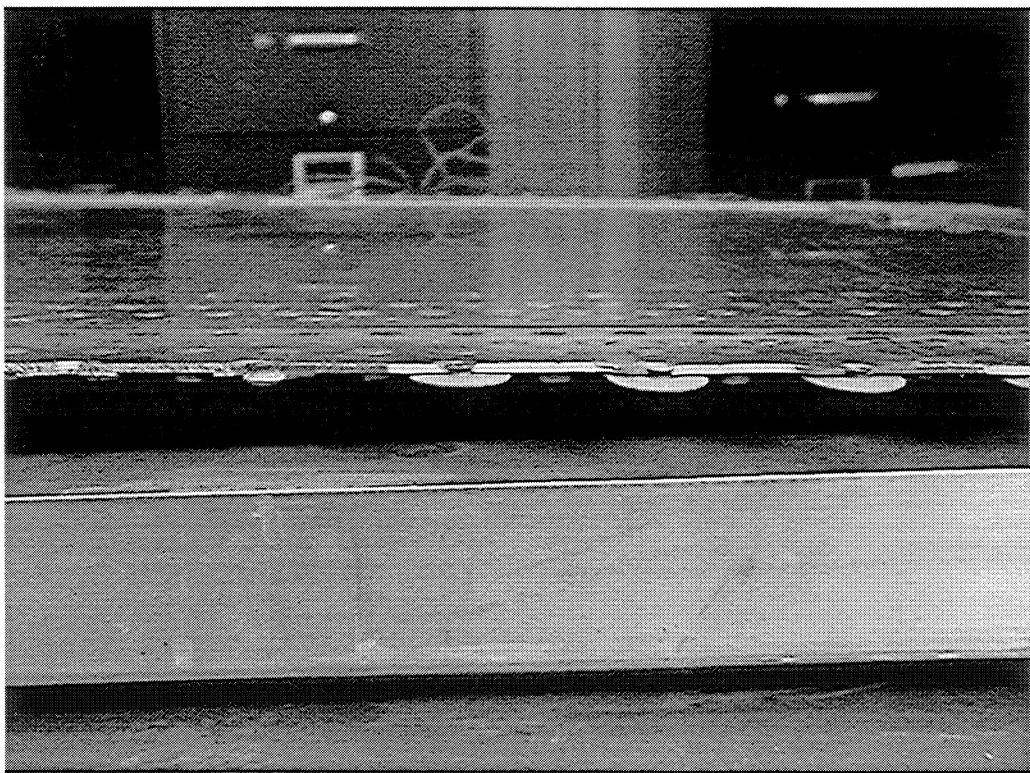
Figure 132
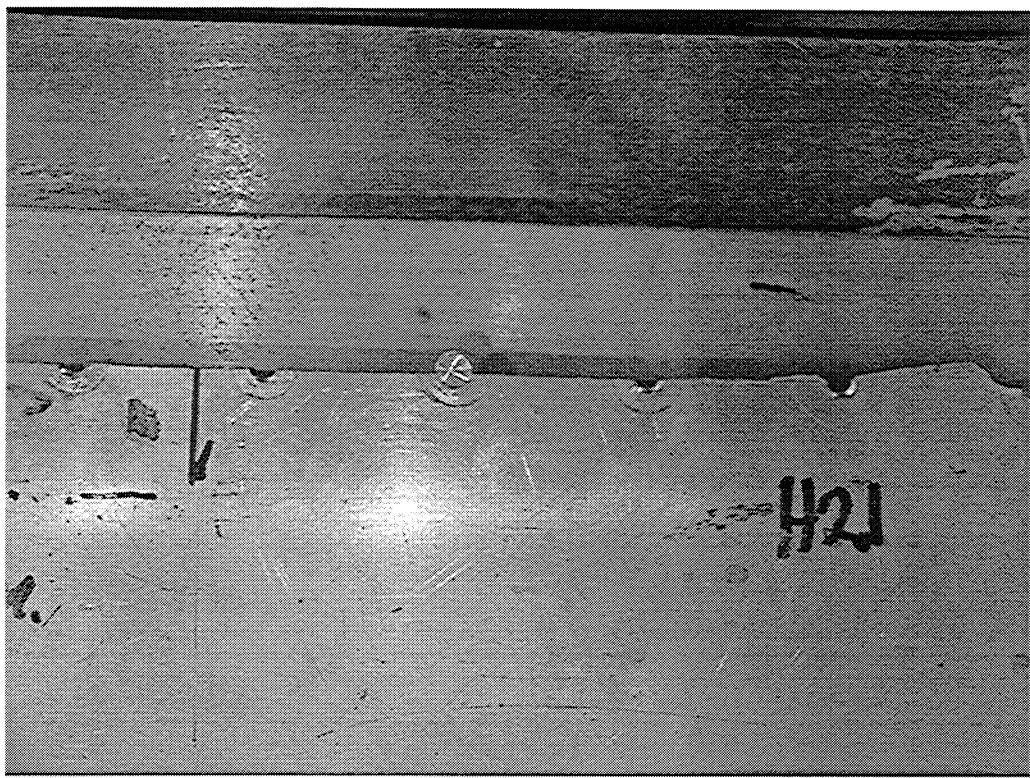
Figure 133
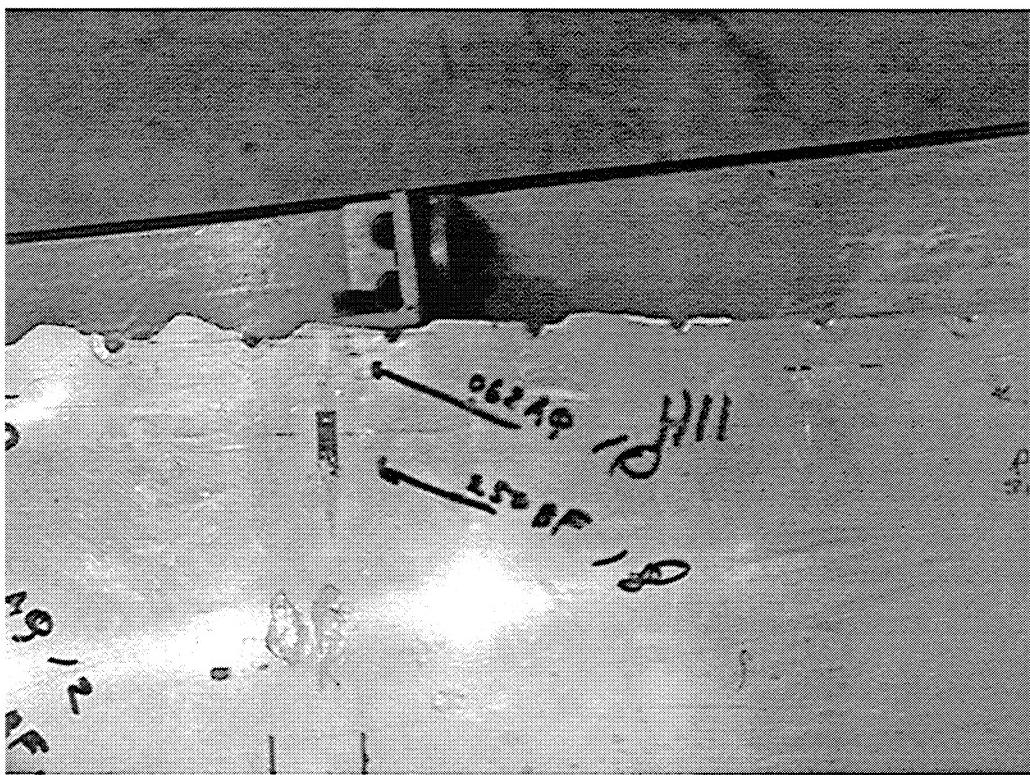
Figure 134
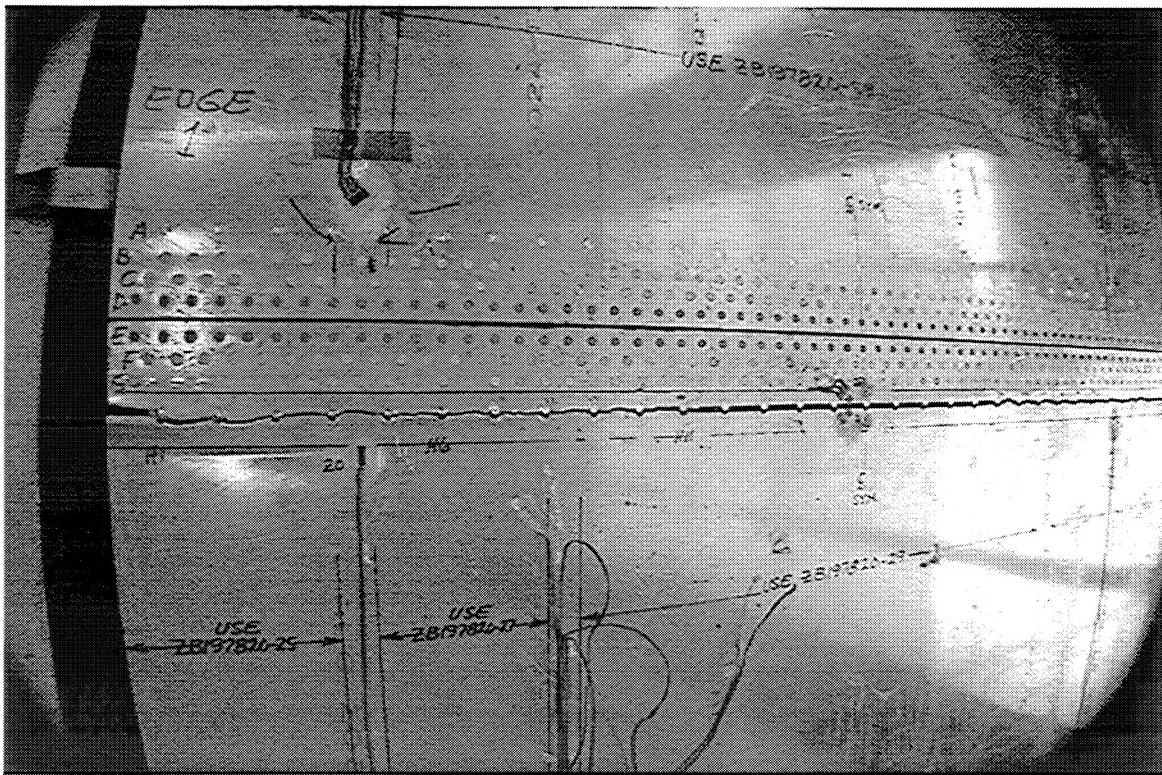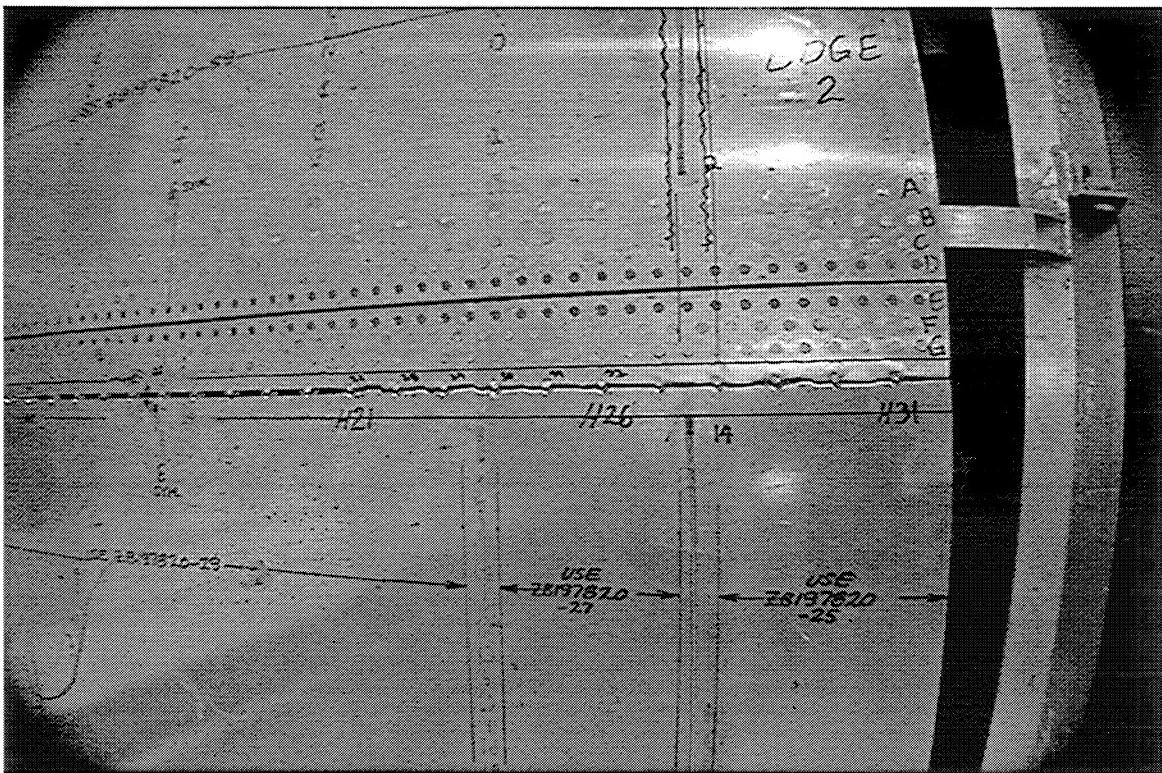
Figure 135

Figure 136
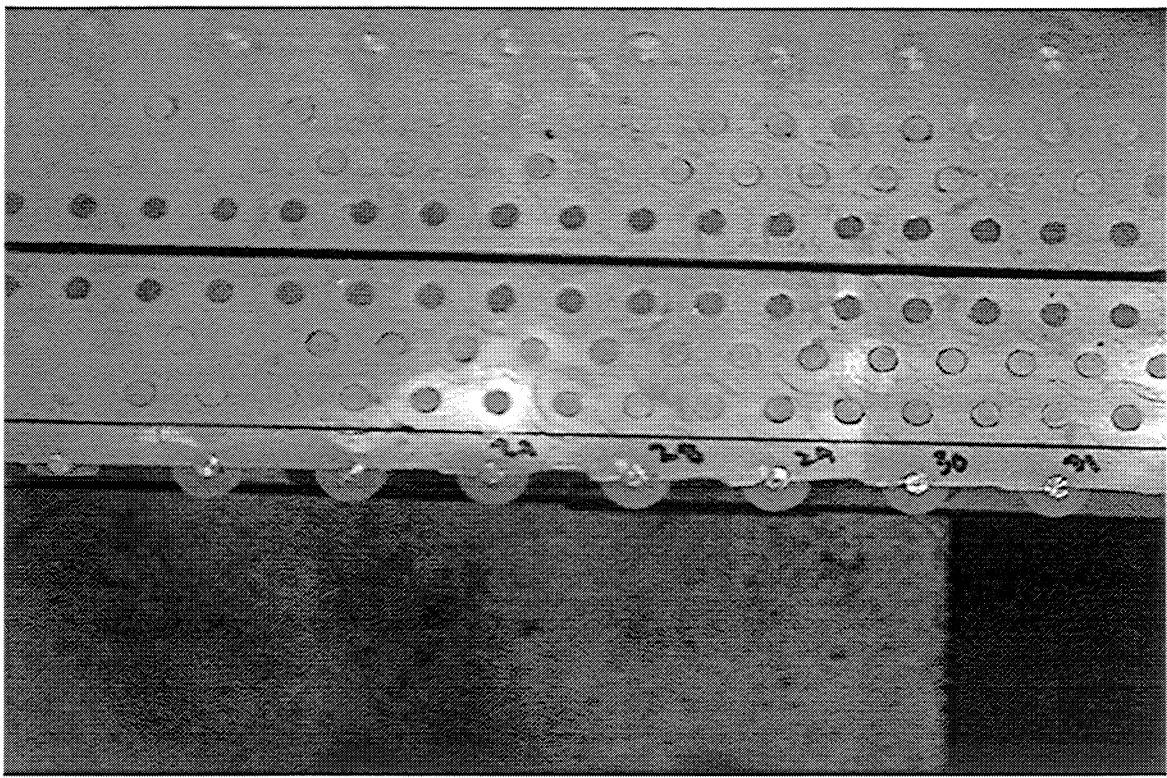
Figure 137

Figure 138
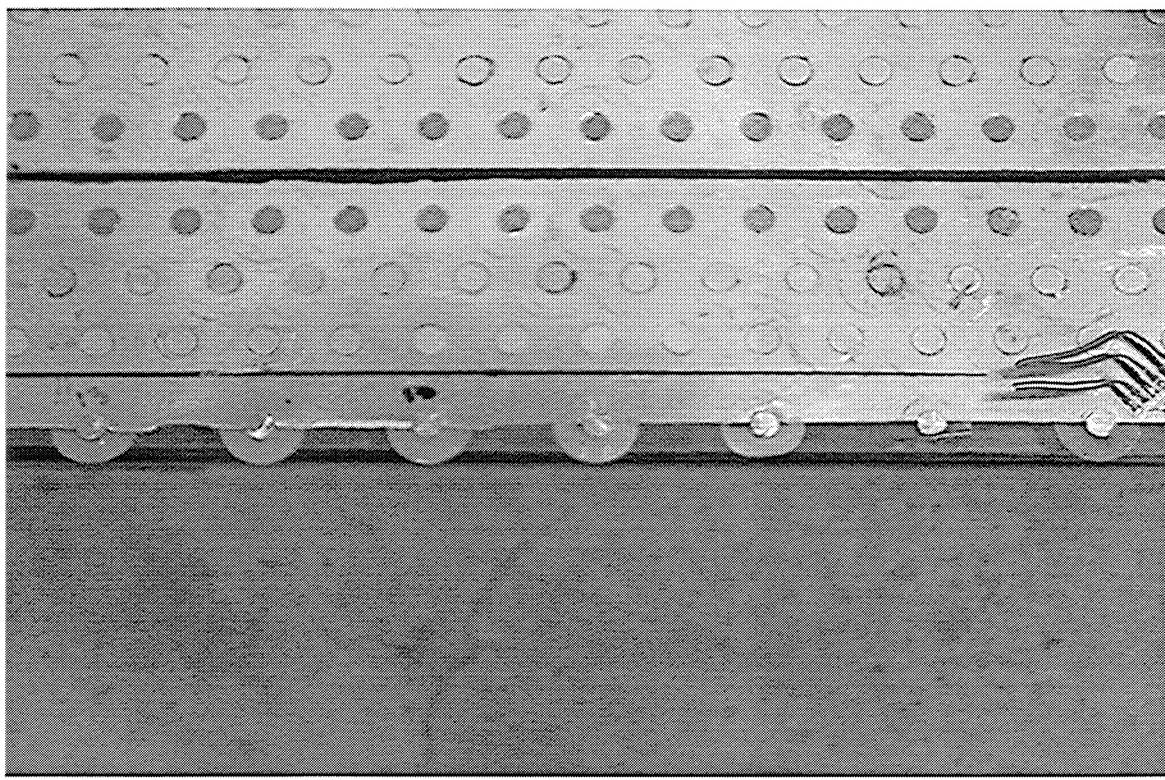
Figure 139
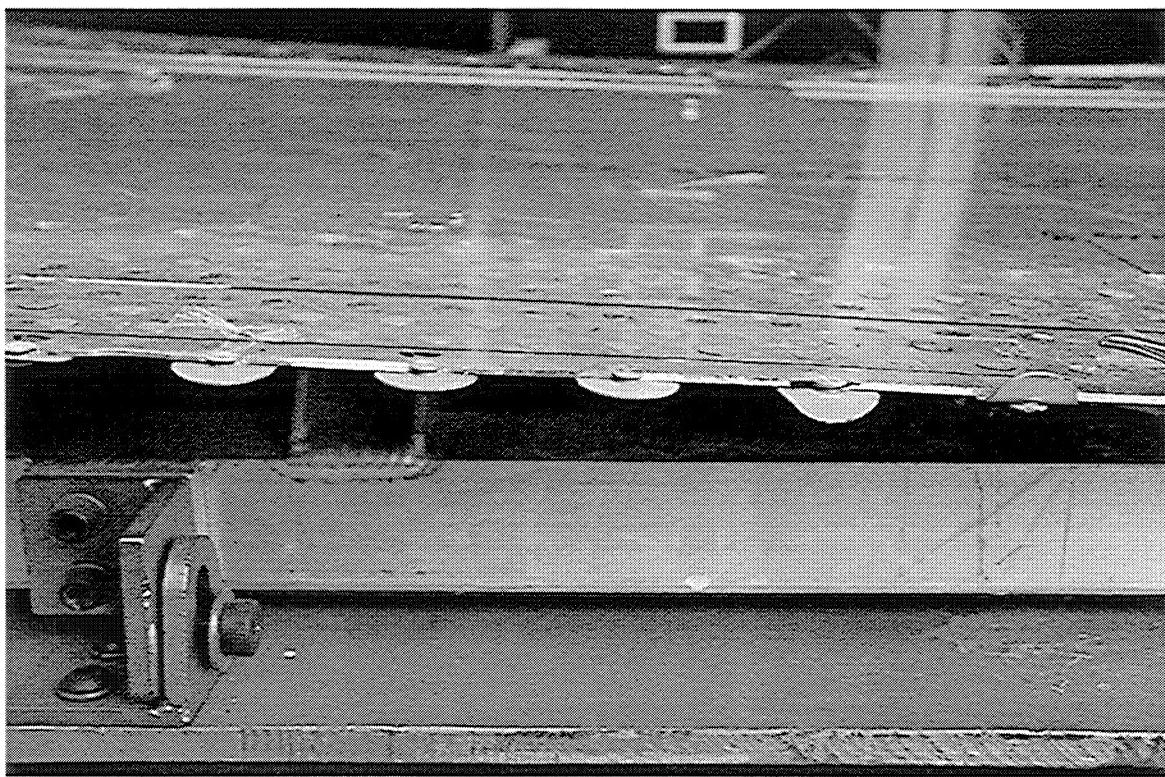
Figure 140
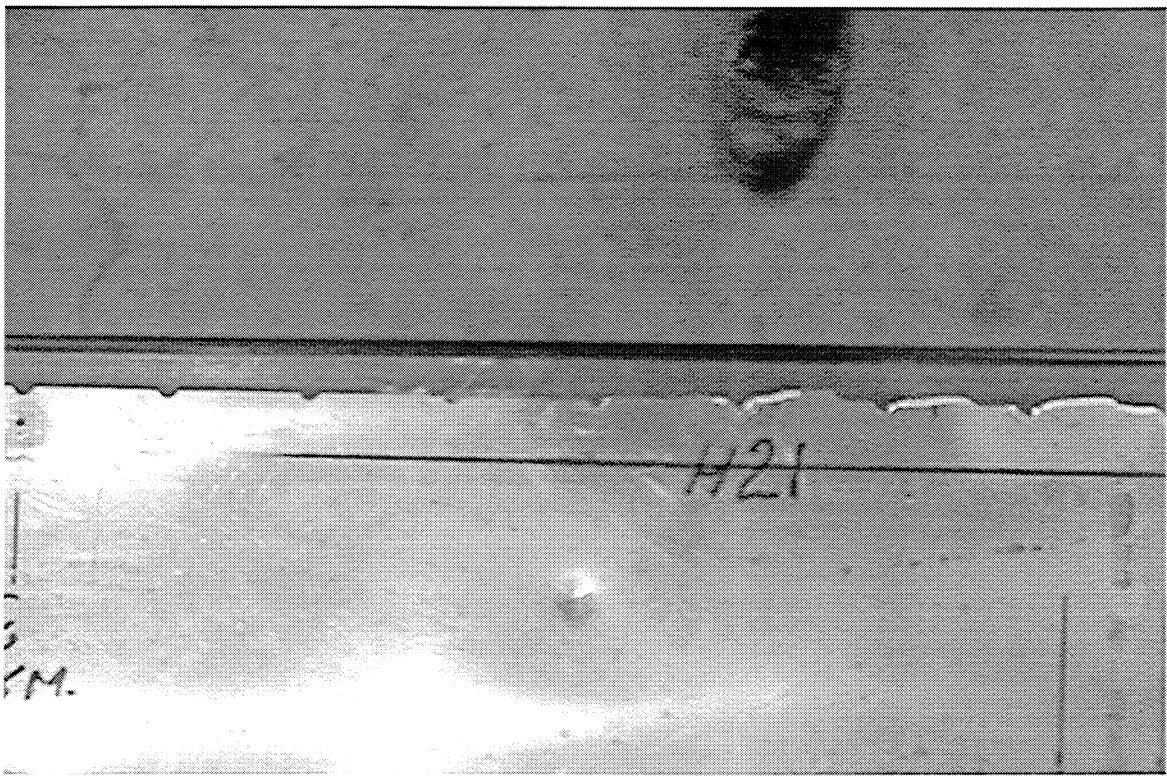
Figure 141

Figure 142
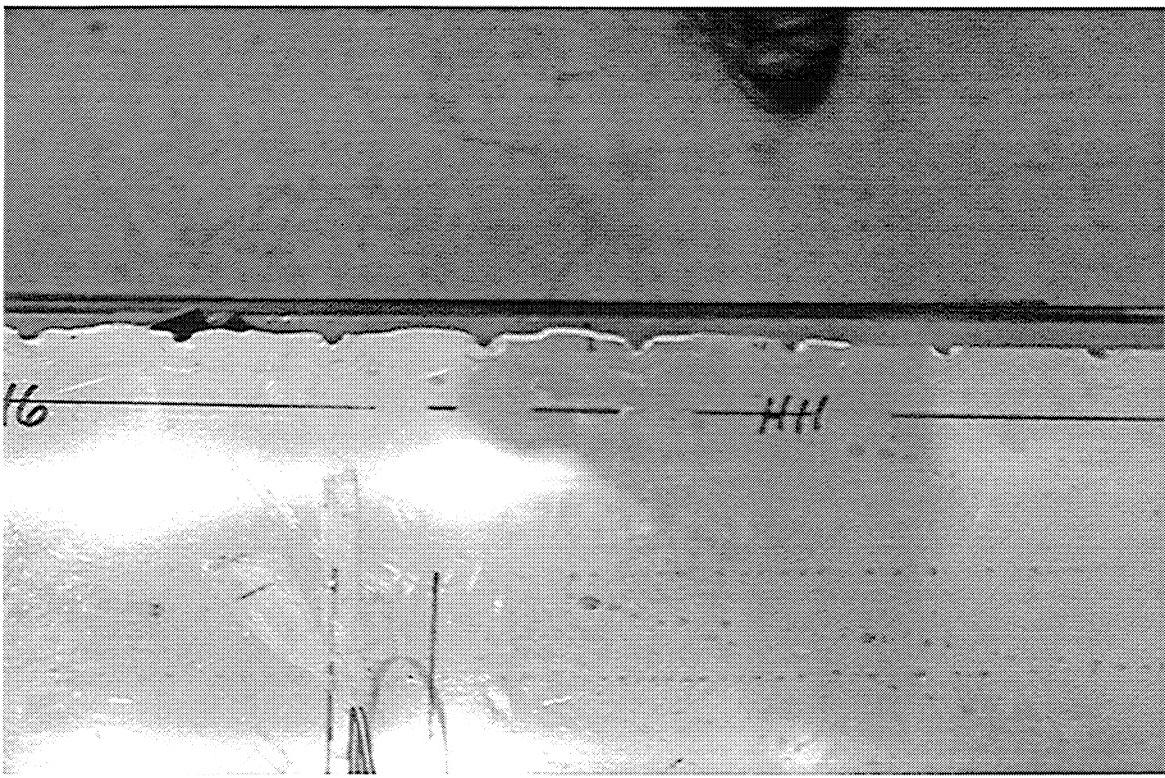
Figure 143
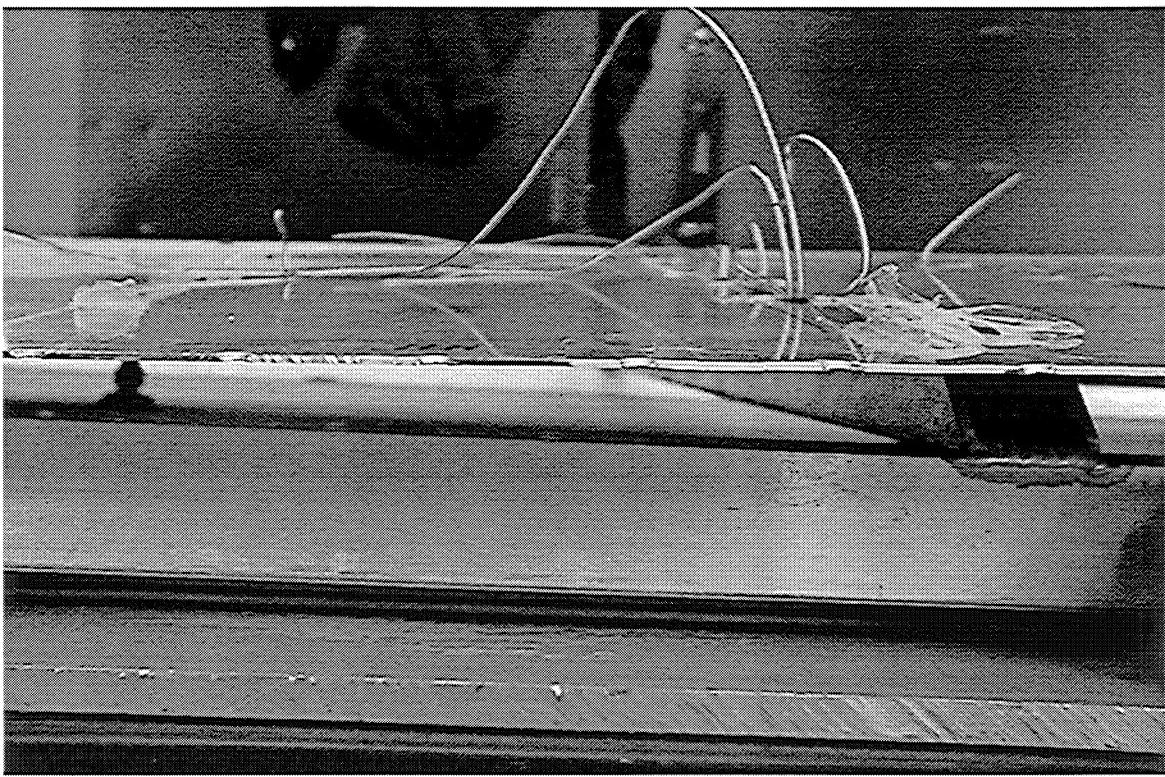
Figure 144
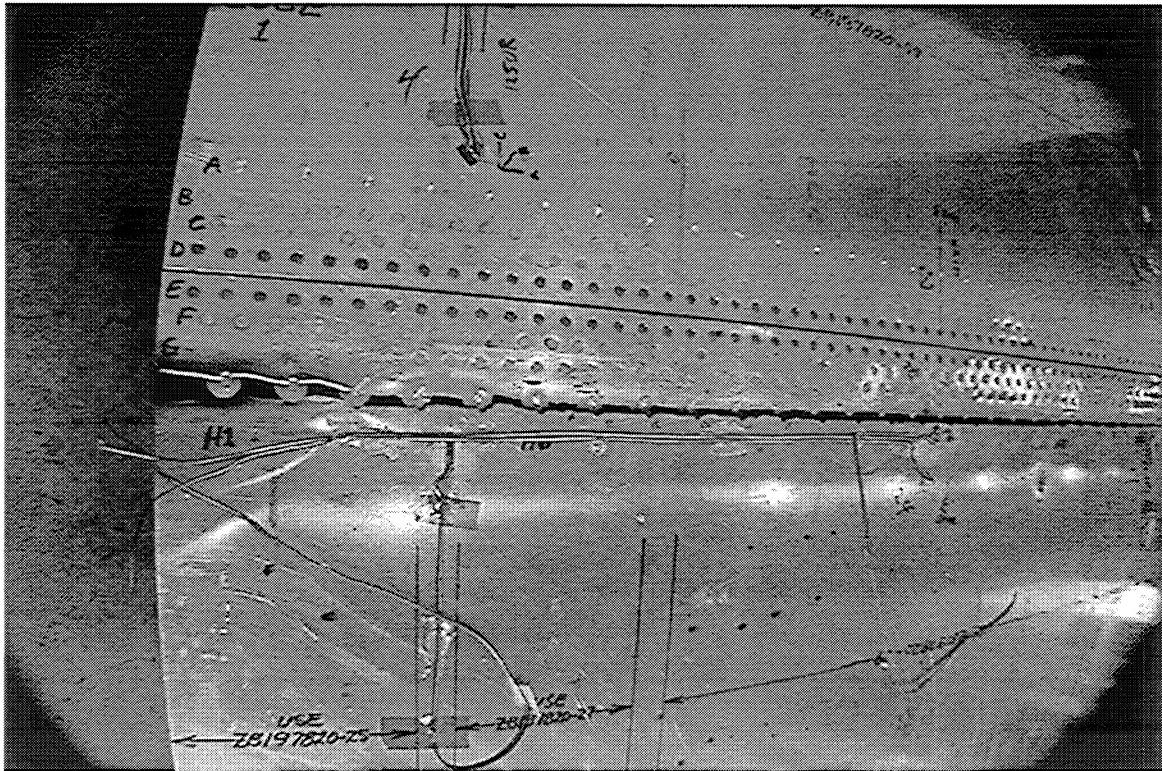
Figure 145
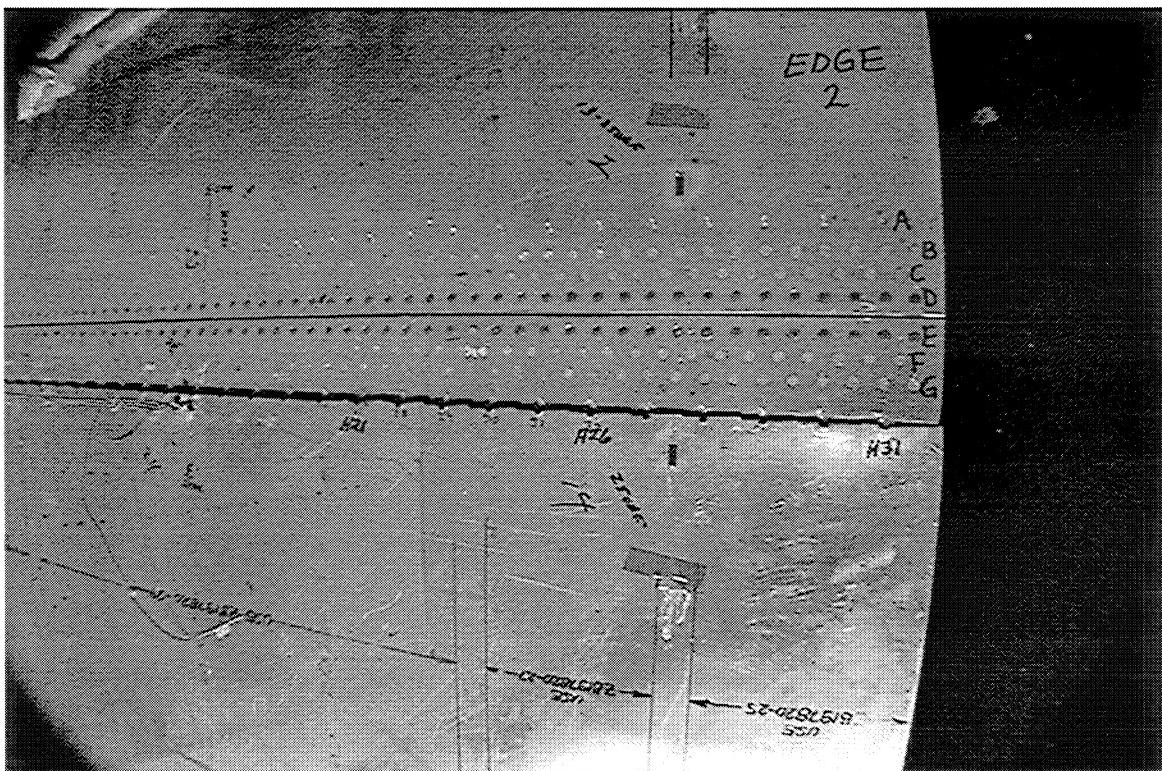
Figure 146
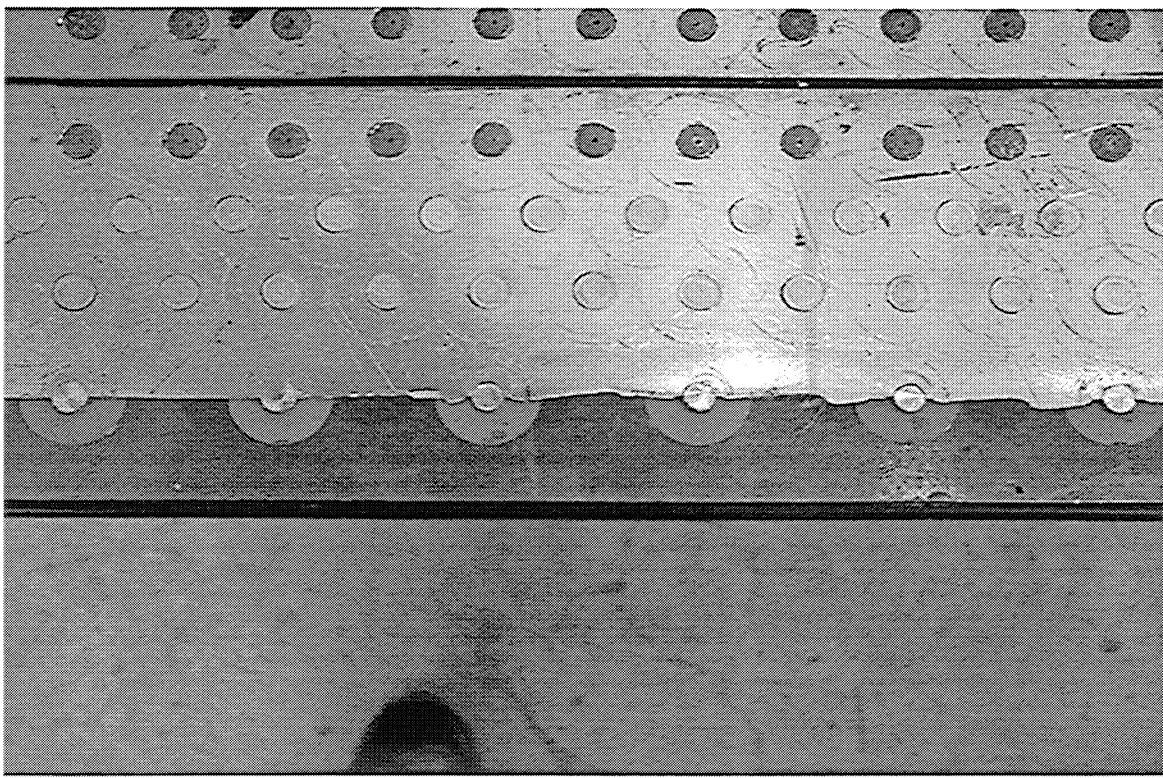
Figure 147

Figure 148
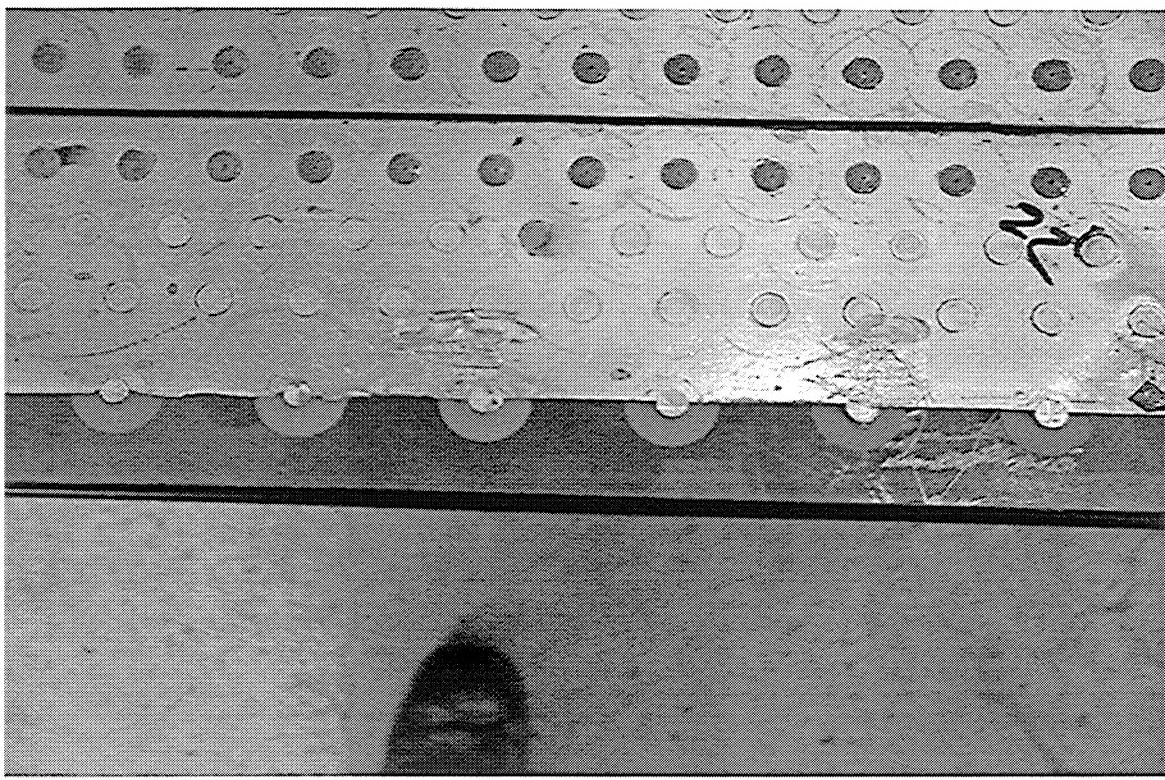
Figure 149

Figure 150

Figure 151

Figure 152